Bulletin of the University of Utah

Vol. 53 May, 1962 No. 21

Bulletin No. 116

of the

UTAH ENGINEERING EXPERIMENT STATION

STRESS AND VELOCITY FIELDS IN GRAVITY FLOW OF BULK SOLIDS

Jerry Ray Johanson

and

Andrew W. Jenike

Salt Lake City, Utah

INTRODUCTION

This paper is an extract from a Ph.D. thesis written by Johanson in the Department of Mechanical Engineering, College of Engineering, University of Utah; it follows earlier publications by Jenike [e.g. 1,5].

The purpose of the work has been to develop a mathematical theory of flow of bulk solids. The term 'bulk solids' encompasses both frictional (granular) and cohesive materials, and specifically describes such solids as ore, coal, concentrates, chemicals, flour, sugar. While there exist papers describing the behavior of these solids in bins and hoppers, the authors believe that this is the first time that stress and velocity fields have been computed mathematically for steady flow in converging channels under the action of gravitational forces. The method used in this paper is based on the concepts of soil mechanics and plasticity adapted by Jenike and Shield [3] to permit the steady flow of frictional solids.

In Chapter I the applicable features of the theory of steady state flow are stated. The solution of the general problem of stress and velocity fields for plane strain and axial symmetry requires the solution of two systems, each comprising two hyperbolic differential equations.

In Chapter II the differential equations are transformed into difference equations in preparation for the numerical work which follows in Chapter IV. Types of possible boundary conditions are considered and the difference equations are adapted to those types. Useful combinations of boundary conditions are then described.

A particular solution, called the radial stress field, is described

in Chapter III. This solution applies to converging channels with straight walls and has been treated at length in reference 5. In this paper experimental observations are given to substantiate the existence of such fields.

Certain cases of more general boundary conditions are computed and observed in Chapter IV. They substantiate the existence of radial stress fields and verify experimentally the physical assumptions made in the derivation of the theory.

ACKNOWLEDGEMENTS

The results presented in this paper were obtained in the course of work conducted under a National Science Foundation grant to the project: "Flow of Rigid-Plastic Solids in Converging Channels Under the Action of Body Forces".

TABLE OF CONTENTS

NOTATIONS

x, y, z	rectangular coordinates
r, θ, α	spherical coordinates
t	time
γ	bulk density
δ	effective angle of friction of a solid
ϕ	angle of internal friction of a solid
ϕ'	angle of friction between a flowing solid and a wall
θ'	angle of inclination of the wall of a channel measured from the vertical axis
$\mu = \pi/4 - \delta/2$	Angle between the directions of major pressure and of the stress characteristics
ν'	the acute angle between a wall and the direction of the major pressure
ω	the angle between the x-axis and the direction of the major pressure measured counterclockwise from the x-axis
$\sigma_x, \sigma_y, \sigma_z$	pressure components in the x, y and z direction
σ_1, σ_2	major and minor principal pressures in the x-y or r-θ planes
σ_3	third principal pressure
$\sigma = \frac{1}{2}(\sigma_1 + \sigma_2) = \frac{1}{2}(\sigma_x + \sigma_y)$	mean pressure in the x - y plane
$\tau_{xy}, \tau_{xz}, \tau_{yz}$	shear strain rate components in rectangular coordinates
$\epsilon_x, \epsilon_y, \epsilon_z$	normal strain rate components in the x, y and z direction
$\gamma_{xy}, \gamma_{zx}, \gamma_{yz}$	shear strain rate components in rectangular coordinates
u, v	Velocity components in the x and y direction
V	magnitude of the velocity vector in the x - y plane
V_1, V_2	velocity components in the first and second characteristic directions
ϵ	Angle of inclination from the horizontal to a traction-free top boundary.

CHAPTER I

THEORY OF STEADY FLOW

The reader may find many of the concepts encountered in the theory of bulk solids flow very similar to those found in soil mechanics and plasticity. However, when applied to bulk solids, these concepts undergo subtle but significant changes. In this chapter the physical as well as the theoretical meaning of steady flow as it relates to some of the well known concepts of plasticity and soil mechanics is discussed.

The Steady Flow Condition

The stress and velocity fields discussed in this paper apply to conditions of steady flow. This means that the stress and velocity at any point are unchanged with time. The boundaries are also assumed unchanged with time. As the solid flows out of a channel the channel is refilled at the top in such a way as to maintain constant boundaries. In applications this condition is rarely achieved, however, if the change with time is small and continuous, the steady flow fields calculated from the boundary conditions at a given time will closely approximate the real fields.

Steady flow in a converging channel is characterized by a continuous deformation without change in the stress at a given point. It appears from experimental evidence that this type of flow occurs only for certain stress conditions. Results of the shear test procedure proposed by Jenike [1] show that Mohr circles representing a steady flow stress are approximately tangential to a straight line through the point of zero

stress, Figure 1. De Jong [2] shows the same results in a test in which $\sigma_1 + \sigma_2$ is held constant and $\sigma_1 - \sigma_2$ is increased until continuous deformation occurs without change in stress. The envelope of Mohr circles defined in this manner is termed the effective yield locus, EYL, and is expressed by the equation $\frac{\sigma_1 - \sigma_2}{\sigma_1 + \sigma_2} = \sin \delta$ where σ_1 and σ_2 are the major and minor principal stresses in the plane of deformation with compression taken as positive. From experimental evidence it appears that the value of δ is essentially independent of the magnitude of the third principal stress σ_3. The EYL transforms into σ_1, σ_2, σ_3 coordinates as the plane

$$\sigma_1(1 - \sin \delta) - \sigma_2(1 + \sin \delta) = 0 \qquad (i)$$

which passes through the σ_3 axes and makes an angle $\beta = \tan^{-1}\left(\frac{1 - \sin \delta}{1 + \sin \delta}\right)$ with the σ_1 axis Figure 2. By cyclic renumbering of the variables in equation (1), six such planes can be constructed each passing through one of the axes and making an angle β with one of the other axes. The surface formed by these planes, Figure 3, is called the effective yield pyramid. Stress conditions for steady flow are represented by points lying on the surface of this pyramid. Since the plane of any side of the pyramid can be derived from any other plane simply by permutating the subscript of σ_1, σ_2, σ_3 one need only consider one of the sides in order to represent all possible stress conditions. If the principal stresses are ordered so that $\sigma_2 \leq \sigma_3 \leq \sigma_1$ then the pyramid side AFO need only be considered. Along OA $\sigma_1 = \sigma_3 > \sigma_2$ and along OF $\sigma_3 = \sigma_2 < \sigma_1$.

The strength of a bulk solid varies with the pressure under which it was consolidated. This is shown experimentally by subjecting a sample

of solid to continuous steady flow with a given σ_{1s} Figure 1. Observe that the Mohr circle for this condition is tangential to the EYL. The stress is removed in such a way that no further deformation occurs. The sample now has certain strength properties which can be determined by restressing several such samples under different σ_{1f} values where the subscript f indicates failure conditions. The result of such a test carried out as outlined in [1] is shown in Figure 1. It is necessary that $\sigma_{1s} > \sigma_{1f}$ because for the condition $\sigma_{1s} \leqslant \sigma_{1f}$ the solid would again assume a condition of flow and different stength properties would develop.

The Mohr circles for failure are tangent to a line called the yield locus, YL, which represents the normal and shear stress on slip-planes of the solid along which full frictional conditions develop. In steady flow the stress at the slip planes are located at point E. In general, a different σ_{1s} will have a different YL. The YL near point E can be approximated by a straight line indicated by the dashed line. This line in σ_1, σ_2, σ_3 coordinates, transforms, as did the EYL, into a pyramid, Figure 4, where the planes of the sides are given by

$$\sigma_1(1 - \sin\theta) - \sigma_2(1 + \sin\theta) - 2\cos\phi = 0. \qquad (2)$$

Jenike and Shield [3] have proposed that this pyramid be terminated by a base plane perpendicular to the octahedral axis Point E, Figure 1, then corresponds to a point at the intersection of the base plane with the side planes. The intersection of a given EYL function and the plane of the YL function is shown in Figures 2 and 3 as a vertical line AF. As σ_3 changes along this line of constant σ_1 and σ_2, the base of the YL pyramid must also change for steady flow. In general, steady flow

requires not only the base of the YL pyramid to change but the entire pyramid must change from one stress condition to another. The physical interpretation of this is that a solid flowing in a channel has a strength at a generic point dependent on the stress condition at that point.

Plastic Potential and Steady Flow

Plastic potential or normality states that

$$\epsilon_i = \lambda \frac{\partial F}{\partial \sigma_i}$$

where F is the yield function. Geometrically this means that when ϵ_i and σ_i coordinates are aligned, the vector formed by the ϵ_i components is normal, or perpendicular, to the yield surface. In this paper σ_i and ϵ_i are positive for compression and contraction, respectively. In particular, consider one side of the yield pyramid given by equation (2), then

$$\epsilon_1 = \lambda \frac{\partial F}{\partial \sigma_1} = \lambda(1 - \sin\phi),\ \epsilon_2 = \lambda \frac{\partial F}{\partial \sigma_2} = -\lambda(1 + \sin\phi)\ \epsilon_3 = \lambda \frac{\partial F}{\partial \sigma_s} = 0.$$

The ϵ vector is $\lambda[(1 - \sin\phi), -(1 + \sin\phi), 0]$, normal to the given plane. At the sharp edges or corners of the yield function, ϵ_i is defined only to within the limits imposed by the intersecting surfaces [4]. For steady flow the stresses are located on the base of the yield function thus giving the maximum freedom to the direction of the ϵ vector.

The continuity of the solid is expressed by

$$\epsilon_1 + \epsilon_2 + \epsilon_3 = \epsilon_x + \epsilon_y + \epsilon_z = \frac{1}{\gamma}\frac{d\gamma}{dt}$$

where γ is the specific weight of the solid and, in general, is a function of x, y, z and t. It has been shown that γ can be assumed constant without

greatly affecting the solution [3]. The resulting condition

$$\epsilon_1 + \epsilon_2 + \epsilon_3 = 0 \qquad (3)$$

restricts the strain rate vector to a plane perpendicular to the octahedral axis. The strain rate vector $\lambda[(1 - \sin\phi), -(1 + \sin\phi), 0]$ normal to the side of the yield pyramid does not satisfy this condition. One now sees the necessity that point E, Figure 1, correspond to a point on the base of the pyramid, where the ϵ vector has enough freedom to satisfy this condition. It should be noted that plastic potential implies normality with respect to the yield surface not to the effective yield surface.

In the case of plane strain, which is characterized by deformation in one plane only, eg. σ_1, σ_2 plane, velocity is zero in the direction of the σ_3, this implies $\epsilon_3 = 0$, which together with (3) define the direction of the strain rate vector such that the normality limitations can only be satisfied at point F, Figure 3. Thus, with no density change, normality limits the plane strain stresses to $\sigma_2 = \sigma_3 < \sigma_1$. In the case of axial symmetry a unique direction of the strain rate vector is not specified. However, in a converging channel it seems natural to assign the circumferential stress as major since the solid contracts along the circumference. This assumption restricts the stress to point A on the yield pyramid where $\sigma_2 < \sigma_3 = \sigma_1$. Normality at this point gives certain limits for the ϵ vector but does not specify it uniquely.

Isotropy in Steady Flow

In steady flow different points in the material may have different yield functions, however, material properties at any one point are assumed isotropic, i.e. independent of direction. It will be shown that this

usually implies that the directions of principal stress and strain rate coincide. This coincidence is expressed by

$$\frac{2\tau_{xy}}{\sigma_x - \sigma_y} = + \tan 2\omega = \frac{\gamma_{xy}}{\epsilon_x - \epsilon_y} \qquad (4)$$

where ω is the angle measured counter clockwise from the x direction to the direction of major principal stress and strain rate, Figure 5.

To show the coincidence of directions consider the most general expression for the shear strain rate

$$\gamma_{xy} = G(\sigma_x, \sigma_y, \sigma_z, \tau_{xy}, \tau_{yz}, \tau_{xz}, \epsilon_x, \epsilon_y, \epsilon_z, \gamma_{xz}, \gamma_{yz})$$

Since the solid is isotropic the function G will be the same regardless of orientation of x, y, and z. In particular, consider the coordinates aligned with the directions of principal stresses. The terms τ_{xy}, τ_{yz}, τ_{xz} are now zero. A new coordinate system formed by rotating the original by 180° about the y axis is given by $x' = -x$, $y' = y$, $z' = -z$ and

$\gamma'_{xy} = G(\sigma'_x, \sigma'_y, \sigma'_z, \tau'_{xy}, \tau'_{xz}, \tau'_{yz}, \epsilon'_x, \epsilon'_y, \epsilon'_z, \gamma'_{xz}, \gamma'_{yz})$,

where $\sigma'_x = \sigma_x$, $\sigma'_y = \sigma_y$, $\sigma'_z = \sigma_x$, $\tau'_{xy} = \tau'_{xz} = \tau'_{yz} = 0$, $\epsilon'_x = \epsilon_x$, $\epsilon'_y = \epsilon_y$, $\epsilon'_z = \epsilon_z$, $\gamma'_{xz} = -\gamma_{xz}$, $\gamma'_{yz} = -\gamma_{yz}$, $\gamma'_{xy} = -\gamma_{xy}$.

Hence $\gamma_{xy} = G(\sigma_x, \sigma_y, \sigma_z, \epsilon_x, \epsilon_y, \epsilon_z, \gamma_{xz}, \gamma_{yz}) = -\gamma'_{xy} =$

$$= - G[\sigma_x, \sigma_y, \sigma_z, \epsilon_x, \epsilon_y, \epsilon_z, (-\gamma_{xz}), (-\gamma_{yz})]$$

If G is an even function with respect to γ_{xz} and γ_{yz} that is if

$$G[(-\gamma_{xz}), (-\gamma_{yz})] = G(\gamma_{xz}, \gamma_{yz}), \text{ then}$$

$G = -G = 0 = \gamma_{xy}$ and therefore x, y, and z are directions of principal strain rates coinciding with directions of principal stresses. Since most stress-strain relationships involve shear

strain rates as a function of stress only as is the case of plastic potential, the restriction that G be even is usually satisfied.

Basic Equations

The equilibrium equations

$$\frac{\partial \sigma_x}{\partial x} + \frac{\partial \tau_{xy}}{\partial y} = \gamma \qquad (5)$$

$$\frac{\partial \tau_{xy}}{\partial x} + \frac{\partial \sigma_y}{\partial y} = 0$$

for plane strain, and

$$\frac{\partial \sigma_x}{\partial x} + \frac{\partial \tau_{xy}}{\partial y} + \frac{\tau_{xy}}{y} = \gamma \qquad (6)$$

$$\frac{\partial \tau_{xy}}{\partial x} + \frac{\partial \sigma_y}{\partial y} + \frac{\sigma_y - \sigma_1}{y} = 0$$

for axial symmetry, together with the steady flow condition (1), and appropriate boundary conditions are sufficient to define a stress solution. The x, y coordinates are shown in Figure 6, where gravity acts in the positive x-direction. The axis of symmetry coincides with the x-axis These equations can be combined with the aid of Mohr circle geometry to

$$(1 + \sin\delta \cos 2\omega)\frac{\partial \sigma}{\partial x} + \sin\delta \sin 2\omega \frac{\partial \sigma}{\partial y} - 2\sigma \sin\delta \sin 2\omega \frac{\partial \omega}{\partial x} +$$

$$+ 2\sigma \sin\delta \cos 2\omega \frac{\partial \omega}{\partial y} = \gamma - m\frac{\sigma}{y}\sin\delta \sin 2\omega \qquad (7)$$

$$\sin\delta \sin 2\omega \frac{\partial \sigma}{\partial x} + (1 - \sin\delta \cos 2\omega)\frac{\partial \sigma}{\partial y} + 2\sigma \sin\delta \cos 2\frac{\partial \omega}{\partial x} +$$

$$+ 2\sigma \sin\delta \sin 2\omega \frac{\partial \omega}{\partial y} = m\frac{\sigma}{y}\sin\delta(1 + \cos 2\omega).$$

where $\sigma = \frac{\sigma_1 + \sigma_2}{2} = \frac{\sigma_x + \sigma_y}{2}$, m = 0 for plane strain and m = 1 for axial

symmetry [5].

Equations (3) and (4) describing continuity with no density change and isotropy, respectively, are sufficient to define the velocity field in plane strain and in axial symmetry. In accordance with Figure 4, u and v are velocity components in the x and y directions and by definition, taking contracting strain rates as positive,

$$-\epsilon_x = \frac{\partial u}{\partial x}, \quad -\epsilon_y = \frac{\partial v}{\partial y}, \quad \text{and} \quad -\gamma_{xy} = \frac{\partial v}{\partial x} + \frac{\partial u}{\partial y}.$$

In plane strain $\epsilon_z = 0$ while in axial symmetry $\epsilon_\alpha = -\frac{v}{y}$ for symmetry conditions, where α is the circumferential coordinate. With these definitions, equations (3) and (4) become, respectively,

$$\begin{aligned} &\frac{\partial u}{\partial x} + \frac{\partial v}{\partial y} + m\frac{v}{y} = 0 \\ &\tan 2\omega = \frac{\frac{\partial u}{\partial y} + \frac{\partial v}{\partial x}}{\frac{\partial u}{\partial x} - \frac{\partial v}{\partial y}}. \end{aligned} \tag{8}$$

These equations with well posed boundary conditions on the velocity can be solved provided ω is known. Since ω is determined by the stress field, this condition ties the velocity and stress fields together, however, the velocity field is not dependent upon the magnitude of stress σ and the stress boundary conditions do not determine the velocity boundary conditions. Hence, it is not uncommon for the stress field to be symmetric while the velocity field is nonsymmetric.

It is of interest to note that the plastic potential or normality does not influence the basic equations in any way. The discussion of normality was simply to show that the conditions of steady flow do not violate this principle.

Physical Limitations of Steady Gravity Flow

The requirement of steady gravity flow imposes certain restrictions on the stress and velocity field that are not inherent in the equations. These are:

1. Due to the nature of the EYL, stress must always be compressive.
2. Since gravity is the only outside force acting on the solid there should be no upward component of velocity, (i.e., $u \geqslant 0$).
3. Assuming density to be a function of pressure it follows that discontinuities in pressure imply discontinuities in density. If the solid were to flow from one stress (and density) region to another an infinite acceleration would have to occur. Since this is physically impossible stress discontinuities in steady flow can only occur along streamlines. Since discontinuities usually start at some streamline boundary and continue away from the boundary, stress discontinuities seldom occur in the interior of the field.
4. Singular points of stress, that is multiple values of σ and ω at a single point are physically impossible because multiple σ values would imply multiple density values at the same point. However, in the case where $\sigma = 0$ multiple values of ω are permitted.
5. Accelerations of individual particles must be finite. This means that a particle cannot flow across a velocity discontinuity.

Boundary Conditions for Gravity Flow

Figures 6 and 7 illustrate the most common boundary conditions occurring in gravity flow. In Figure 6 the bulk solid flows along a rigid side wall such as a steel plate while in Figure 7 the solid flows along itself. One can also visualize combinations of these conditions. The top boundary of the bulk solid is assumed traction-free. If in addition to being traction-free the surface also satisfies the EYL condition for steady flow, the stress state of the surface is defined by point 0 in Figure 1 and is therefore, stress-free.

The Mohr circle for this condition degenerates to a point $\sigma = \tau = 0$, however, the direction of principal stress ω can be determined as a function of the angle of inclination ϵ of the stress-free boundary, Figure 6. This is accomplished by observing that the directional derivation of σ

$$d\sigma = \frac{\partial \sigma}{\partial x} dx + \frac{\partial \sigma}{\partial y} dy$$

along $\frac{dx}{dy} = -\tan \epsilon$ is zero. This condition together with equations (7) for $\sigma = 0$ can be solved for ϵ and ω_s giving

$$\text{Sin } (2\omega - \epsilon) = -\frac{\sin \epsilon}{\sin \delta},$$

the pertinent root of which is

$$2\omega_s = \epsilon + \sin^{-1} \frac{\sin \epsilon}{\sin \delta} + \pi. \qquad (9)$$

The subscript s indicates the values along a stress-free boundary. It should be noted here that for $\sigma = 0$ all terms in equations (7) involving m disappear; hence equation (9) applies for both axial symmetry and plane strain.

When the solid flows on rigid side walls the normal and shear stresses along the wall are found experimentally to lie approximately on a straight line as shown in Figure 1 by the 'wall yield locus', WYL. The angle ϕ' is said to be the angle of friction between the rigid wall and the solid under steady flow. The angle between the direction of the major principal stress and the slope of the wall is called ν'. From the geometry of Figure 1 one obtains the relation

$$\sin(\pi - \phi' - 2\nu') = \frac{\sin \phi'}{\sin \delta},$$

the pertinent root of which is

$$2\nu' = \pi - \sin^{-1} \frac{\sin \phi'}{\sin \delta} - \phi' \qquad (10)$$

Thus ν' is a function of the solid property δ and the angle of friction between the solid and the wall ϕ'. Figure 6 shows angle θ' defined in such a way that $\frac{dy}{dx} = \tan(-\theta')$ is the equation of the right side wall where $\theta' = \nu' - \omega'$. (10a)

At the point of intersection of a stress-free boundary and a rigid side wall (e.g., point P in Figure 6), the direction of the principal stress is defined by the wall and does not coincide with the direction defined by the stress-free boundary unless

$$\omega' = \nu' - \theta' = \omega_s = \tfrac{1}{2}[\epsilon + \sin^{-1} \frac{\sin \epsilon}{\sin} + \pi].$$

In other words the relation

$$\epsilon + \sin^{-1} \frac{\sin \epsilon}{\sin \delta} = - \phi' - \sin^{-1} \frac{\sin \phi'}{\sin \delta} - 2\theta'$$

must be satisfied between ϵ, ϕ', θ' and δ. In the case when $\omega' > \omega_s$ (as illustrated in the upper Figure 8), the direction of the principal

stress can be rotated from ω_s to ω' without causing a stress discontinuity in the interior of the material. The singularity of ω at P is admissible since $\sigma = 0$ and therefore no singularity in σ occurs. Such a stress condition is referred to as a centered fan in [6]. For the case of $\omega' < \omega_s$ illustrated in the lower Figure 8, a discontinuity in stress is required. As was previously stated in the limitations of steady flow, a discontinuity must coincide with a streamline. In this case the streamline at point P would coincide with the wall, the discontinuity would be in the interior of the solid, therefore, this condition is not acceptable.

The solid near point P would not deform but would remain rigid (or elastic), it would either flow or remain in place. In this case the top boundary would be traction-free, but the stresses would not be those defined by the effective yield condition. It should be noted here that the condition $\omega_s < \omega'$ is only a necessary condition and not sufficient to guarantee deformations at point P. The complete boundary condition is the determining factor not one point alone.

When the solid flows on itself there no longer exists a frictional surface as with a rigid side wall where the material flows along the specified shape of the wall. In flowing along itself the solid is quite free to choose its own flow pattern dependent on the top boundary conditions. The normal stress and the shear stress along such a side boundary must satisfy the slip-line condition for the solid, point E, Figure 1. The wall is then defined by $\frac{dy}{dx} = \tan [\omega - (\frac{\pi}{4} - \frac{\phi}{2})]$ where ϕ is the angle of internal friction at point E. This angle is found experimentally to be bounded by

$$\delta > \phi > 0$$

Since this wall has the greatest frictional value of all the walls, it will be referred to as a 'rough wall', while walls made of extraneous materials will be referred to as 'weak walls'.

CHAPTER II

SOLUTION BY METHOD OF CHARACTERISTICS

In this chapter the characteristic equations of the stress and velocity solutions are introduced and their properties, as they relate to the flow of bulk solids are discussed. The numerical solution of the stress and velocity fields by the method of characteristics using a high speed digital computer is given in detail.

Equations of the Characteristics

Equations (7) and (8) can be expressed as the matric equation

$$A\,U_x + B\,U_y + d = 0$$

where A and B are n x n matrices,

$$U_x = \left\| \begin{matrix} \frac{\partial U_1}{\partial x} \\ \vdots \\ \frac{\partial U_n}{\partial x} \end{matrix} \right\| , \quad U_y = \left\| \begin{matrix} \frac{\partial U_1}{\partial y} \\ \vdots \\ \frac{\partial U_n}{\partial y} \end{matrix} \right\| ,$$

and d is a n x 1 matrix. If the system is subjected to a non-singular linear transformation T such that $T\,A = C\,T\,B$ where C is diagonal [7], the system reduces to $T\,A\,U_x + T\,B\,U_y + T\,d = 0$ or $C\,A^*\,U_x + A^*\,U_y + d^* = 0$ where $A^* = T\,B$ and $d^* = T\,d$. A single equation of the system is of the form

$$\sum_{i=1}^{n} a^{*Ki} \left(C^K U_x^i + U_y^i\right) + d^{*K} = 0$$

where C^K is the K^{th} diagonal element of C. Now consider the direction

$$\frac{dx}{dy} = C^K$$

then

$$C^K U_x^i + U_y^i = \frac{dx}{dy} U_x^i + U_y^i = \left(U_x^i\,dx + U_y^i\,dy\right) \frac{1}{dy} = du\,\frac{1}{dy}$$

where du is the directional derivitive of u in the direction

$$\frac{dx}{dy} = C^K .$$

This direction is called the K^{th} characteristic direction and

$$\frac{dx}{dy} = C^K$$

is the equation of the K^{th} characteristic. It is evident from this that the characteristic directionshave the property that the partial derivatives of the dependent variables become total directional derivatives in these directions. This property makes the characteristics important in solving a problem numerically. A necessary condition for $T\,A = C\,T\,B$ is that the diagonal elements of C be solutions of $|A - \lambda B| = 0$. For hyperbolic type equations the λ's will be real and distinct so that the above interpretation of them is always possible.

In the particular case of equations (8)

$$A = \begin{Vmatrix} 1 & 0 \\ \text{Tan } 2\psi & -1 \end{Vmatrix}, \quad B = \begin{Vmatrix} 0 & 1 \\ -1 & \text{Tan } 2\psi \end{Vmatrix}, \quad U_x = \begin{Vmatrix} \frac{\partial u}{\partial x} \\ \frac{\partial v}{\partial x} \end{Vmatrix}$$

$$U_y = \begin{Vmatrix} \frac{\partial u}{\partial y} \\ \frac{\partial v}{\partial y} \end{Vmatrix} \qquad d = \begin{Vmatrix} \frac{m\,v}{y} \\ 0 \end{Vmatrix}$$

and the characteristic directions are

$$\frac{dy}{dx} = \text{Tan } (\omega \pm \frac{\pi}{4}).$$

In these directions equations (8) become

$$du + dv \frac{dx}{dy} \pm \frac{\frac{m\,v}{y}}{\text{Cos } 2\omega}\, dx = 0$$

These equations can be expressed in the cannonical form

$$\frac{\partial y}{\partial \beta} = \frac{\partial x}{\partial \beta} \text{ Tan } (\omega + \frac{\pi}{4}) \qquad (a)$$

$$\frac{\partial u}{\partial \beta} + \frac{\partial v}{\partial \beta} \operatorname{Tan}\left(\omega + \frac{\pi}{4}\right) + \frac{\frac{m\ v}{y}}{\cos 2\omega} \cdot \frac{\partial x}{\partial \beta} = 0 \qquad \text{(b)}$$

(11)

$$\frac{\partial y}{\partial \alpha} = \frac{\partial x}{\partial \alpha} \operatorname{Tan}\left(\omega - \frac{\pi}{4}\right) \qquad \text{(c)}$$

$$\frac{\partial u}{\partial \alpha} + \frac{\partial v}{\partial \alpha} \operatorname{Tan}\left(\omega - \frac{\pi}{4}\right) - \frac{\frac{m\ v}{y}}{\cos 2\omega} \frac{\partial x}{\partial \alpha} = 0 \qquad \text{(d)}$$

where α and β are functions of x and y such that α is constant along the first characteristic

$$\frac{dy}{dx} = \operatorname{Tan}\left(\omega + \frac{\pi}{4}\right)$$

and β is constant along the second characteristic

$$\frac{dy}{dx} = \operatorname{Tan}\left(\omega - \frac{\pi}{4}\right).$$

The cannonical equations for the stress equations (7) can be derived in a similar way and are

$$\frac{\partial u}{\partial \beta} = \frac{\partial x}{\partial \beta} \operatorname{Tan}(\omega + \mu)$$

$$\frac{\partial \sigma}{\partial \beta} + 2\sigma \operatorname{Tan} \delta \frac{\partial \omega}{\partial \beta} = a \frac{\partial x}{\partial \beta}$$

(12)

$$\frac{\partial y}{\partial \alpha} = \frac{\partial x}{\partial \alpha} \operatorname{Tan}(\omega - \mu)$$

$$\frac{\partial \sigma}{\partial \alpha} - 2\sigma \operatorname{Tan} \delta \frac{\partial \omega}{\partial \alpha} = b \frac{\partial x}{\partial \alpha}$$

where

$$\mu = \frac{\pi}{4} - \frac{\delta}{2}$$

$$\left.\begin{matrix} a \\ b \end{matrix}\right\} = \begin{matrix} - \\ + \end{matrix} \frac{\gamma \operatorname{Sin}(\omega \mp \mu)}{\operatorname{Cos} \delta \ \operatorname{Cos}(\omega \pm \mu)} \begin{matrix} + \\ - \end{matrix} m \frac{\operatorname{Cos} \omega \ \operatorname{Cos} \mu}{y \operatorname{Cos}(\omega \pm \mu)} \sigma \tan \delta$$

and α is constant along the first characteristic and β is constant along the second characteristic.

The velocities determined from equations (11) are unique to an arbitrary multiplicative constant. The stress solution can also be found in terms of an arbitrary constant length ℓ by defining new variables: $x' = x/\ell$, $y' = y/\ell$, and $\sigma' = \sigma/\gamma\ell$. Equations (12) in terms of these new variables are the same as shown except $\gamma = 1$ in a and b. In plotting these non-dimensional variables no scale is shown. The reader may assume any scale as long as the dimensions of ℓ and γ are compatible. These new variables will be used throughout the remainder of the paper.

In the xy plane the stress characteristics are at angles $\pm \mu$ from the direction of major principal stress while the velocity characteristics are at $\pm \pi/4$ as shown in Figure 5. The stress and velocity characteristics do not coincide except for the case of $\delta = 0$. Figure 9 shows the shape of the characteristics in a typical symmetric converging channel. Because of this physical interpretation of characteristics and their role in defining the regions of unique solutions, the types of boundary problems as applied to gravity flow of bulk solids will now be reviewed.

Boundary Problems

The first type of a well posed boundary problem, or Cauchy problem [8], is when sufficient conditions are imposed on a line that at no point coincides in direction with a characterisitic. Figure 10 shows such a line AB. The region in which a unique solution is defined is the curvilinear rectangle ACBD formed by the characteristics through the end points of AB. In all of the figures the first characteristics will be represented by a long and short dashed line and the second characteristics by a dashed line. The most common problem of this type occurring in gravity flow is that of a stress free surface as illustrated by AB in Figure 13. This boundary is nowhere characteristic, (provided $|\epsilon| < \delta$), and the two dependent variables σ and ω are determined by the shape of AB. The region of

unique solution for the stress field is the triangle ABC. For this boundary to be a Cauchy problem in a velocity field the velocity would have to be given along AB and, after the stress field had been calculated the unique solution for this boundary would be in a corresponding triangle formed by the velocity characteristics.

Another type of well posed boundary problem is when only part of the unknowns are specified along two intersecting lines. (This is often referred to as a mixed boundary value problem.) One common occurrence of this problem is when one of the lines is a given characteristic and the other is non-characteristic with one of the dependent variables given along it. Figure 11a shows the region ABCD in which a unique solution is determined if the given characteristic is long in relation to the given non-characteristic line. Figure 11b shows the region ABC defined when the non-characteristic line is long.

An example of this problem, illustrated in Figure 13, is the stress characteristic BC previously calculated and the rigid side wall BF along which $\omega' = \theta' - \nu'$ where ν' is given by equation (10). The region determined is BCD. A similar situation in the velocity field occurs when a velocity characteristic is determined by a Cauchy problem along AB and the wall BF is a streamline, that is

$$\frac{v}{u} = -\text{Tan } \theta'.$$

In a symmetric channel the centerline condition $\omega = \pi/2$ with the characteristic AC serve to define a well posed problem for the stress field.

A third type of problem is when two lines, both characteristic, are given. (This is referred to as a Goursat problem in [8].) As shown in Figure 12 the region of solution is the curvilinear rectangle ABCD. This problem is illustrated in Figure 13 by the characteristics EC and DC determined from previous calculations. The region of solution is CDHE. By repeated application of the last two boundary problems discussed, the calculation can be completed to the first characteristic GF, Figure 13, where F is the

last point given on the wall. It should be noted that a characteristic with dependent and independent variables given along a segment of it does not define uniquely a region of solution.

Properties of Stress and Velocity Solutions

Without actually solving the equations, one can draw some general conclusions about the solutions in certain regions or along certain lines. In this section some of these conclusions will be discussed.

Consider a solution of a system of hyperbolic type equations, such as equation (7) or (8), given in region R, Figure 14. The solution defined by a well posed boundary value problem with boundaries in R and boundary values in accordance with the given solution is equal to the given solution at every point common to R and to the region of unique solution of the boundary problem. This follows directly from the uniqueness of solution of a well posed problem. In particular, if a non-characteristic line AB has assigned dependent variables along it in accord with the given solution in R, the Cauchy problem thus described will yield the given solution in region ACBD. Similarly the given solution would be determined in region ACBD by the problem defined by having both dependent variables given along characteristic AC and any one dependent variable given along AB in accord with the given solution. The solution of a boundary value problem is continuously dependent on the initial data [8]. Hence, if the dependent variables assigned in the problems described above closely approximate the given solution, the solution defined by such boundary values will approximate the original solution in region ACBD.

These properties of hyperbolic systems yield some interesting results when applied to equations (7) and (8). The condition $u = c$, $v = (1 - m)d$ where c and d are constants, is a solution to equations (8). Hence, if condition $u = c$, $v = 0$ is assigned along the non-characteristic top boundary AD of Figure 15, the resulting Cauchy problem enforces this solution in ABC. The problem formed

by the characteristic AC and the centerline condition v = 0, compatible with the described solution, enforces this solution in ACD. If the weak wall BE is vertical, thus causing v = 0 along it, the wall, together with BD, enforces this solution in region BDE. The constant solution continues down to a first characteristic FG where F is the lowest point at which the wall is vertical.

Suppose velocity was not assigned along AB but it was observed that u = c along the portion of the vertical wall BE. This would enforce the solution u = c, v = 0 in region ABFG. The conclusion from this is that if the velocity along a sufficient portion of a vertical weak wall is observed constant, the velocity field must be constant down to the point at which the wall no longer is vertical. The length of the observed portion must be such that the unique field determined by it includes at least one point along the centerline. If u is approximately constant along such a section, then the field determined would approximate u = c, v = 0.

The solution of equation (7) for $\omega = \pi/2$, $\sigma = \sigma(x)$ is

$$\frac{d\sigma}{dx} = \frac{\gamma}{1 - \sin \delta}$$

or

$$\sigma - \sigma_o = \frac{\gamma}{1 - \sin \delta} (x - x_o).$$

An example of a boundary defining such a field is the horizontal stress-free boundary shown in Figure 16. Since $\epsilon = 0$ equation (9) implies $\omega = \pi/2$ while $\sigma = 0$ along $x = 0$; hence, $\sigma = \frac{\gamma x}{1 - \sin \delta}$ in region ABC. If the x axis is the centerline, thus enforcing $\omega = \pi/2$ along it, then this solution also occurs in the region ACD.

Properties of Characteristics

Consider a first stress characteristic given by $y = f(x)$, then $y' = \text{Tan}\ (\omega + \mu)$ or $\omega = \text{Tan}^{-1} y' - \mu = \omega(x)$. The characteristic equation

$$\frac{d\sigma}{dx} + 2\sigma \text{ Tan } \delta \frac{d\omega}{dx} = a(\omega)$$

reduces to the form

$$\frac{d\sigma}{dx} + \sigma F(x) = G(x)$$

where

$$F(x) = 2 \operatorname{Tan} \omega \frac{d\omega(x)}{dx}$$

and

$$G(x) = a\big(\omega(x)\big).$$

This can be integrated to give σ as a function of x to within an arbitrary constant. A similar equation can be derived for a given second characteristic.

In the velocity field, if a first velocity characteristic is given as $y = f(x)$, then $\omega = \omega(x)$, and if a relation between u and v, $u = u(v)$, is given along the characteristic, then equation (16) becomes

$$\frac{du(v)}{dx} + \frac{dv}{dx} + \frac{\frac{m\,v}{y}}{\cos 2\omega} = 0$$

which can be solved for $v = v(x)$ along the characteristic.

This illustrates the property of the characteristics that if one dependent variable is given along a characteristic, the other may be calculated to within an arbitrary constant. This constant is usually determined by some physical boundary condition. Thus if in a symmetric channel such as is shown in Figure 13, the shape of the characteristic AD was given as $\omega = \omega(x)$ and σ at point A was given as $\sigma = 0$, then σ would be determined along characteristic AD. Since AG is the centerline along which $\omega = \pi/2$, then AG, AD, and the wall conditions of DF would be sufficient to determine a unique solution in region ADFG.

The velocity characteristic equations (11b) and (11d) can be rewritten in terms of components of velocity V_1 and V_2 along the first and second characteristics respectively [5]. The equations resulting from the transformation of

$$u = -V_1 \sin\left(\omega - \frac{\pi}{4}\right) + V_2 \sin\left(\omega + \frac{\pi}{4}\right)$$

$$v = V_1 \cos\left(\omega - \frac{\pi}{4}\right) + V_2 \cos\left(\omega + \frac{\pi}{4}\right)$$

are

$$\frac{\partial V_1}{\partial \beta} + V_2 \frac{\partial \omega}{\partial \beta} + \frac{m}{2y}\left[V_1 + V_2 \tan\left(\omega - \frac{\pi}{4}\right)\right] \frac{\partial y}{\partial \beta} = 0$$

$$\frac{\partial V_2}{\partial \alpha} - V_1 \frac{\partial \omega}{\partial \alpha} + \frac{m}{2y}\left[-V_1 \tan\left(\omega + \frac{\pi}{4}\right) + V_2\right] \frac{\partial y}{\partial \alpha} = 0$$

where V_1 and V_2 are velocity components in the direction of the first and second characteristics respectively. Two properties of velocity characteristics can be readily seen with the equations in this form: First, if the velocity characteristic is also a streamline (i.e., $V_2 = 0$ for the first characteristic and $V_1 = 0$ for the second), then the velocity component in the direction of the characteristic is $V_1 = Ay^{-m/2}$ and $V_2 = By^{-m/2}$ for the first and second characteristics respectively. Second, if the characteristic is straight (i.e., d $d\omega = 0$), the velocity in the direction of the characteristic is constant in plane strain.

In the section on boundary problems, it was pointed out that a characteristic with dependent and independent variables completely given along it does not uniquely determine a solution in a region. However, any non-characteristic line with all variables given along it does define a region of unique solution since it forms a Cauchy problem. With this in mind, consider the right black drawn line in the photograph of Figure 49. In this picture the upper right side region was observed to move with a uniform velocity in the direction of the wall. Along the black line the velocity changes magnitude and direction as is shown by the break in the white lines. Material is flowing through the black line and, therefore, it cannot be a velocity discontinuity because, if it were, the particles crossing DE would have to undergo an infinite acceleration which is physically impossible. The only alternative is for velocity along the black line to have the same value as in the upper side region. The break in the white lines is caused by a rapid change in velocity that starts at the black line and continues over a short but definite width.

Lines along which rapid changes in velocity occur must be velocity characteristics. This is easily shown by assuming that such a line is not a velocity characteristic. Since velocity is given along it, a region of similar velocity would be determined in the region of unique solution of the Cauchy problem; hence, no rapid change could occur along it. In the particular case of plane strain, if velocity along such a line is constant, the Cauchy problem defines a constant velocity in its region of definition. However, if AB is a characteristic, no unique field is determined and an additional boundary condition may be assigned to give the observed rapid change in velocity.

The proof is now complete that rapid changes in velocity may occur only along velocity characteristics. However, one should note that discontinuities in velocities, which are characterized by absence of flow across them, need not be velocity characteristics, but the direction of principal stress is governed by the frictional conditions between the two solids on either side of the discontinuity. In the case of flow of the solid on itself, such a discontinuity would have full friction developed between the flowing and the non-flowing solid, and would, therefore, be a slipline.

This property of rapid changes occurring along characteristics is not unique to the velocity field. In Figure 43 one observes that the oscillations in σ values are reflected along stress characteristics. For example, the peak σ value at point A on the centerline is reflected along the second characteristic AB to a peak value at point B at the wall, and this maximum in σ is reflected from point C at the wall to point D at the centerline along the first characteristic CD.

The First Basic Type of Numerical Calculation

The numerical solution by the method of characteristics consists of replacing the differential equations of the characteristics by finite difference equations and then calculating along the characteristics.

The calculation proceeds from a known point on a characteristic to an unknown point on the same characteristic. Let the known values be denoted with a subscript 1 and 2 for a calculation along a first and second characteristic, respectively. Let the unknown values be denoted by the subscript p. With this notation, the characteristic equations for stress can be written in finite difference form

$$\frac{y_1 - y_p}{x_1 - x_p} = \text{Tan}\ (\omega + \mu) \qquad \text{(a)}$$

(13)

$$(\sigma_1 - \sigma_p) + 2\sigma(\omega_1 - \omega_p)\ \text{Tan}\ \delta = a_1\ (x_1 - x_p) \qquad \text{(b)}$$

for the first characteristic, and

$$\frac{y_2 - y_p}{x_2 - x_p} = \text{Tan}\ (\omega - \mu) \qquad \text{(a)}$$

(14)

$$(\sigma_2 - \sigma_p) - 2\ \sigma\ (\omega_2 - \omega_p)\ \text{Tan}\ \delta = b_2\ (\ x_2 - x_p\ ) \qquad \text{(b)}$$

for the second characteristic, where a and b are defined in equations (12). For the velocity equations (11), the finite difference form is

$$\frac{y_1 - y_p}{x_1 - x_p} = \text{Tan}\ (\omega + \frac{\pi}{4}) \qquad \text{(a)}$$

(15)

$$\frac{u_1 - u_p}{x_1 - x_p} + \frac{v_1 - v_p}{x_1 - x_p} + m\ \frac{v}{y\ \cos\ 2\ \omega} = 0 \qquad \text{(b)}$$

for the first characteristic and

$$\frac{y_2 - y_p}{x_2 - x_p} = \text{Tan}\ (\omega - \frac{\pi}{4}) \qquad \text{(a)}$$

$$\frac{u_2 - u_p}{x_2 - x_p} + \frac{v_2 - v_p}{x_2 - x_p} - m \frac{v}{y \cos 2\omega} = 0 \qquad \text{(b)} \qquad (16)$$

for the second characteristic.

In these finite difference equations, the dependent variables ω, σ, u, and v occur other than as differences. The mean value theorem of calculus states that if $\frac{dy}{dx} = f(x)$, then

$$\frac{y_1 - y_p}{x_1 - x_p} = f(X)$$

where X is a point in the interval from point 1 to p. In particular, if the curve connecting 1 and p is an arc of a circle, then X is the midpoint between points 1 and p. With this motivation it appears that the accuracy of the finite difference calculation can be improved by evaluating the dependent variables not occurring in differences at the midpoints of the interval rather than at the ends of the interval. For the first stress characteristic this means

$$\omega = \frac{\omega_1 + \omega_p}{2} \quad \text{and} \quad \sigma = \frac{\sigma_1 + \sigma_p}{2} .$$

In calculating from the boundary conditions previously discussed two basic types of calculations will suffice to determine the solution. When the dependent variables are known at two adjacent points not on the same characteristic, they can be computed at a third point lying at the intersection of characteristics through the given points. This type of calculation is the only one used in calculating a Cauchy problem. Figure 17 shows an example of this situation where 1 and 2 are the given points and p is at the intersection of the first characteristic through 1 and the second characteristic through 2.

Using average ω and σ values, equations (13a) and (14a) are combined to give

$$x_p = \frac{x_1 \operatorname{Tan}\left(\frac{\omega_p + \omega_1}{2} + \mu\right) - x_2 \operatorname{Tan}\left(\frac{\omega_p + \omega_2}{2} - \mu\right) + y_2 - y_1}{\operatorname{Tan}\left(\frac{\omega_p + \omega_1}{2} + \mu\right) - \operatorname{Tan}\left(\frac{\omega_p + \omega_2}{2} - \mu\right)} \qquad (17)$$

$$y_p = (x_p - x_1) \operatorname{Tan}\left(\frac{\omega_p + \omega_1}{2} + \mu\right) + y_1. \qquad (18)$$

Equations (13b) and (14b) are combined to give

$$\omega_p = \frac{F + A}{G + B}$$

$$F = b_2 (x_2 - x_p)(\omega_1 \operatorname{Tan} \delta - 1) + a_1 (x_1 - x_p)(\omega_2 \operatorname{Tan} \delta + 1)$$

$$+ (\sigma_1 - \sigma_2)(\omega_2 - \omega_p)(\omega_1 - \omega_p) \operatorname{Tan}^2 \delta$$

$$A = (\sigma_1 + \sigma_2)(\omega_1 + \omega_2) \operatorname{Tan} \delta + \sigma_1 - \sigma_2$$

$$G = \operatorname{Tan} \delta \left[a_1 (x_1 - x_p) + b_2 (x_2 - x_p)\right]$$

$$B = 2 \operatorname{Tan} \delta (\sigma_1 + \sigma_2)$$

$$\sigma_p = \frac{a_1 (x_1 - x_p) + \sigma_1 \left[1 - (\omega_1 - \omega_p) \operatorname{Tan} \delta\right]}{1 + (\omega_1 - \omega_p) \operatorname{Tan} \delta}$$

where

$$a_1 = \frac{-\sin\left(\frac{\omega_p + \omega_1}{2} - \mu\right)}{\cos \delta \cos\left(\frac{\omega_p + \omega_1}{2} + \mu\right)} + m \frac{\cos\left(\frac{\omega_p + \omega_1}{2}\right) \cos \mu}{y_1 \cos\left(\frac{\omega_p + \omega_1}{2} + \mu\right)} 2\sigma_1 \operatorname{Tan} \delta$$

$$b_2 = \frac{\sin\left(\frac{\omega_p + \omega_2}{2} + \mu\right)}{\cos \delta \cos\left(\frac{\omega_p + \omega_1}{2} - \mu\right)} - m \frac{\cos\left(\frac{\omega_p + \omega_2}{2}\right) \cos \mu}{y_2 \cos\left(\frac{\omega_p + \omega_2}{2} - \mu\right)} 2\sigma_2 \operatorname{Tan} \delta$$

These four independent equations are solved for the four unknown values x_p, y_p, ω_p, and σ_p at point C. An initial guess for ω_p is made; then from equation (17) an approximate x_p is found. Using this x_p and ω_p in the right hand side of equation (19), a refined ω_p is found. A refined x_p is now calculated using this new ω_p in equation (17). Using this x_p and ω_p equation (19) yields an even greater refined ω_p. This process can be iterated until consecutively calculated values of ω_p agree to a specified accuracy. With the final x_p and ω_p one can now use equations (18) and (20) to find y_p and σ_p, and the calculation is complete. The thought pattern or flow chart for this procedure is given in Figure 18.

One problem encountered in using this first basic calculation in the stress field is the convergence of the iteration at certain points near a stress-free boundary. At these points the successively calculated points would oscillate about the true value with increasing amplitude. In order to avoid this, the value of x used as the n^{th} approximation was taken as

$$x = \frac{x_n + x_{n-1}}{2} .$$

In this manner convergence of the iterative scheme was achieved everywhere.

The first type of calculation for the velocity equations proceeds in somewhat of a different manner since ω_p is given by the stress field. Equations (15a) and (16a) can be combined to

$$x_p = \frac{x_1 \operatorname{Tan}\left(\frac{\omega_1 + \omega_p}{2} + \frac{\pi}{4}\right) - x_2 \operatorname{Tan}\left(\frac{\omega_2 + \omega_p}{2} - \frac{\pi}{4}\right) + y_2 - y_1}{\operatorname{Tan}\left(\frac{\omega_1 + \omega_p}{2} + \frac{\pi}{4}\right) - \operatorname{Tan}\left(\frac{\omega_1 + \omega_p}{2} - \frac{\pi}{4}\right)} \qquad (21)$$

$$y_p = y_1 + (x_p - x_1) \operatorname{Tan}\left(\frac{\omega_1 + \omega_2}{2} + \frac{\pi}{4}\right) . \qquad (22)$$

Since ω is a known function of x and y an initial guess of ω_p is made. Then x_p and y_p are calculated from equations (21) and (22).

With these, a new ω_p is calculated from the given function $\omega(xy)$. This process is iterated until consecutive values of ω_p agree to within a prescribed limit. Equations (15b) and (16b) combine to

$$v_p = \frac{u_1 - u_2 + v_1 \frac{y_1 - y_p}{x_1 - x_p} - v_2 \frac{y_2 - y_p}{x_2 - x_p}}{\frac{y_1 - y_p}{x_1 - x_p} - \frac{y_2 - y_p}{x_2 - x_p} + \frac{m}{y_p \cos 2\omega}\left[(y_1 - y_p) + (y_2 - y_p)\right]} \tag{23}$$

$$u_p = u_1 - (y_1 - y_p)\left(\frac{v_1 - v_p}{x_1 - x_p} + m\frac{v_p}{y_p}\right) \tag{24}$$

and with proper values of x_p, y_p, and ω_p calculated as above, u_p and v_p can be found. The flow chart for this procedure is given in Figure 19.

A major problem in using this velocity calculation is in determining $\omega(x, y)$ from the stress field calculations. Since the velocity and stress characteristics do not coincide, the point of calculation in the velocity field will not be the same as in the stress field. It is, therefore, necessary to interpolate values of ω as calculated from the stress field. At first it was felt that a high order polynomial could be fitted thoughout the entire field by a least squares method. This proved to be very inaccurate. After having the same problem of inaccuracy after dividing the field into several small regions, it was concluded that the best method would be linear interpolation between the closest points to the point in question. This method required the storage of all the calculated stress points as well as a great deal of time for the computer to search out the closest of these points to the point in question. The limited capacity of the computer, therefore, eliminated the possibility of velocity calculation except for radial stress in which case ω is a function of one variable only and interpolation is feasible.

The Second Basic Numerical Calculation

In calculating a mixed boundary value problem the situation arises as illustrated in Figure 20 where the dependent variables are given at points along the characteristic OA and relationships between them are given along an intersection line OB. In calculating a point p on OB near O, the calculation proceeds from a given point 2 on OA, along the segment of characteristic 2p. The calculation is carried out by the use of the finite difference equations of the characteristic from 2 to p and the given information at p.

In particular consider the case for the stress field when OB is a straight rigid side wall with angle of friction ϕ'. Then ω_p is determined from equation (10a) when the slope of the wall is given. If 2p is a second characteristic, the relations

$$\frac{y_2 - y_p}{x_2 - x_p} = \text{Tan}\left(\frac{\omega_2 + \omega_p}{2} - \mu\right) \tag{25}$$

$$(\sigma_2 - \sigma_p) - (\sigma_2 + \sigma_p)\,\text{Tan}\,\delta\,(\omega_2 - \omega_p) = b_2\,(x_2 - x_p) \tag{26}$$

from the characteristic equations and

$$y_p = A\,x_p + B \tag{27}$$

as the equation of the line OB, where ω_p is given, are combined to

$$x_p = \frac{y_2 - x_2\,\text{Tan}\left(\frac{\omega_2 + \omega_p}{2} - \mu\right) - B}{A - \text{Tan}\left(\frac{\omega_2 + \omega_p}{2} - \mu\right)} .$$

Equation (26) then yields

$$\sigma_p = \frac{b_2\,(x_2 - x_p) - \sigma_2\left[1 - \text{Tan}\,\delta\,(\omega_2 - \omega_p)\right]}{1 - \text{Tan}\,\delta\,(\omega_2 - \omega_p)} \tag{26a}$$

and point p is completely determined.

At the centerline of the channel a similar calculation is encountered along a first characteristic. The centerline condition is expressed by $\omega_p = \pi/2$ and $y_p = 0$ which can be combined with equations (13) to give x_p and σ_p at the centerline in terms of the variables at the neighboring point 1. It should be noted here that the axial symmetry term in the expression for a_1 is not determined at the centerline and is, therefore, approximated by its value at point 1.

In a more general case of this type of calculation when the line is not straight but given by $x = f(y)$ and $\omega = \omega(y)$ the solution of point p may be more complicated and an approximate iterative method may be needed. As an illustration of this, consider a weak wall given by

$$x = f(y) \tag{28}$$

The direction of principal stress is found from equation (10a) to be

$$\omega = -\theta - \nu = -\cot^{-1} f'(y) - \nu. \tag{29}$$

If 2p is a second characteristic, then equations (25) and (26) apply and equation (25) can be expressed as

$$y_p = -\left[x_2 - f(y_p)\right] \operatorname{Tan}\left(\frac{\omega_2 + \omega_p}{2} - \mu\right) + y_2 . \tag{30}$$

The iterative scheme is shown in the flow chart Figure 21 and consists of making an initial approximation for y_p, calculating x_p and ω_p from equations (28) and (29), then using these values in equation (30) to calculate a new y_p. This process is then iterated until consecutive y_p values agree to within a specified accuracy. One must use this procedure cautiously, however, since it may diverge instead of converge, depending on f(y) and the closeness of the initial y_p approximation to the actual y_p.

The second type calculation in the velocity field usually occurs when the direction of the velocity vector is given along some line like the wall of a channel or a centerline. In such a

case the calculation of x_p and y_p is essentially the same as for the stress field except μ is replaced by $\pi/4$. The variables u_p and v_p can usually be calculated directly when x_p and y_p are known. For example, consider the situation shown in Figure 20 when the line $x = f(y)$ is the wall of the channel so that $\frac{u}{v} = f'(y)$ along the wall. Consider 2p as a second velocity characteristic. Then x_p and y_p are determined as for the stress field. Equation (16b) applies from 2 to p. When this is combined with

$$\frac{u_p}{v_p} = f'(y_p)$$

one obtains

$$v_p = \frac{u_2 + v_2}{f'(y_p) + 1 + m \frac{x_2 - x_p}{\frac{1}{2}(y_2 + y_p) \operatorname{Cos}(\omega_p + \omega_1)}},$$

$$u_p = v_p f'(y_p).$$

The condition for the second type calculation along the centerline is even simpler because $v_p = 0$. After calculating x_p and y_p in the same way as in the stress calculation except μ is replaced by $\pi/4$, u_p can be calculated directly from equation (15b) for $v_p = 0$.

The examples discussed in connection with this type of boundary are certainly not the only possibilities. However, these will serve as a basis for dealing with others.

Combining Calculations Into a Complete Solution

So far only the calculation of individual points has been discussed. In order to calculate a stress or velocity field, literally thousands of these calculations must be performed. When one considers the time required to calculate just one point, especially with the iteration involved in some of the calculations, the necessity of the use of the high speed digital computer becomes evident. To make

the computer program flexible enough so that any type of boundary problem could be solved, separate programs for each type of basic calculation were written. These programs for the Burroughs 205 computer are found in the appendix along with instructions on how to use them. They were written in such a way that all the required data for a calculation is assumed stored in place before the program is started. The calculated values are stored in certain locations and then the program stops. In order to be useful, these basic calculation programs must be manipulated and entered by a master correlation program which, in general, will differ with different type boundary problems. To illustrate this, the example given in Figure 13 is considered. Figure 22 shows this same example to a larger scale. The given boundary AB is divided into several segments by an arbitrary number of points. For illustrative purposes three points are used here. However, in practice many more would probably be used because the accuracy of the calculation is a function of the length of the divisions.

The order in which the calculations are performed is somewhat arbitrary. The order presented here was found to be useful for automatic high speed calculation. Points 33 and 22 are used in the first basic calculation to find point 32. Point 32 is then used in a second type of calculation with the centerline to determine point 42. Again using the first type of calculation, points 22 and 11 determine 21, 21 and 32 determine 31, and 42 and 31 determine 41. The point 41 is then used in a second type calculation to find 51. Point 21 is used in a second type calculation with the wall to find point 20. Points 20 and 31 are used to calculate 30. The calculation proceeds as above until point 60 is calculated. The pattern is now established. The first characteristic is calculated point by point from its uppermost point to its last. Each time the characteristic is started with a second type calculation to the wall and is ended with a second type calculation to the centerline with all intermediate calculations of the first type. It is seen that this scheme can be

continued as far as the wall conditions are defined. The flow chart describing this procedure is found in Figure 23. The programs for the Burroughs 205 Computer are found in the appendix.

One of the major problems with this numerical calculation along characteristics is the spacing of the points. One can not rely on a uniform spacing of the original data points to give uniform spacing to further calculations. In fact, the characteristics usually have the tendency to become closer together in some places and farther apart in others. When the characteristics become closer, or bunch up, the efficiency of the calculation is greatly reduced because the same accuracy could be achieved with less points calculated. Even more important, the characteristics may become so close together, or the mesh of characteristics may become so elongated in one direction, that the errors of calculation cause characteristics of the same family to appear to cross. This crossing if it were to occur legitimately would imply a discontinuity of some sort [9], however, if it is due merely to improper spacing of the points, it simply invalidates the calculation from that point on. To eliminate this problem, the spacing of the points along the wall was kept constant. If one reviews the proceeding paragraph on the combined calculation it is evident that, in general, the spacing of points along the wall is determined by the initial data spacing, but is unpredictable. In order to achieve the desired uniform spacing along the wall, the points determined by the initial data were used to interpolate points of uniform spacing along the wall. By controlling the spacing, any irregularities introduced by the original spacing can be controlled and eliminated in subsequent calculation. If with this controlled spacing, crossing of characteristics of the same family still occurs, then chances are good that there is an actual discontinuity in the neighborhood of the crossing.

The procedure that will now be discussed is built into the second type wall calculations. A typical calculation situation is shown in Figure 24. The spacing is controlled by a constant vertical distance Δx between points along the wall. The second type

calculation is employed from point 12 to the wall, point 22. If $|x_{11} - x_{22}| < \Delta x$, as in the case illustrated, the second type calculation is repeated for point 13 to the wall and again $|x_{11} - x_{22}|$ is checked to see if it is greater than Δx. If it is not, the process is repeated until a point along the first characteristic is found such that the difference between x_{11} and the x of calculated point is greater than Δx. In the example point 23 satisfies this condition. Values at point p are then calculated by linearly interpolating between points 11 and 23. In the case of a straight wall with constant frictional condition, one has

$$x_p = x_{11} + \Delta x \ , \qquad y_p = \Delta x \ \mathrm{Tan}\ \theta' - y_{11} \ ,$$

$$\omega_p = \omega_{11} \ , \qquad \sigma_p = \Delta x \ \frac{\sigma_{11} - \sigma_{23}}{x_{11} - x_{23}} + \sigma_{11} \ .$$

This control was used in most of the examples of calculated fields shown in this paper and was found to be very satisfactory.

CHAPTER III

THE RADIAL STRESS SOLUTION

In this chapter a particular stress solution will be discussed: the direction of principal stress is radially symmetric about an origin. This condition is compatible with the direction of the velocity vector being radial, but is also admissible to other velocity fields. The numerical solution of this stress field is discussed and the solutions are given for a range of parameters for symmetric channels in plane strain and axial symmetry. Solutions are also given for a limited number of non-symmetric channels in plane strain. The last three sections of this chapter show by calculation from general boundary conditions and by experimental observations that radial stress occurs, or at least is closely approached in all regions, where the side wall conditions in symmetric channels are compatible with it. Thus, this stress field seems to be very basic to the flow of bulk solids in axial symmetry and plane strain.

Equations for Radial Stress and Velocity

Equations (7) written in plane polar co-ordinates with the changes of variables

$$\sigma = \gamma\, r\, s(\theta, r)$$

$$\omega = \psi + \theta$$

are

$$\frac{\partial s}{\partial \theta} + s\, f(r,\theta) + g(r,\theta) = 0$$

$$r\frac{\partial s}{\partial r} + s\, h(r,\theta) + j(r,\theta) = 0 \qquad (31)$$

With the assumption $\psi = \psi(\theta)$ it can be shown that $s = s(\theta)$ which is by definition radial stress [5], page 59, and f, g, h, and j evaluate at

$$f(\theta) = 2\left(\frac{d\psi}{d\theta} + 1\right)\frac{\sin\delta}{\cos^2\delta}\sin 2\psi +$$

$$+ m\,\frac{\sin\delta}{\cos^2\delta}(1 + \sin\delta)\,[\sin 2\psi - \cot\theta(1 + \cos 2\psi)],$$

$$g(\theta) = -\frac{\sin\delta}{\cos^2\delta}\sin(\theta + 2\psi) \quad \frac{\sin\theta}{\cos^2\delta}$$

$$h(\theta) = 1 + 2\left(\frac{d\psi}{d\theta} + 1\right)\frac{\sin\delta}{\cos^2\delta}(\cos 2\psi - \sin\delta) +$$

$$+ m\frac{\sin\delta}{\cos^2\delta}(1 + \sin\delta)(\cot\theta \sin 2 + \cos 2\psi - 1),$$

$$j(\theta) = -\frac{\sin\delta}{\cos^2\delta}\cos(\theta + 2\psi) + \frac{\cos\theta}{\cos^2\delta};$$

and equations (31) become

$$\frac{ds}{d\theta} = \frac{F_1 + m F_2}{A} = F$$

$$\frac{d\psi^*}{d\theta} = \frac{G_1 + m G_2}{2A} = G \qquad (32)$$

where

$$F_1 = \sin(2\psi^* + \theta) + s \sin 2\psi^*$$

$$F_2 = -s \sin\delta\,[(1 - \cos 2\psi^*)\cot\theta + \sin 2\psi^*]$$

$$G_1 = \frac{\cos\theta + \sin\delta\cos(2\psi^* + \theta) + s\cos^2\delta}{s\sin\delta} - 2A$$

$$G_2 = -(1 + \sin\delta)(\sin 2\psi^* \cot\theta + \cos 2\psi^* + 1)$$

$$A = \cos 2\psi^* + \sin\delta$$

$$\psi^* = \psi - 90^\circ .$$

These equations can be written in an alternate form:

$$\frac{d\theta}{ds} = \frac{A}{F_1 + m F_2} = F^*$$

$$\frac{d\psi^*}{ds} = \frac{G_1 + m G_2}{2(F_1 + mF_2)} = G^*. \qquad (33)$$

The velocity equations (8) when written in terms of polar co-ordinates with velocities u_r and u_θ in the r and θ directions respectively become

$$\frac{\partial}{\partial r}\left[\gamma\, u_r\, r\, (r \sin\theta)^m\right] + \frac{\partial}{\partial \theta}\left[\gamma\, u_\theta\, (r \sin\theta)^m\right] = 0$$

and

$$\text{Tan } 2\psi\ (r, \theta) = \frac{\dfrac{\partial u_r}{r\partial\theta} + \dfrac{\partial u_\theta}{\partial r} - \dfrac{u_\theta}{r}}{\dfrac{\partial u_r}{r} - \dfrac{u_r}{r} - \dfrac{\partial u_\theta}{r\partial\theta}}.$$

For radial velocity

$$u_r = V, \quad u_\theta = 0$$

and the velocity equations can be combined to give

$$\psi = \psi\ (\theta)$$

$$V = V^\circ \left(\frac{r^\circ}{r}\right)^{1+m} e^{-(2+m)\int_{\theta^\circ}^{\theta} \text{Tan } 2\psi\, d\theta}$$

where V°, r°, and θ° are given constants. If some particular $r = r^\circ$ is considered and if the centerline velocity is assigned as one, then $V^\circ = 1$ for $r^\circ = r$, and $\theta^\circ = 0$. One observes from this solution that $\psi = \psi\ (\theta)$ implies $\omega = \omega(\theta)$ which is the condition for radial stress [5]. Thus, radial velocity implies radial stress. However, the converse is not true as will be shown by an example in a later section.

One observes that the radial stress equations are total differential equations and involve only one co-ordinate θ. This makes the solution much easier to obtain than in the general case with the partial differential equations. However, no closed form solution is found and numerical methods must be used.

Numerical Solution of Radial Stress

The numerical method used was the fifth order Runga-Kutta method for simultaneous first order equations, described in [10]. When applied to equations (32) with θ as the independent variable, successive values of s and ψ are given by

$$s_{n+1} = s_n + \frac{1}{6}(K_o + 2K_1 + 2K_2 + K_3) + O(h^5),$$

$$\psi_{n+1} = \psi_n + \frac{1}{6}(m_o + 2m_1 + 2m_2 + m_3) + O(h^5),$$

where

$$h = \theta_{n+1} - \theta_n;$$

$$K_o = hF(\psi_n, s_n, \theta_n),$$

$$K_1 = hF(\psi_n + \frac{1}{2} m_o, s_n + \frac{1}{2} K_o, \theta_n + \frac{1}{2}h),$$

$$K_2 = hF(\psi_n + \frac{1}{2} m_1, s_n + \frac{1}{2} K_1, \theta_n + \frac{1}{2} h),$$

$$K_3 = hF(\psi_n + m_2, s_n + k_2, \theta_n + h);$$

$$m_o = hG(\psi_n, s_n, \theta_n),$$

$$m_1 = hG(\psi_n + \frac{1}{2} m_o, s_n + \frac{1}{2} K_o, \theta_n + \frac{1}{2} h),$$

$$m_2 = hG(\psi_n + \frac{1}{2} m_1, s_n + \frac{1}{2} K_1, \theta_n + \frac{1}{2} h),$$

$$m_3 = hG(\psi_n + m_2, s_n + K_2, \theta_n + h).$$

The error term $O(h^5)$ is small, provided h is small. This method has the advantage in that the size of h can be changed at any point without upsetting the previous calculations and without additional calculation. This same method may be used on equations (33) with s as the independent variable and ψ and θ as dependent variables.

For boundary conditions in a symmetric channel, one has $\theta = 0$ and $\psi = \pi/2$ or $\psi^* = 0$ at the centerline. Denoting the value of s at the centerline by s°, the functions involved evaluate to

$$F_1]_{s^\circ} = 0$$

$$F_2]_{s^\circ} = \lim_{\substack{\psi^* \to 0 \\ \theta \to 0}} s^\circ \sin\delta[(1 - \cos 2\psi^*)\cot\theta] =$$

$$= \lim_{\substack{\psi \to 0 \\ \theta \to 0}} s^\circ \sin\delta \; 2\frac{\sin^2\psi^*}{\sin\theta}\cos\theta = 0,$$

$$G_1]_{s^\circ} = \frac{1 + \sin\delta + s^\circ \cos^2\delta - 2(1 + \sin\delta)}{s^\circ \sin\delta},$$

$$G_2]_{s^\circ} = \lim_{\substack{\psi^* \to 0 \\ \theta \to 0}} -(1 + \sin\delta)(\sin 2\psi^* \cot\theta + 2) = -(1 + \sin\delta)\left(2\frac{d\psi^*}{d\theta} + 2\right),$$

$$A]_{s^\circ} = 1 + \sin\delta,$$

$$\left.\frac{ds}{d\theta}\right]_{\substack{\psi^* = 0 \\ \theta = 0 \\ s = s^\circ}} = 0,$$

$$\left.\frac{d\psi}{d\theta}\right]_{\substack{\psi^* = 0 \\ \theta = 0 \\ s = s^\circ}} = (1 - \frac{m}{2})\left(\frac{1 + \sin\delta + s^\circ \cos^2\delta}{2\, s^\circ \sin\delta\,(1 + \sin\delta)} - 1\right) - \frac{m}{2},$$

whereas the derivatives in equations (33) are not defined. For this reason equations (32) were used to start calculating from the centerline. When A = 0, the derivatives in this equation become undefined and equations (33) are used to continue the calculations in the neighborhood of A = 0.

Since the magnitude of the various derivatives varies greatly in different parts of the solution, it is necessary to change h accordingly, so as to maintain accuracy and yet allow h to be as large as possible in order to shorten the time of calculation. The flow chart in Figure 25 shows the scheme used to accomplish this and also to decide when to use equations (33) instead of equations (32). The various constants $\Delta\psi^*$ maximum, $\Delta\psi^*$ minimum, $\Delta\theta$ maximum, $\Delta\theta$ minimum, $\Delta\theta$ change, and Δs maximum were determined by trial and error until two standard sets of constants were found to be suited to most problems. The accuracy of

the calculation was checked by comparing the solution obtained using the standard program with the solution obtained using much smaller h values and checking the agreement of the two solutions at the extreme points from the original starting point.

The computer program for the Burroughs 205 digital computer with instructions on how to use it is found in the thesis [11]. With only slight modifications, as outlined in the thesis, the non-symmetric case of plane strain can be run, and with additional changes, the program can be used to run the stress field with density as a function of σ in the form $\gamma = \gamma_o \sigma^{\beta}$ where β is a constant determined experimentally. In addition to the values of s, ψ, and θ, this program also gives the radial velocity V, flow factor ff, vertical force q, shear stress τ_n, and normal stress σ_n acting on a radial wall.

The general flow chart for the calculations is given in Figure 26. Since this chart gives only a rough overall view of the calculation, a more detailed flow chart of each section will now be discussed.

The solution by the Runga-Kutta method involves calculation of F and G at various points near the given point. Thus, a program is needed to calculate $F(\psi_n + a, s_n + b, \theta_n + c)$ and $G(\psi_n + a, s_n + b, \theta_n + c)$ where a, b, and c are arbitrary constants. The flow chart for this is shown in Figure 27. It is assumed that for this part of the program ψ_n, s_n, θ_n, a, b, and c are already stored in locations as required by the program. This program is called "Calculation of K_i and m_i," in the Runga-Kutta program shown in flow chart form in Figure 28. This Runga-Kutta solution program presupposes that ψ_n, s_n, and θ_n are given in the proper locations for calculation as the input to this program. The output of the program is ψ_{n+1}, s_{n+1}, and θ_{n+1}. After this calculation, the equations of radial stress are essentially solved. However, for applications, it is desirable to calculate the vertical force acting on a horizontal cross section, the radial velocity profile, the flow factor as described in [5] , and the shear and normal stress components along the wall of the channel.

The vertical force Q on a symmetric cross section of width B and length L in plane strain, or of diameter B in axial symmetry is given by $Q = 2\pi^m L^{1-m} \int_o^y \sigma_x \; y^m \, dy$. For radial stress this transforms to

$$Q = q \gamma L^{(1-m)} B^{(2+m)}$$

where

$$q = 2\pi^m \left(\frac{\cot \theta'}{2}\right)^{2+m} \int_o^\theta s \frac{\tan^m \theta}{\cos^3 \theta} [1 + \sin \delta \cos 2(\theta + \psi)] \; d\theta$$

see reference [5], page 82. For calculation of q, the integral is approximated by

$$\sum_{n=0}^{n=N} \left[\frac{s_{n-1} + s_n}{2}\right] \left[\frac{1 - \sin \delta \cos 2\left(\frac{\psi^*_{n-1} + \psi^*_n}{2} + \frac{\theta_{n-1} + \theta_n}{2}\right)}{\cos^3\left(\frac{\theta_{n-1} + \theta_n}{2}\right)}\right] \tan^m \left(\frac{\theta_{n-1} + \theta_n}{2}\right) \Delta\theta.$$

It is evident from this that it is necessary to have values of ψ_{n-1}, s_{n-1}, and θ_{n-1} as well as ψ_n, s_n, and θ_n in order to perform this calculation. Therefore, provision for keeping these values had to be made in the Runga-Kutta solution of the equations.

The radial velocity solution for $r = r^\circ$, $V^\circ = 1$, and $\theta^\circ = 0$ is given by

$$V = e^{-(2 + m) \int_0^\theta \tan 2\psi \, d\theta}.$$

As with the vertical force calculation, the integral is approximated by

$$\sum_{n=0}^{n=N} \tan 2\left(\frac{\psi^*_{n+1} + \psi^*_n}{2}\right) \Delta\theta.$$

The values calculated by the program are typical for any constant radius. One observes that at $\psi^* = \pi/4$, $V = 0$, because $\tan 2\psi \rightarrow \infty$ at this point. In order to calculate the radial velocity field for $\psi^* > \pi/4$ an arbitrary constant had to be assigned. Therefore, the magnitude of V for $\psi^* > \pi/4$ is not related to the magnitude of V for $\psi^* < \pi/4$. Since this velocity calculation is elementary, no flow chart is given.

The computed solutions of the stress fields are shown in Figures 29 through 38 for plane strain symmetry and axial symmetry for various values of the parameter δ. The radial velocity field is shown for $\delta = 50^\circ$ in Figures 69 and 70. In plane strain, the radial stress field is not limited to symmetry. Figures 39 to 41 show the radial fields calculated for one vertical wall with $\delta = 50^\circ$ and various angle of friction values for the solid against the wall. For the interpretation of these graphs, it is convenient to use ϕ' in place of ψ^*. The relation between them as seen from the geometry of Figure 6 is $\psi^* = \pi/2 - \nu$, where ν is given as a function of ϕ' and δ by equation (10). In using these graphs to determine the radial stress field in the symmetric case, one needs only to know the angle of friction ϕ' for the wall and solid, the slope of the wall θ', and the effective angle of friction δ. With the appropriate graph chosen for the δ value, one now finds the point on the graph of the given θ' and ϕ' where ϕ' is plotted vertically at the right side and θ' is plotted horizontally. The curve that passes through the given point describes the radial field for this symmetric boundary condition. Note that different boundary conditions may have the same radial solution in certain regions. For example, in Figure 31 for plane symmetry $\delta = 50^\circ$, wall conditions $\phi' = 41^\circ$, $\theta' = 30^\circ$ have the same solution as $\phi' = 33^\circ$, $\theta' = 13^\circ$ in the region between $\theta' = 0$ and $\theta' = 13^\circ$.

For a non-symmetric channel, the solution has an additional parameter in that θ' and ϕ' must be given along both boundaries. The case illustrated in Figures 39 through 41 is for one vertical wall. The appropriate frictional value along the vertical wall determines which chart to use. Then θ' and ϕ' of the sloping wall determine the curve describing the field. As before, different boundary conditions may have the same solution in certain regions.

Calculated Examples of Convergence to Radial Stress Field

In this section are given some examples of stress fields with boundary conditions chosen at random, which may or may not represent actual physical conditions. In each case the radial field compatible with the given straight wall conditions is closely approached in regions away from the

the stress-free top boundary. It must be remembered that, although certain regions may be assigned as plastic or as non-plastic, the actual size of the plastic and non-plastic regions is governed by more than mere equilibriu of forces and may differ from those assigned in the examples. It will be shown in a later section that the actual physical boundary is such as to approach radial possibly closer than in the examples given here. These examples not only show the convergence tendency to radial stress, but also serve as a check point on the validity of the calculated radial stress fields and the method of characteristics calculations.

In the following examples σ is shown to approach radial value at the centerline and at the wall. To show that the stress fields in the given examples approach radial, it is sufficient to show that the value of σ along the centerline approaches radial. This follows from the discussion on page 20 concerning the continuous dependence of the solution upon the boundary conditions in the region of unique solution defined by such conditions. In these examples, the centerline has $\omega = \pi/2$, which is one condition necessary for symmetric radial stress. If $\sigma = \gamma r s(\theta)$, then the region of unique solution defined by the characteristics and shown by the shaded region in Figure 42 is approximately radial. The value of σ at the wall is also shown, even though it is not necessary to establish the convergence to radial stress.

Figure 43 shows a symmetrical top boundary with a non-flow region. The convergence is very rapid for this situation. At one-half width, w/2 down from the point P the value of σ° at the centerline deviates only 8% from radial while the value of σ'' at the wall deviates by 15%. The σ value oscillates about the radial value with a decreasing frequency and amplitude as the vertex is approached.

Figure 44 shows the stress field in a steeper channel with no dead region. The oscillations about radial are more severe near the top than in the previous example. This is due to the greater curvature of the stress free top boundary required to make the slope at point P compatible with the wall conditions. Here, as before, deviation from radial is within 20% at w/2 down from P.

Sometimes a channel is formed by a vertical top portion and a sloping bottom section, joined by a sharp transition as shown in Figure 45. In such a case a non-flow region may occur at the sharp transition. A possible stress solution in such a case is shown in Figure 45. There is a rapid drop in σ at the centerline caused by the transition. This disturbance soon damps out and radial stress is again closely approximated.

Experimentally Observed Examples of Convergence

In this section it is shown experimentally that in large portions of a symmetric straight-walled converging channel, the stress field is radial or at least as close to radial as the experimental technique used could measure. It is conjectured on the basis of this evidence that, if a radial stress field can develop, it will. Furthermore, if conditions are not suitable for radial stress, the region where radial stress cannot exist will either not be plastic or will not flow steadily. Examples substantiating this are given in the following paragraphs.

In the experiments, conditions of plane strain and axial symmetry were observed. The equipment for the plane strain tests, pictured in Figure 46, simply consists of a box with glass both front and back so that the flow patterns can be observed. To achieve a uniform and controlled feed of solid out of the box, a cylindrical roller was used, as shown. To eliminate the effect of the direction of rotation of the roller, a 2 inch vertical skirt section feeds the solid from the bottom of the box onto the roller. The inside dimensions of the box are 23 1/2 inches long, 9 1/2 inches deep, and 20 inches high. The width of the slot opening at the bottom is 3/16 of an inch. Inside the box, various wall conditions can be achieved as illustrated by the photographs throughout this chapter. In order that the flow patterns be observed and photographed, it was necessary to place thin horizontal layers of white powdered clay against the glass on the front side. These layers then deformed, showing the flow pattern. Caution should be used in interpreting the deformations of the layers,

because the result observed is the integrated effect of the flow pattern on the layers. For this reason, only the initial deformations are considered significant.

The axial symmetry equipment consists of right circular cones made of galvanized metal. After being constructed, these cones were reinforced by metal bands and then cut in half along a vertical plane of symmetry, as shown in Figure 54. In performing an experiment, the cone is assembled in the vertical position. Thin layers of white clay are used as markers, as in the plane strain model. Some of the solid is allowed to flow slowly out of the cone. The level of the solid is then made even with the top of the cone and both top and bottom are sealed. The cone is then placed with its axis horizontal, and the upper half of the cone is removed. The solid is scraped off to about 1/16 of an inch above the bottom section of the cone. The remainder of the solid is removed by gently blowing it away. The white layers of clay have sufficient cohesion to remain intact while the dark material, which is essentially cohesionless, is removed. With this technique, the results of the action inside of the solid can be observed without actually disturbing it while the test is being run.

The material used in all of these tests was iron concentrate with $\delta = 50°$ and an internal angle of friction $\phi = 33°$. This is the most common value of δ for commercially handled materials. In the tests, various wall materials were used. The angle of friction ϕ' for the solid on the wall was determined experimentally as outlined in [5].

Figure 47 shows the plane strain model filled with the solid and with a horizontal top boundary. The walls are inclined from the vertical at $\theta' = 29°$ with $\phi' = 24°$. In this case, the entire solid was moving, including the upper side regions that appear undisturbed in the photograph. Hence, the observed breaks in the white lines must occur along velocity characteristics as discussed in the previous chapter. The equation of these characteristics is

$$\frac{dy}{dx} = \text{Tan}\ (\omega - \pi/4).$$

Figure 48 shows one of the family of the solutions to this equation as calculated, assuming ω to be given by the radial stress field for the boundary conditions $\theta' = 29°$, $\phi' = 24°$, and $\delta = 50°$. This characteristic was determined by a graphical solution of

$$\frac{dy}{dx} = \text{Tan } (\omega - \pi/4)$$

along an appropriately interpolated solution curve in Figure 31. The other members of the family of solutions are exactly of the same shape with respect to θ and differ only by a scale factor in r, because $\omega = \omega(\theta)$ for radial stress. Figure 49 shows the same photograph as Figure 47, except a centerline is drawn in and the velocity characteristic is plotted starting at the same point on the centerline as the velocity characteristics observed in the model. The higher characteristic observed in the model on the left deviates from the radial characteristic as it approaches the wall. However, the lower characteristic at the right coincides with the radial characteristic as closely as can be determined from the photograph. From this it can be observed that the radial stress is closely approached, for if $\omega = \omega(\theta)$ is given as radial, then, as was pointed out earlier in this chapter, the stress field is radial. The deviation from the radial characteristic exhibited by the upper left characteristic is to be expected since it starts at the centerline very close to the top, stress-free boundary which requires $\sigma = \frac{\gamma x}{1-\sin \delta}$ for a horizontal boundary with x measured from it.

To give an indication of the effect that deviation from radial stress has on the shape of the characteristics, a comparison between two stress characteristics in Figure 43 is given. In the figure, AB is the characteristic computed from the boundary conditions as shown, and AE is the stress characteristic for the radial stress field, compatible with the wall conditions. One observes that there is a noticeable difference in the two characteristics. The calculated value of σ differs by about 15% from the radial value. One would expect the velocity characteristic from point A to show an even greater deviation from the radial characteristic since the relative length of them is greater than for the stress characteristics shown.

Figure 50 shows the plane strain model with $\theta' = 29°$ but with the walls slightly rougher than in the previous case. As before, the appropriate radial velocity characteristic is plotted and good agreement occurs between the radial velocity characteristic and the observed characteristic.

Convergence to radial stress is not limited to horizontal stress-free boundaries. As was indicated in the calculated fields, convergence also occurs in a straight wall section below a vertical transition. Figure 51 shows such a case for $\theta' = 29°$ and $\phi' = 24°$. As before, there is good agreement between the radial characteristics and the observed characteristics.

The examples given thus far all involve straight walls and the radial stress fields involved are determined by the slope θ' and frictional condition ϕ' of the walls. However, when there are no walls, there seems to be no basis for assuming that radial stress should occur. Figure 52 shows the plane strain flow pattern for a flat bottom. In this case, the side regions did not flow. Only the center portion flowed. The boundary between the flowing and the non-flowing regions has the possibility of being either a velocity characteristic or a slipline. The interior lines, however, must be velocity characteristics, because the whole mass in which they occur is flowing. One observes that the interior lines intersect the boundary line between the flowing and non-flowing. Since characteristics of the same family cannot intersect, one concludes that the boundary is not a velocity characteristic, and, hence, is a slipline. The line drawn in the photograph that closely approximates the boundary is a slipline from the radial stress solution for $\delta = 50°$ and $s° = 0.105$. This slipline, shown in Figure 53, has been calculated graphically as the solution of

$$\frac{dy}{dx} = \text{Tan}\,[\omega - (\pi/4 - \phi/2)]$$

where $\phi = 33°$ is the angle of internal friction for the solid. This example indicates that even without walls compatible with the radial

stress field, the stress solution closely approaches radial, if at all possible. In the case of the flat bottom, the radial stress field approached will be determined by the cohesive properties of the flowing solid, or, more specifically, by the flow-factor [5].

In axial symmetry, radial fields occur only for certain boundary conditions. For example, if the wall has an angle of friction $\phi' = 20°$ for a solid with $\delta = 50°$, Figure 36 shows that $\theta' = 26°$ is the maximum that the half angle of the cone can be placed and still develop a radial stress field. To investigate the flow pattern in axial symmetry, cones with three different θ' angles were used. The friction of the cones was changed by covering them with sand paper and high gloss paper. The points plotted in Figure 36 are actual test points. The circled points indicate that flow along the walls was observed, and the square points indicate no flow along the walls.

Figure 54 shows the flow pattern in a cone with $\theta' = 15°$ and $\phi' = 24°$. In this case, the θ', ϕ' point in Figure 36 is well within the radial stress region. The radial stress velocity characteristic is plotted in the photograph and seems to agree with the actual velocity characteristic. Figure 55 shows the flow pattern for a cone with $\theta' = 21°$, $\phi' = 24°$. This point lies just on the critical line of Figure 36. As can be readily seen, most of the flow occurred in the middle of the cone, however the sides did flow somewhat as is evidenced by the upward curvature of the white lines along the wall of the cone. It is of interest to note that for the same cone with $\phi' = 23°$ the flow along the walls was much more rapid than for the case pictured in Figure 55 where $\phi' = 24°$. Figure 56 shows a cone with $\theta' = 30°$ and $\phi' = 24°$, which point lies outside of the radial stress region in Figure 36. As can be seen, no flow occurred along the edges of the cone, but instead flow occurred only in a central plug. The remainder of the cases plotted in Figure 36 are not shown in pictures because they exhibited the same behavior as the three points already discussed. Thus it is seen that if the ϕ', θ' values lay in the radial stress region, then flow occurred along the walls. If the point was outside the radial stress region, then only a vertical pipe flowed.

The conclusion from this experimental evidence is that the radial stress field is a very basic element in axi-symmetric and plane strain gravity flow of bulk solids: wherever possible the stress field will be very close to radial, and where radial stress field is not possible, the flow will be somewhat restricted as is evident in axial symmetry. Perhaps the most startling example of approximation to radial stress was the channel for a flat bottom plane strain model. This again substantiates the hypothesis that if a radial field can develop, it will.

The Velocity Field for Radial Stress

The photographs shown thus far often indicate a non-symmetric velocity field, especially in the region near the top boundary. This non-symmetric velocity does not enforce a non-symmetric stress field, because, under our assumptions, the only connection between velocity and stress fields is ω. The choice of velocity boundary conditions therefore is independent of the stress conditions. However, it is only fair to point out that if inertial effects are included in the equilibrium equations, then the stress and velocity fields are dependent on each other and the non-symmetric velocity would influence the stress in a non-symmetric manner. Since velocities and accelerations are small in magnitude, the interrelationship between the velocity and the stress fields produces a negligible effect, and a slight change in the stress field may be accompanied by a drastic change in the flow pattern and velocity field.

Some calculated examples of symmetric velocity fields in plane strain will now be discussed. The assumption of symmetry restricts the use of these fields to the lower region of a converging channel where symmetry in the velocity field is usually observed even though the top region of the channel may exhibit non-symmetric flow. In the first section of this chapter, the condition for radial velocity was shown to be $\psi = \psi(\theta)$ and it was pointed out that this condition enforces radial stress. Hence, a radial velocity field cannot occur unless there is a radial stress field. However, a radial stress field

does not enforce radial velocity. In the following discussion of velocities, it is assumed that the stress is radial, that is $\omega = \omega(\theta)$ determined by the stress field. With ω given, the shape of the velocity characteristics is also given. Figure 57 shows some of these characteristics in a field where $\phi' = 48°$. It is observed that one of these characteristics is a straight radial line. Such a characteristic has the property that the component of velocity along it is constant in plane strain.

If velocity is assigned along a non-characteristic line AB, Figure 9, the velocity field is only determined down to the first velocity characteristic CB. To continue the field further, velocity must be assigned along the wall. In the examples, a constant velocity was assigned. This assignment is in accord with observed velocity fields in tests with plane strain models. Figure 58 shows two velocity profiles along the arc DE. The unbroken vectors are the velocity from a constant radial velocity assigned along AB. The dash-dot vectors are the velocity resulting from a velocity decreasing proportionally to the distance from the centerline assigned along AB. In both cases in the region between the centerline and the straight characteristic, the velocities closely approach the radial profile as determined from Figure 69 and given by the dashed line in Figure 58. The velocity profile calculated in this way will never reach radial completely, because the radial profile demands the velocity to be zero at the straight characteristic.

It must be remembered that this convergence to radial was for a constant velocity along the wall. If the requirement that the velocity at point F, Figure 57, go to zero is imposed, and the wall velocity is allowed to change accordingly, a drastic deviation from radial velocity is observed along the first characteristic FG, Figure 58. The deviation is allowed by the freedom of choice of the velocity along the wall. If the wall had frictional conditions such that the field did not include the straight velocity characteristic, such deviation would not be possible without deviation from the radial stress field, because the velocity along the wall would be uniquely

defined by the conditions along the non-characteristic line AB.

Figure 59 shows the velocity along the arc PQ for the case of a wall coinciding with the straight velocity characteristic. The velocity along AB for the example was assigned constant and radial. One can see from Figure 59 that the radial profile is not approximated very well near the wall, since the radial field requires zero velocity there. However, at a sufficient vertical distance from A, the wall velocity will be negligible compared to the centerline velocity, thus improving convergence to the radial velocity profile. This is because: to preserve continuity of the solid, the average vertical velocity must change inversely as the area through which it flows; since the wall velocity is constant the velocities at other points must become larger than the wall velocity as the vertical distance from A increases and the area decreases in a converging channel. A similar reasoning can be applied as an indication of convergence to radial velocity to the previous case in which the field contained the straight characteristic and had constant velocity along the wall. However, in this case, one would consider the velocity of the region between the straight characteristic and the wall as negligible compared with the velocities in the interior region of the straight characteristic. In these examples the velocity field tends to approach radial when the stress field is of the form $\omega = \omega(\theta)$.

CHAPTER IV

STRESS AND VELOCITY SOLUTIONS OTHER THAN RADIAL

In the previous chapter the importance of the radial stress solution was emphasized and it was shown that a large portion of a converging channel approximated radial stress. In this chapter the stress and velocity solution outside the regions of radial stress are discussed with emphasis on their limitations and relation to radial stress.

Straight Wall Symmetric Channels

The top, traction-free boundary of a channel may take many shapes. The shape shown in the experiments discussed is straight and horizontal. Other possible shapes are the convex type such as shown in Figures 43 and 44 and the concave type shown in Figure 60. If the solid is allowed to flow in the channel without refilling, it usually assumes either a horizontal or a concave shape. In both cases the velocity field in plane strain is not symmetric; the solid will flow more rapidly from one side for awhile, then shift and flow more rapidly from the other side. In axial symmetry the velocity field in both cases tends to be more symmetric than in plane strain. Figure 49 shows an example of a channel in which the boundary tends to remain horizontal. Figure 61 shows the horizontal position of the top boundary in this same channel after it has been nearly emptied. Figure 62 shows a channel of the same shape but with a slightly greater $\phi' = 26.5°$. In this case one clearly sees the tendency to form the concave type boundary where the slope of the top is at the angle of repose of the solid. The coefficient of friction at which a convex top occurs could be calculated approximately by assuming that the side regions in which deformation does not occur are rigid. The forces acting on this rigid wedge could then be summed, and in this way the required frictional force, and therefore ϕ', could be approximated. This type of calculation is not carried out here but is left for some future date.

In chapter three it was shown that radial stress is closely approached in the lower regions of a symmetric channel with straight walls. This solution requires $\sigma = \gamma r s^\circ$ and $\omega = \pi/2$ for the stress along the centerline. In the region of the horizontal stress free boundary the stress field is given by $\sigma = \frac{x\gamma}{1 - \sin \delta}$ and $\omega = \pi/2$. At some point along the centerline these two stress conditions will be compatible. The calculation of this point is illustrated in Figure 63. Compatibility of the two stress fields requires

$$\gamma R s^\circ = \frac{\gamma x_r}{1 - \sin \delta}$$

or

$$x_r = (1 - \sin \delta) R S^\circ$$

Let us suppose that the actual stress field in a channel is of this form. The resulting σ along the centerline is plotted to the left in Figure 63. The ramifications of such an assumption are: no plastic deformation should be observed along the traction-free boundary beyond A because this would extend the plastic or steady flow solution of $\sigma = \frac{\gamma x}{1 - \sin \delta}$ below x_r. Similarly, no plastic deformations should be observed along the wall above the intersection of the second stress characteristic and the wall, point C, because this would imply a continuation of the radial stress beyond the characteristic BC which would extend the solution $\sigma = \gamma r s^\circ$ above x_r. In other words, the region ABC must flow as a rigid wedge. Figure 49 shows these critical points plotted on the photograph of the flow patterns for a channel $\delta = 50^\circ$, $\theta' = 29^\circ$ and $\phi' = 24^\circ$. Point C was determined by the radial stress characteristic through B. This stress characteristic is shown in Figure 48. As can be seen, the required flow conditions are satisfied at both critical points indicating that this proposed stress condition is possible. One point of interest is that the observed velocity characteristic on the left starts at the centerline at a point above the possible radial stress point, and, hence, is not expected to conform to the radial stress velocity characteristic. This explains the deviation from radial

stress velocity characteristic as shown in Figure 49 and discussed on page 47. The actual stress field for the channel is probably different from the one proposed here. However, the evidence indicates that this relatively simple combination of radial and $\sigma = \frac{\gamma x}{1 \sin \delta}$ stress fields can closely approximate the actual field.

In the case of top boundaries not horizontal one would expect a similar combination of stress fields to approximate the actual condition. However, the σ near the top would not be the same as above but would be determined by the shape of the stress-free boundary. For a convex type boundary, σ along the centerline increases slower than for a horizontal boundary. As shown in Figure 43, σ starts at about the same rate of increase as for a horizontal boundary, but the rate gradually decreases as the curvature of the boundary increases. For this situation x_r would be larger than for a horizontal boundary. One might conjecture that for the convex type boundary x_r would be smaller than for the horizontal boundary.

Transition Regions

In this section the stress solution is considered in the region of a sharp transition between a vertical and a symmetric sloping wall. In the region of the transition three different flow patterns are observed: Flow may occur at the transition, a dead non-flowing region that is terminated by the vertical wall may form, or a dead region may form that is not terminated at the vertical wall, but is terminated by the traction-free top boundary. Each of these conditions will be discussed.

Figure 64 shows an example of the first case when flow occurs at the transition. In this figure the velocity characteristics are smooth in the region of the transition, which implies that ω is continuous in this region. Equation (10a) gives $\omega' = \nu' - \theta'$ where θ' is the slope of the wall and ν' is a function of the friction condition along the wall. If it was assumed that ν' has the same value for the sloping wall as for the vertical wall, a discontinuity in ω would be required at the intersection of the walls. Since no such discontinuity is observed, ν' must not be the same for the vertical wall as for the

sloping wall. If the solid flows along the wall, then ν' is given by (10). From Figure 64 it appears that flow does occur along both of the walls; however, closer inspection of the marking line, shown in Figure 65, reveals a narrow portion of white against the vertical wall. This thin strip of solid tends to make the vertical wall rougher so that ν_v' along it decreases. The minimum that ν_v' can attain is when the slipline condition is reached and $\nu_v' = \pi/4 - \phi/2$. A necessary condition for flow to occur at the transition is that ω_v' of the vertical wall be equal to ω_s' of the sloping wall. If $\omega_s' > \pi/4 - \phi/2$, the vertical wall may exhibit enough roughness with the aid of the thin non-flow region to make $\omega_s' = \omega_v'$. In the event that $\omega_s' < \pi/4 - \phi/2$, the vertical wall cannot be made rough enough to make ω' continuous at the intersection, hence, a dead region must form. It should be noted that $\omega_s' < \pi/4 - \phi/2$ is sufficient but not necessary for a dead region to develop at the transition.

When a dead region forms at the transition, the boundary between the bead or non-flowing solid and the flowing solid is either a velocity discontinuity or a line of rapid change of velocity with velocity at the boundary zero. In the first case, the boundary must be a slipline. In the second case, the boundary must be a velocity characteristic. By considering the possibility of velocity fields for each of these cases, it appears that both are possible. Figure 66 shows the approximate location of the velocity characteristics near the dead region. The dashed lines are velocity characteristics. The solid line CD is the slipline. The value of the coefficient of friction along the vertical wall from C to E changes continuously from full friction or $\nu_v' = \pi/4 - \phi/2$ at C to a smaller amount of friction or $\nu_v' > \pi/4 - \phi/2$ at E. Point A is the proper friction value to make the velocity characteristics tangential to the wall at A. If the boundary of the dead region was a characteristic, then the dead region would be AOB and AB would have velocity assigned as zero. If velocity was assigned along AF, such that at A velocity was zero but rapidly changing to a non-zero value near A, then this rapid change would propagate along AB and also along AG. Hence, the type of flow observed

near the dead region can be achieved when the boundary is a velocity characteristic. It is important to observe that the assigning of velocities along FA and AB does not over-determine the field, but, on the other hand, it does uniquely determine the velocity field in the remaining upper and lower regions.

If the dead region was bounded by a slipline, then velocity along FA could be determined by any arbitrary boundary conditions above FA. In order that the velocity solution calculation be continued, it is necessary that velocity be assigned along ACD, thus determining the velocity field in region ADH. This assigned velocity would have to be in the direction of the boundary ACD. Since the direction of the velocity vector at point D is discontinuous, the magnitude of the velocity must be zero there in order to avoid an infinite acceleration of particles at point D. With these boundary conditions, the velocity field is not over-defined, but is uniquely determined in all regions; hence, the boundary could be a slipline. As the figure indicates, if the boundary is a slipline, the dead region will be smaller for the same wall conditions than if it is a velocity characteristic. If the boundary is a slipline, then there need not be a rapid change of velocity along AG as is required by the velocity characteristic boundary. Therefore, when there is no observed rapid change of velocity above the transition region, the boundary is a slipline. If there is an observed rapid change above the transition, the boundary can be either a slipline or a velocity characteristic.

Figure 67 shows the relation between the wall, the direction of σ_1, and the direction of the slipline or velocity characteristic. For convenience, call the angle between the wall and the slipline or velocity characteristic α. Then $\alpha = \nu'_s - (\pi/4 - \phi/2)$ for the slipline and $\alpha = \nu'_s - \pi/4$ for the velocity characteristic. When $\alpha > \theta'$ a dead region of the type shown in Figure 66 where the boundary of the dead region terminates at the vertical wall will not form because the only possible boundaries for this region tend to go away from the vertical wall. When $\alpha < \theta'$ a dead region of the type shown in Figure 66 may form. When the dead region is not terminated by the vertical wall, it must extend to the top, traction-free boundary. In the event that this top

boundary is at a considerable distance above the transition, it seems very unlikely that the dead region could extend so far, especially when $\alpha < \theta'$. This indicates that there is some critical height for the solid above the transition. If the solid in the vertical section is above this height, then no dead region that does not terminate at the vertical wall will form. If the solid is below this height, then dead regions not terminating at the vertical wall but at the top boundary of the solid will form. By using the radial stress field developed in the previous chapter, this critical height can be determined.

In the discussion of radial stress, it was observed that the stress field tended to be radial wherever possible and where the radial field was not possible the flow tended to be restricted. In the examples of axial symmetry, if radial stress was not possible, the flow was restricted to a vertical pipe. One might suspect that this same hypothesis might apply in determining the critical height at which the flow will become more restricted in the sense that the dead region will increase in size. Figure 68 illustrates a typical situation with a dead region terminating at the vertical wall. Since AB is a straight wall with a constant friction condition, it is compatible with radial stress. Assume that radial stress occurs along AB. AB is then the boundary of a Cauchy problem, and determines radial stress in the region ABCD where BC and AD are first and second characteristics. The centerline condition along DC will automatically be satisfied because of the choice of symmetric radial stress along AB. BC and the centerline condition form a mixed boundary problem with boundaries compatible with radial stress and, therefore, define radial stress in region CBE where BE is a second stress characteristic. It is evident that for radial stress to exist along AB, this same stress condition must prevail up to point E at the centerline. For a horizontal, traction-free boundary, there is a minimum height x_c above E required to have σ at E sufficiently large to be compatible with the radial σ. For any height below this, radial stress cannot develop at point E and, hence, not at point B. By hypothesis, for any height below this critical height, the dead region should increase in size.

As can be seen from the geometry of the channel $h_c = R + x_c - \frac{W}{2} \cot \theta'$ where $x_c = R\, s^\circ(1 - \sin \delta)$. Finally

$$\frac{h_c}{W} = \frac{R}{W}\left[1 + s^\circ(1 - \sin \delta)\right] - \frac{1}{2} \cot \theta' \qquad (34)$$

where R, s°, δ, and W are determined from the geometry and frictional conditions of the channel. Figures 64, 65, 71, 72, and 73 show the plane strain model with a vertical section on a symmetric channel with $\delta = 50°$, $\phi = 33°$, $\theta' = 29°$, and $\phi' = 24°$. For this friction condition $\nu' = 62°$ as calculated from equation (1). Hence, $\alpha = 17°$ for the velocity characteristic boundary and $\alpha = 33.5°$ for the slipline boundary. It is quite evident in Figures 64 and 65 that little if any dead region developed when there was considerable height of material above the transition. Apparently in this case the slipline boundary for the dead region took precedence over the velocity characteristic boundary because the velocity characteristic boundary is such that $\alpha < \theta'$ and, therefore, would require a dead region. By comparing Figure 71 with Figure 72, one sees that flow has occurred in the transition region. Figure 73 shows the pattern after more material has been removed at the bottom. In this case flow has definitely stopped in the region of the transition and the critical height of the material in the vertical section has been reached. In this case, since the dead region was non-existent for sufficient height, the W in equation (34) becomes the width of the channel. Referring to Figure 48, which gives the shape of the radial stress characteristic for this channel, it is observed that $R/W = 1.58$, $s^\circ = 0.24$. Hence, $h_c/W = 0.77$. In Figure 73 flow at the transition had stopped and $h/W = 0.72$. In Figure 72 where flow at the transition was still taking place $h/W = 0.85$. This indicates that the actual critical h is between 0.72 and 0.85 which is in agreement with $h_c/W = 0.77$ predicted on the assumption of radial stress. This gives further evidence of the validity of the hypothesis that radial stress will occur whenever possible.

SUMMARY

The theory of steady flow of bulk solids consists mostly of the well know principles of equilibrium, isotropy and continuity of the solid. The one principle that is unique to the flow of bulk solids is the concept of the effective yield locus. This concept is essentially experimental in nature and is very similar to the yield locus of plasticity and soil mechanics, however it is not the same. A bulk solid will, in general, have both an effective yield locus and an infinite number of yield loci.

The equations of steady flow as derived from the basic concepts can be written as two hyperbolic systems of two partial differential equations, each. One of these systems with proper boundary conditions can be solved for the stress field. The other system can be solved for the velocity field after the stress field is known. These equations do not include the physical limitations of gravity flow. Therefore, these limitations must be stated explicitly and boundary conditions must be assigned so that these limitations are not exceeded anywhere in the field. The side boundary conditions of a flowing solid are determined by the frictional conditions between the flowing solid and the walls. This condition determines the direction of major principal stress in relation to the direction of the walls. The top boundary is traction-free which implies a zero stress condition if the solid is to obey the effective yield locus.

The general solution of the hyperbolic equations was accomplished in this paper by the method of characteristics. The characteristic directions are such that along them the partial derivatives of the hyperbolic equations can be replaced by total derivatives. This makes it possible to solve a problem by integrating in the directions of the characteristics.

The boundary value problems encountered in calculating the stress and velocity fields are of three types: the Cauchy problem in which dependent and independent variables are given along some non-characteristic

line, the mixed boundary value problem where the variables are specified along a characteristic and only partly specified along a non-characteristic line that intersects the given characteristic, and the Goursat problem in which the variables are given along two intersecting characteristics not of the same family. Each of these problems defines a unique solution, in a region bounded by characteristics. The solution is continuously dependent on the initial data. This property of uniqueness implies that if the given variables on a boundary are in agreement with a known solution of the equations being solved, then the known solution is determined throughout the region of unique solution of the boundary value problem. If the given variables in the problem closely approach a known solution, then the known solution is closely approached throughout the region of unique solution of the boundary value problem.

The characteristics of the equations have the property that, if one dependent variable is assigned along one of the characteristics, the other dependent variable may be calculated from the assigned variable to within an arbitrary constant. Another property of the characteristics is that rapid changes in the dependent variables occur along them. This property is very significant in the study of the flow patterns in bulk solids.

The numerical solution of a problem by the method of characteristics calls for only two basic types of calculation. The first type requires that two adjacent points-, not on the same characteristic-, be given. A third point can then be calculated at the intersection of the characteristics through the given points. The second type of calculation requires that one point be given adjacent to a line along which incomplete information is available. A second point can then be calculated at the intersection of the line and the characteristic through the given point. These two basic calculations can be combined to solve whatever boundary problem or combination of boundary value problem may be presented. To facilitate the solution, computer programs for each type of calculation were written as separate parts

and then a master correlation program was written to combine these parts as needed for the specified boundary value problem. In order that a reasonable spacing of the calculated points be achieved in subsequent calculation, it was necessary at times to interpolate points between the calculated points.

A stress field compatible with a channel with straight sloping walls intersecting at point O is found in the radial stress field. This stress field has the property that along every ray the stress is directly proportional to the distance from point O. The direction of principal stress is also constant along any ray through O for this radial stress field. With these conditions the partial differential equations for the stress field reduce to a system of total differential equations. The solution of the equations was not found in closed form, however, a numerical solution by the use of the Runga-Kutta method was used for various solids flowing in symmetric channels. This method of solution was chosen because of the ease in changing the size of the step of the calculation. In the calculation, the size of the step was changed automatically so as to maintain accuracy and yet allow the step to be as large as practical.

The radial stress solution is a very basic element in the gravity flow of bulk solids. When stress fields are calculated by the method of characteristics for various top boundaries with straight walls as side boundaries, the radial stress solution is approached in the lower portion of the channel. The velocity characteristics observed in models of plane strain and axial symmetry correspond to those required by radial stress. When the solid is allowed to flow without the influence of walls the radial stress flow pattern is also observed. The radial stress fields for axial symmetry do not exist for certain boundary conditions for straight walled channels. When the solid is required to flow in such a channel flow will not occur along the walls but in a vertical pipe.

When the solid is required to flow in channels with boundary conditions for which a radial field exists, flow does occur along the walls. These results indicate that if possible the radial stress field tends to develop and if it is not possible for radial stress to develop the flow will be restricted.

Another property of the radial stress field is that it is required if the velocity is to be in the radial direction throughout the field, however, it is not necessary to have radial velocity when the stress field is radial. The velocity field may be non-symmetric and still have a symmetric radial stress field. For certain conditions it appears that radial velocity is approached in the lower region of the radial stress channel.

In straight walled symmetric channels rigid regions form at the sides near the top traction-free boundary. These regions may move with a uniform velocity or they may remain stationary depending on the frictional condition of the wall along which they must flow.

It was proposed that the stress condition of the solid not in these rigid regions be approximated by radial stress except for a small region at the centerline near the top boundary. The minimum size of the rigid regions can be predicted by this stress field and agrees with experimental evidence.

When the channel is formed by straight sloping symmetrical walls in the lower region and vertical walls in the upper region, three flow-patterns may occur at the intersection of the sloping and vertical walls: Flow may occur at the intersection, a small non flowing region terminated by the vertical wall may form at the intersection, or a large non-flowing region terminating at the top boundary may form. The first two conditions occur only when there is sufficient height of solid in the vertical portion of the channel and the third condition occurs whenever the height of the solid is below a certain value. This value can be calculated on the basis of radial stress and shows good agreement with experimental evidence.

One of the major values of the paper is the agreement shown between the theory and the actual observations of flow in channels. This

agreement is most remarkable when the possible chances for introducing errors are considered: In the theory there are certain simplifying assumption such as no inertial effects, isotropy, and no density change. The calculations based on the theory were carried out numerically and are therefore subject to error. Finally, the test procedure determining the flow properties of the solid could possibly introduce errors. The agreement of the calculatedfields with experiment therefore indicates the validity of the theory, calculations and test procedure.

Another contribution of this paper is that the radial stress field is basic to the flow of bulk solids. In reference [5] a proof is given that any stress field with boundaries intersecting at a point converges to radial at the intersection, however, no indication is given as to the validity of radial stress at regions away from the intersection point.

This paper indicates the importance of radial stress in regions removed from the intersection. To prove rigorously that radial stress is basic, it appears that some additional physical concept need be added to the theory.

This becomes evident when the arbitrary size of the rigid regions in a symmetric straight walled channel is considered. The approximate size of these was determined on the basis of radial stress and was observed to conform with experiment results, however, stress fields could be calculated which would require much larger or smaller rigid regions. These stress fields will not be radial near the top but they will still satisfy all the requirements of the theory. It is possible that a concept of minimum energy or the most even distribution of energy dissipation is the additional information required. As a future research project the determination of this additional concept might be undertaken.

FIGURES

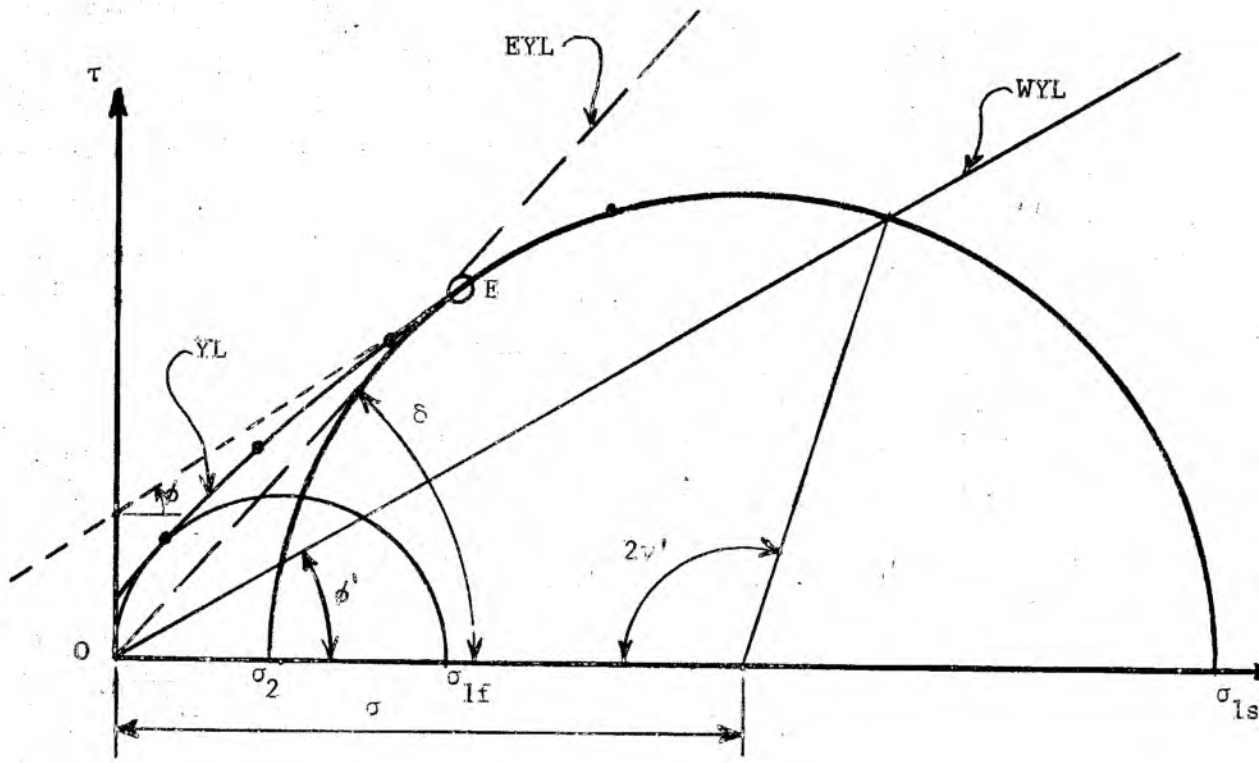

Figure 1.

Experimental results showing the yield, effective yield, and wall yield loci

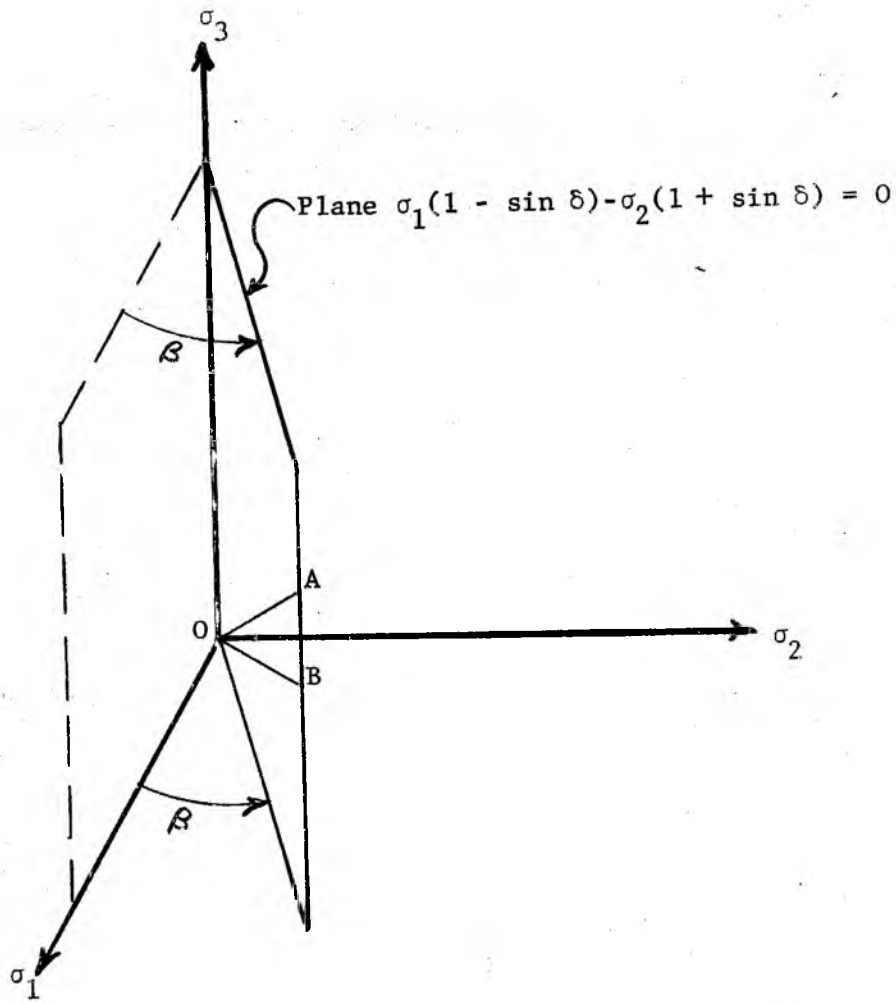

Figure 2.

Construction of the effective yield locus

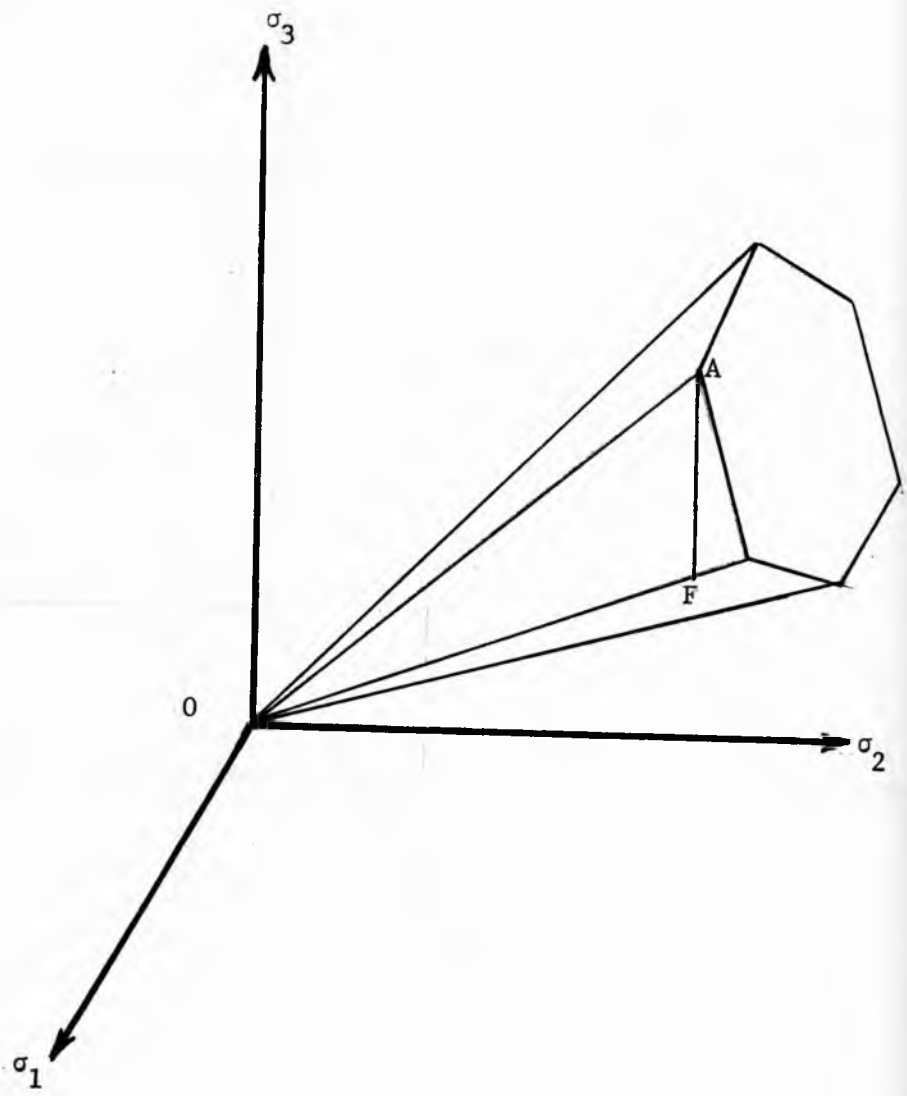

Figure 3.

The effective yield pyramid

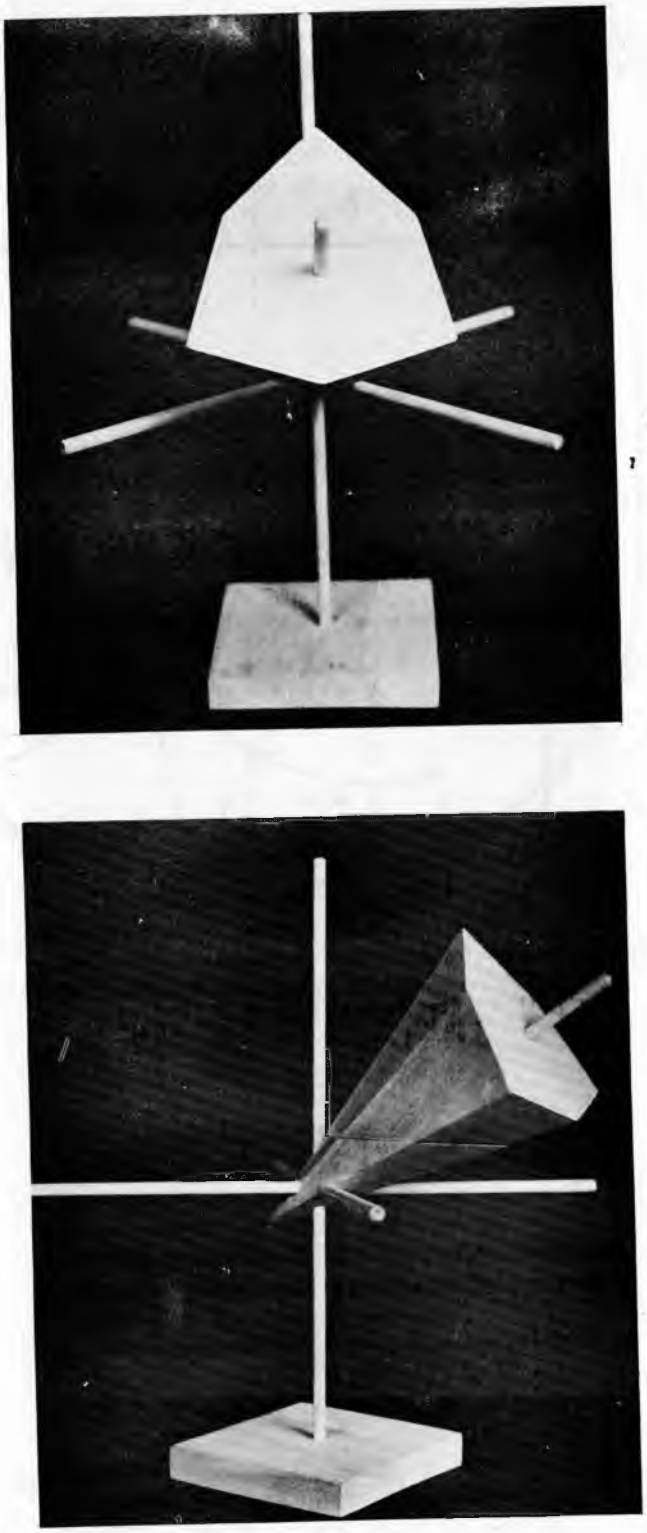

Figure 4

The yield pyramid

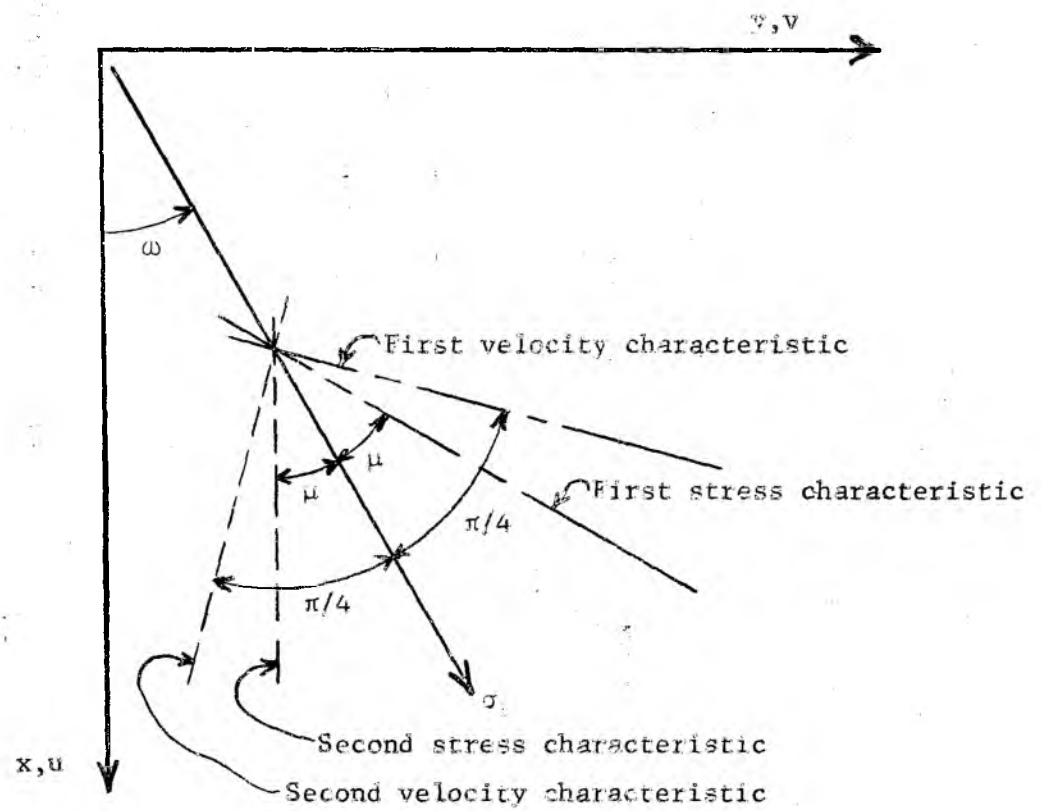

Figure 5.

Orientation of the stress and velocity characteristics with respect to the direction of σ_1

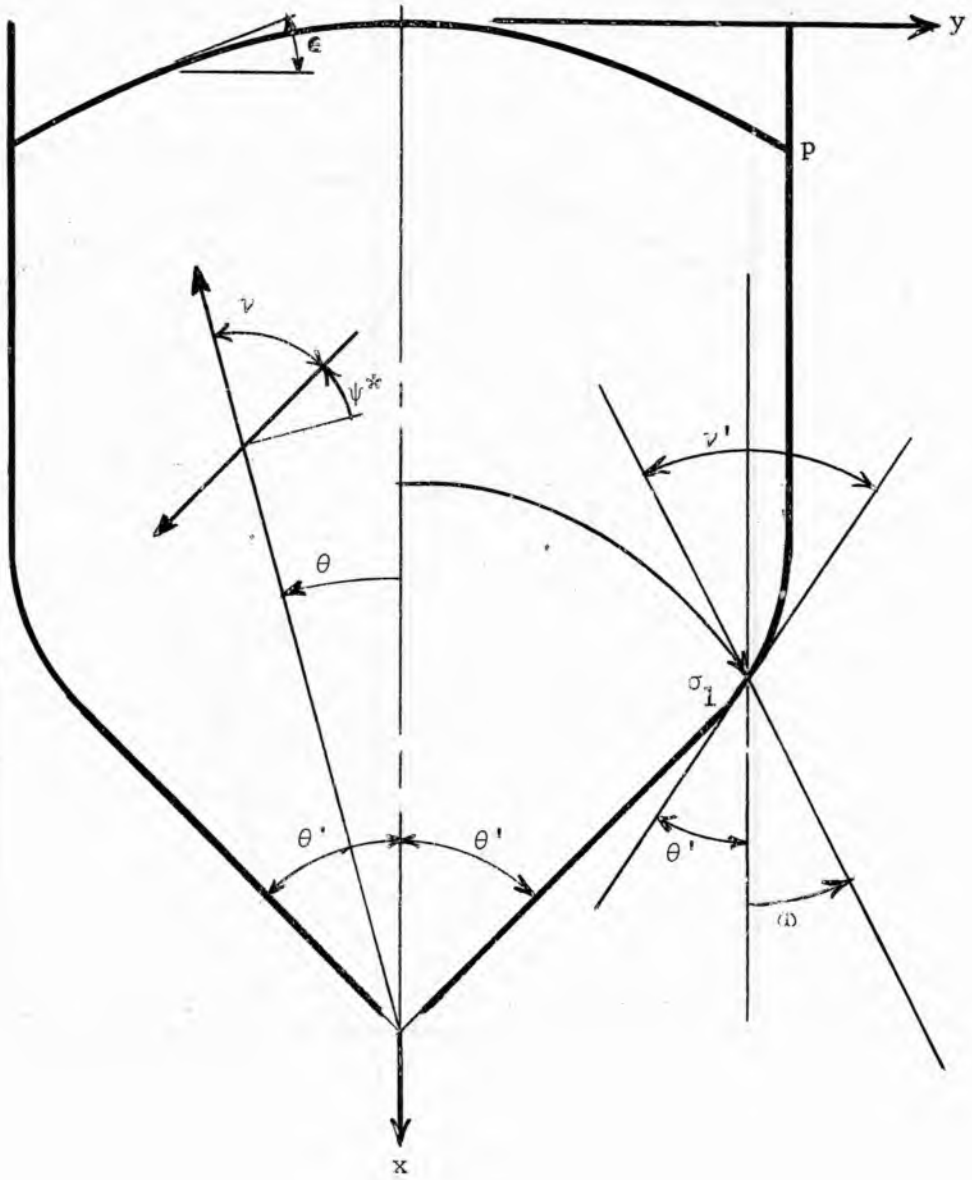

Figure 6.

The co-ordinate system for the symmetrical converging channel

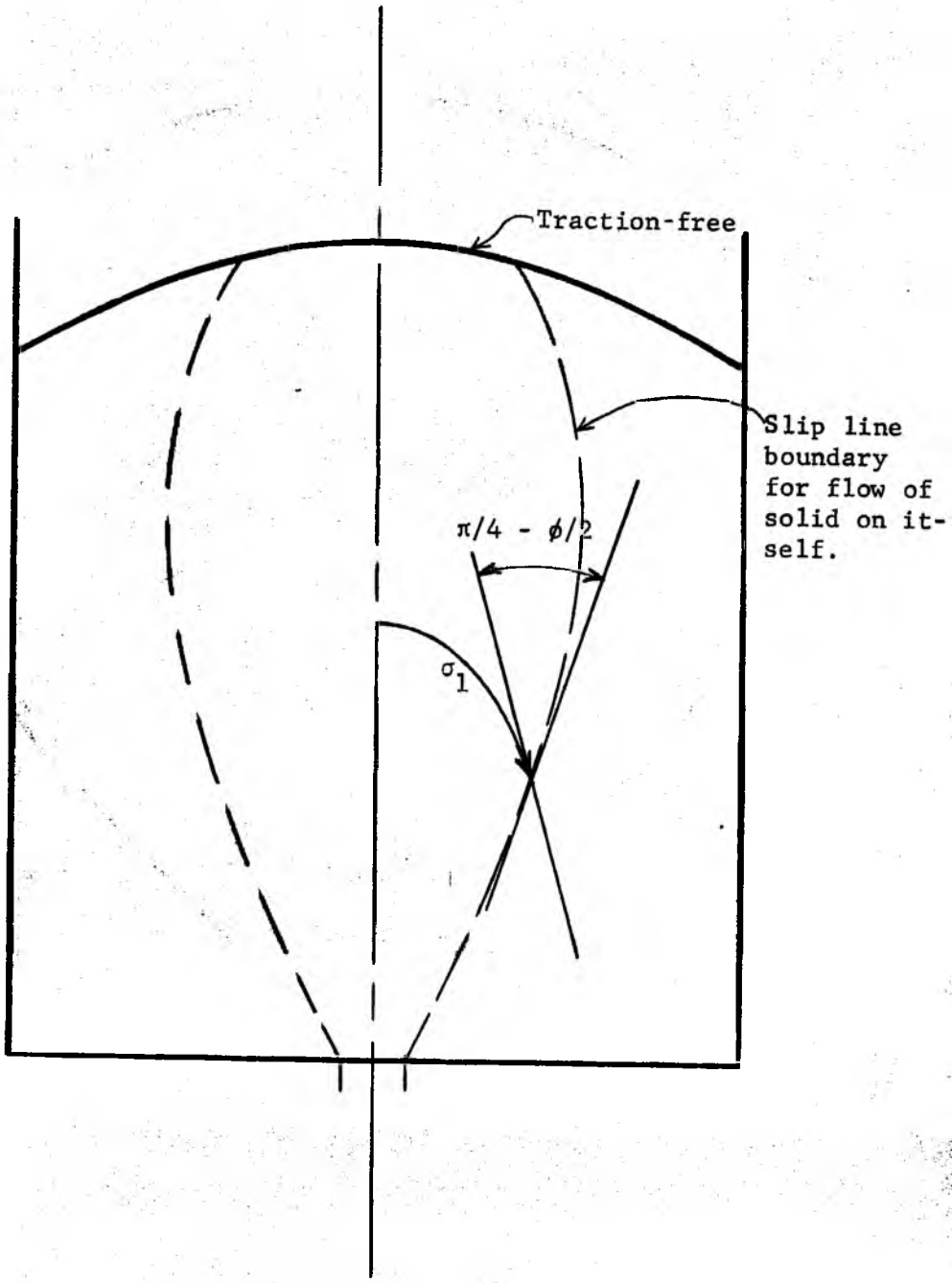

Figure 7

Gravity flow channel for
the solid flowing on itself

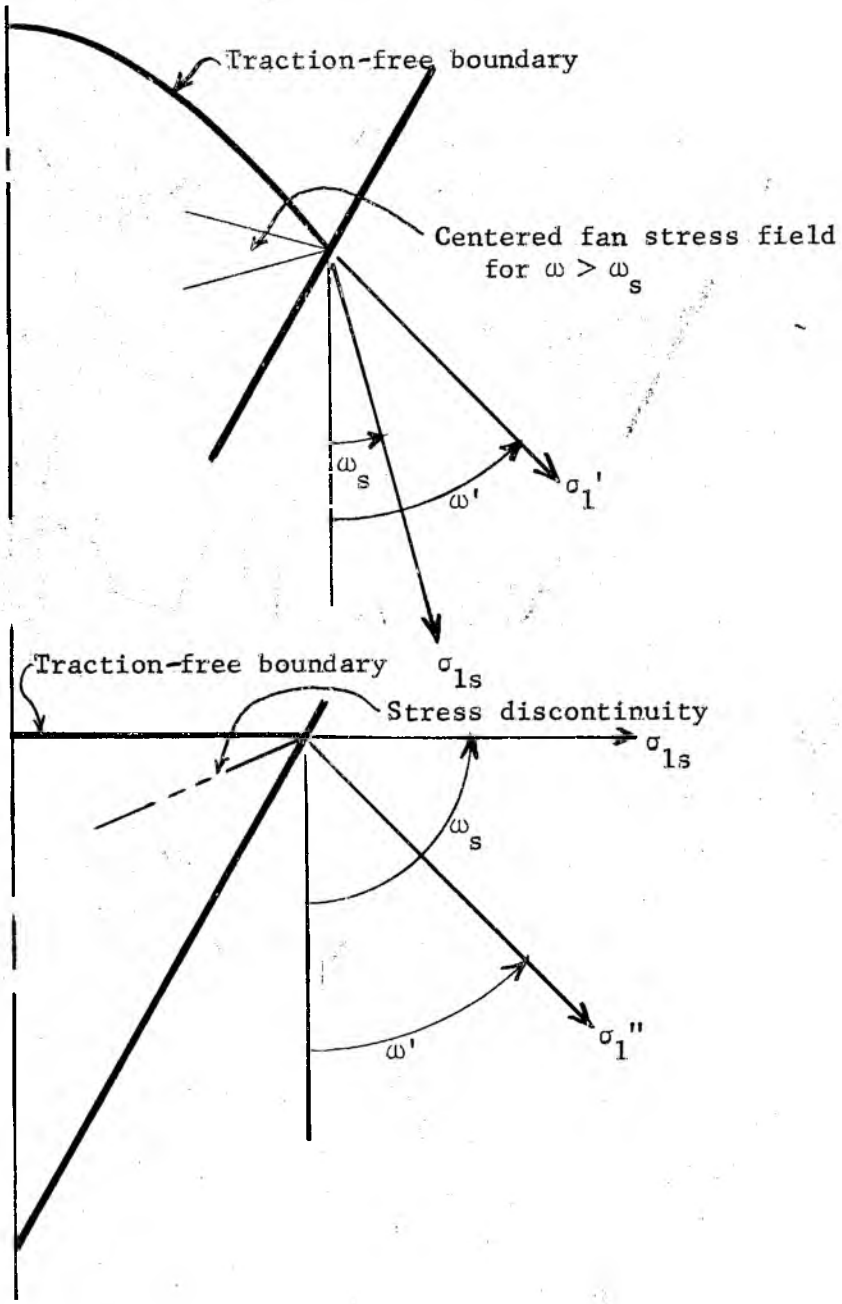

Figure 8.

Possible stress conditions at the
intersection of a stress free boundary and a wall

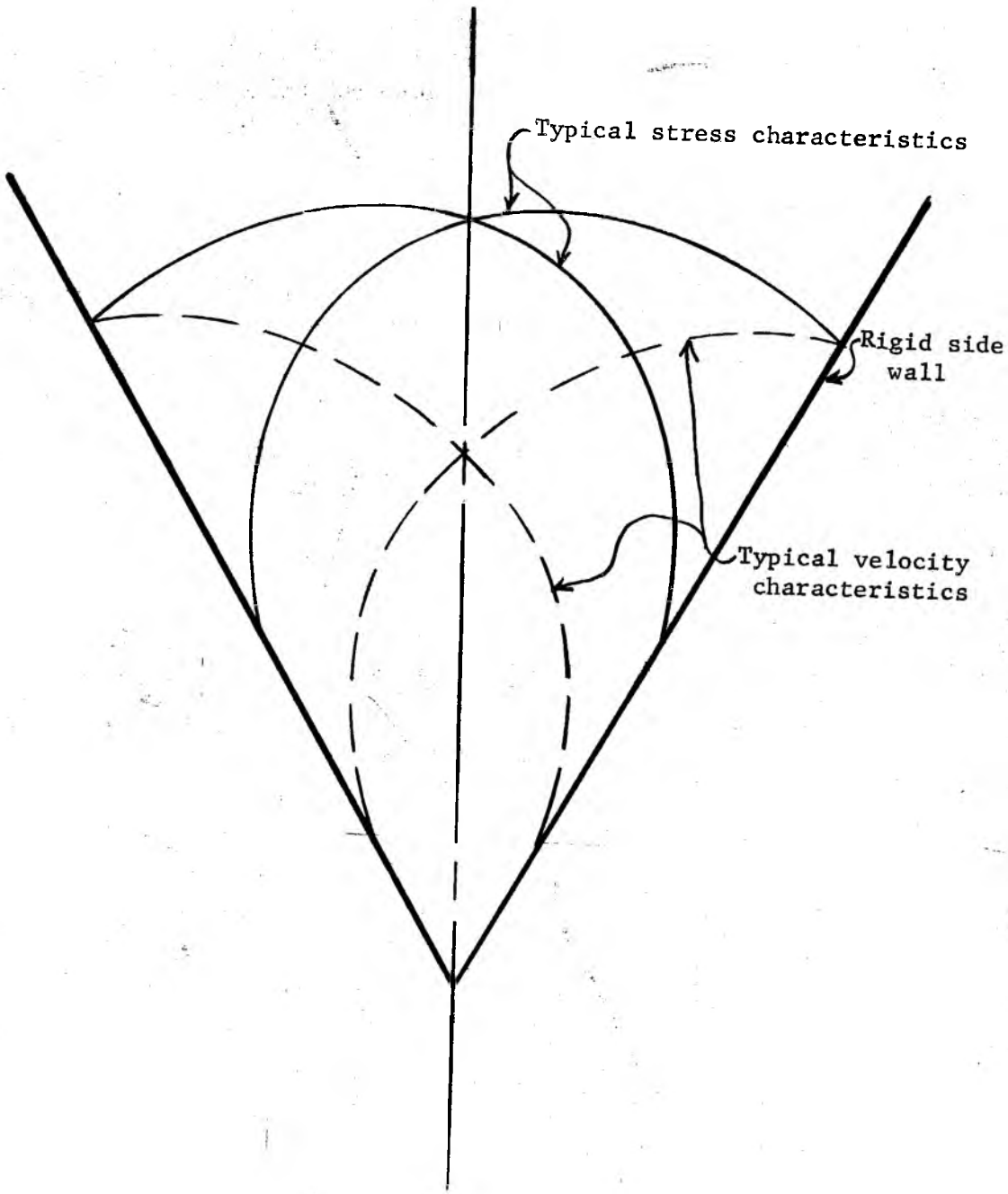

Figure 9.

Shape of the characteristics in a typical symmetric channel

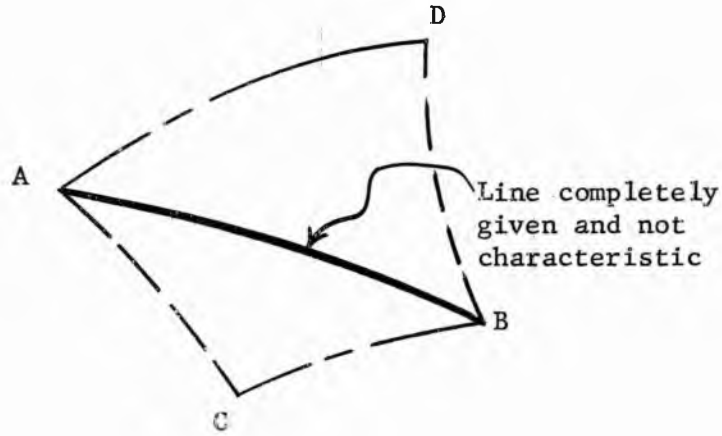

Figure 10.

Cauchy Boundary Problem

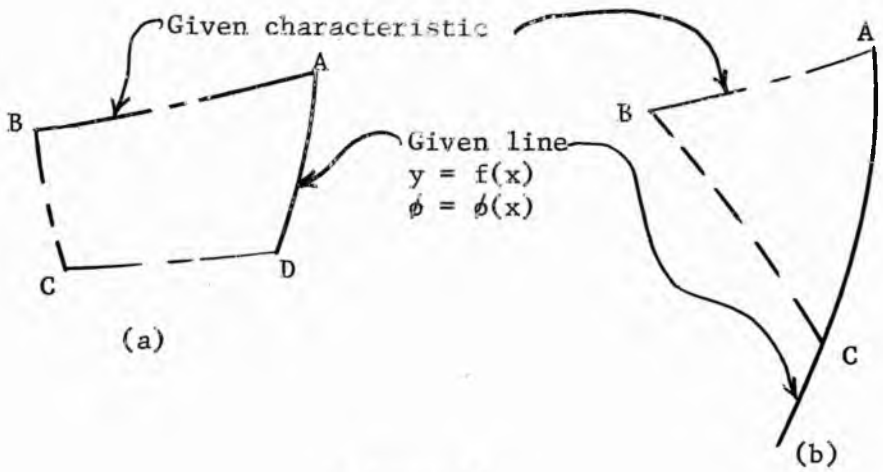

Figure 11.

Mixed boundary problem

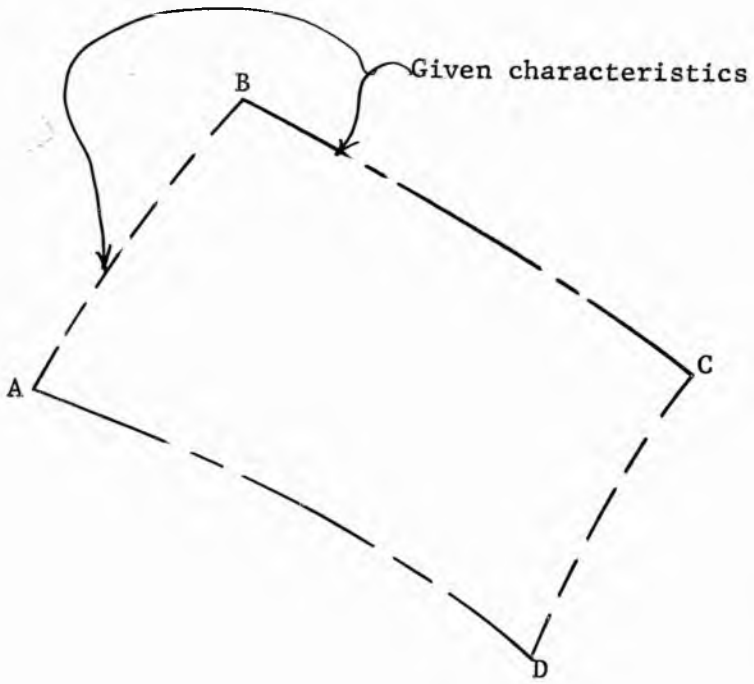

Figure 12

Goursat boundary problem

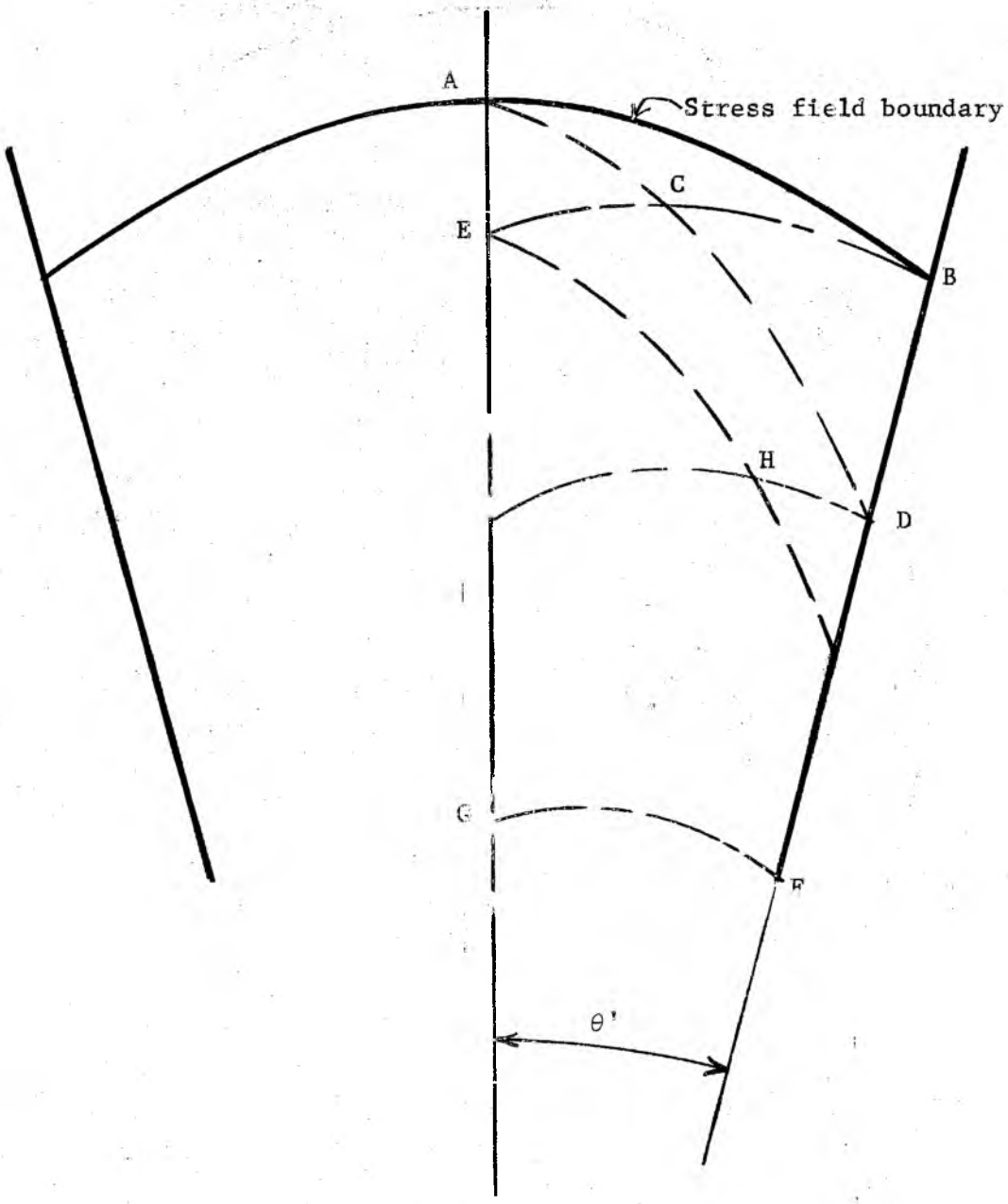

Figure 13.

Application of the boundary problems
to a converging channel

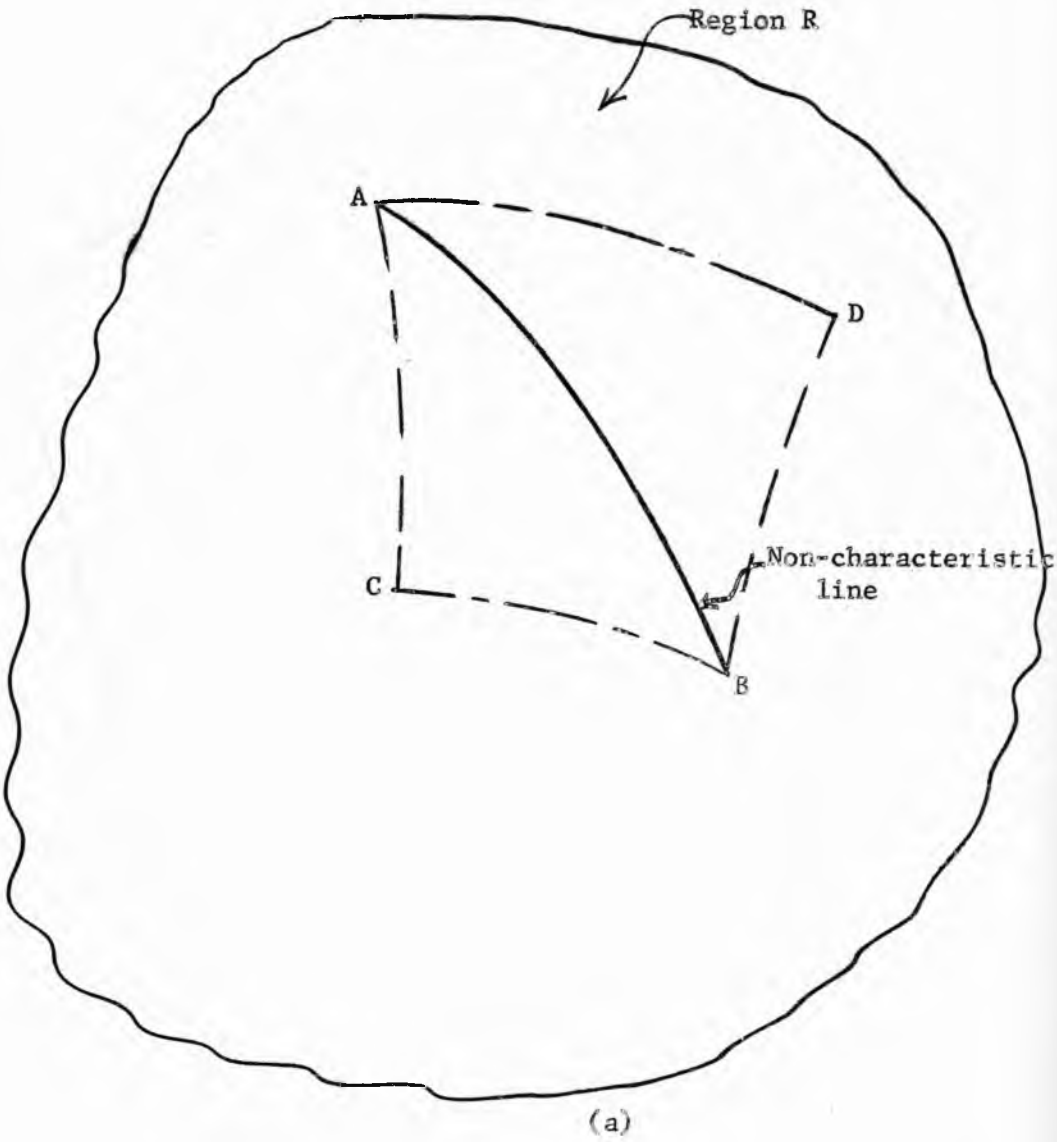

Figure 14

An illustration of uniqueness

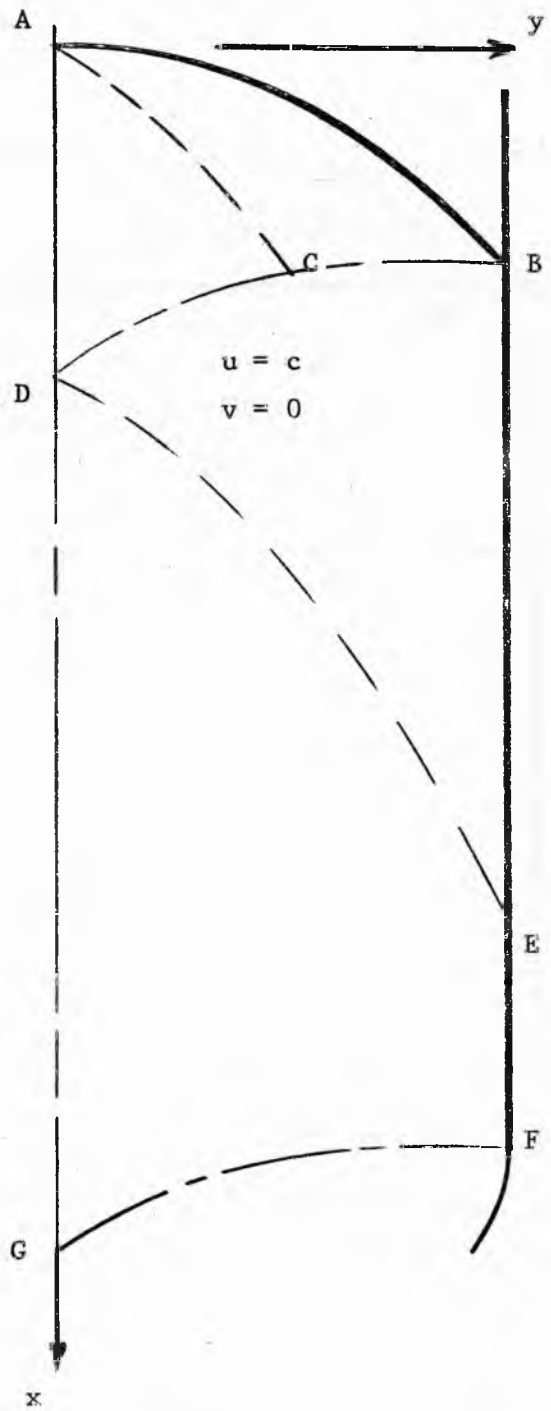

Figure 15

Constant velocity in a vertical channel

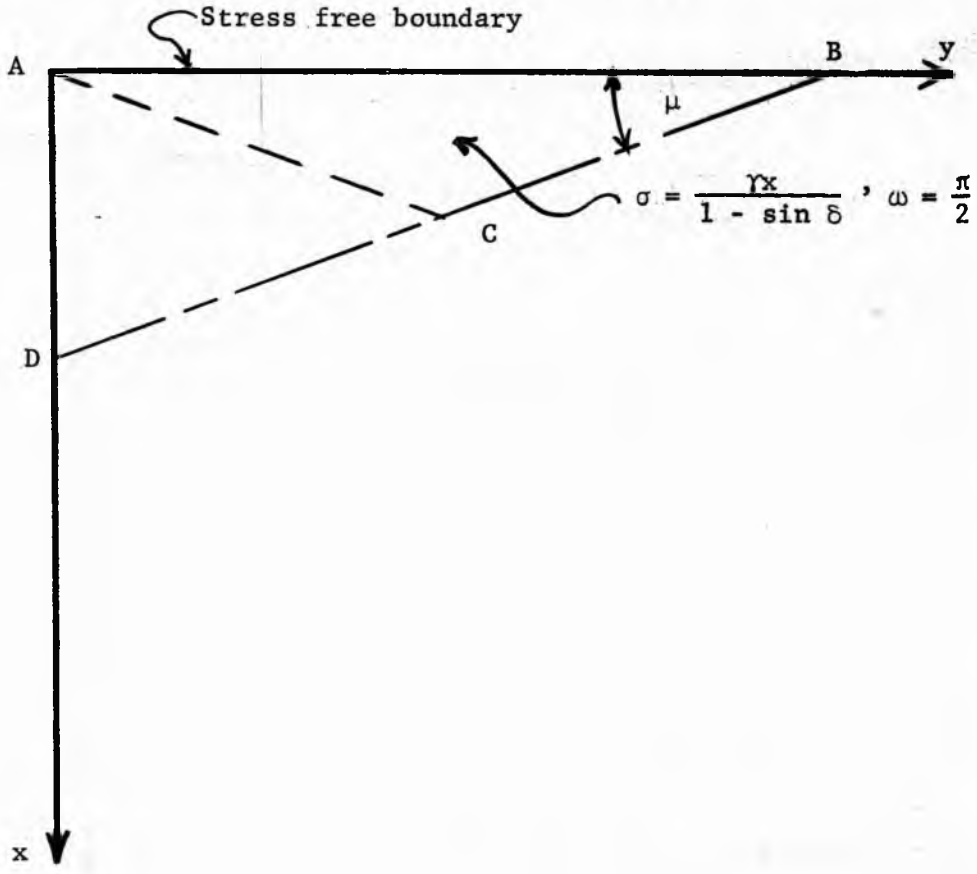

Figure 16

Horizontal stress free boundary

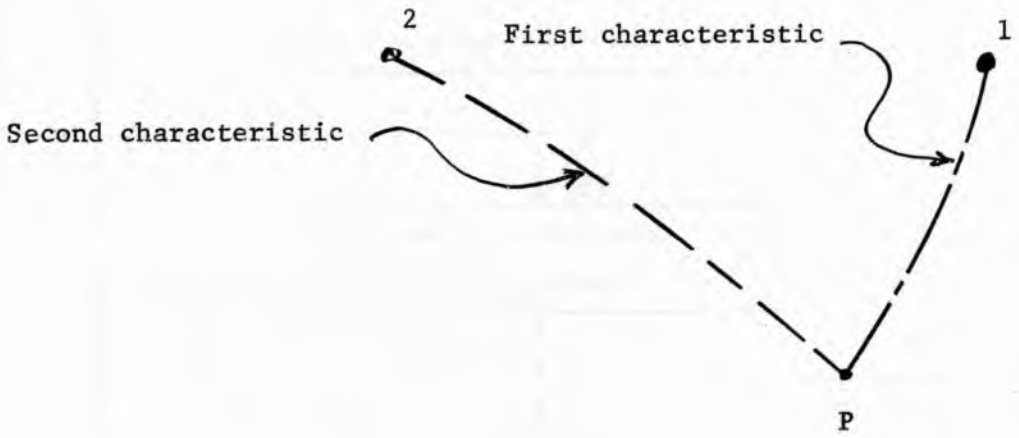

Figure 17

The first basic numerical calculation

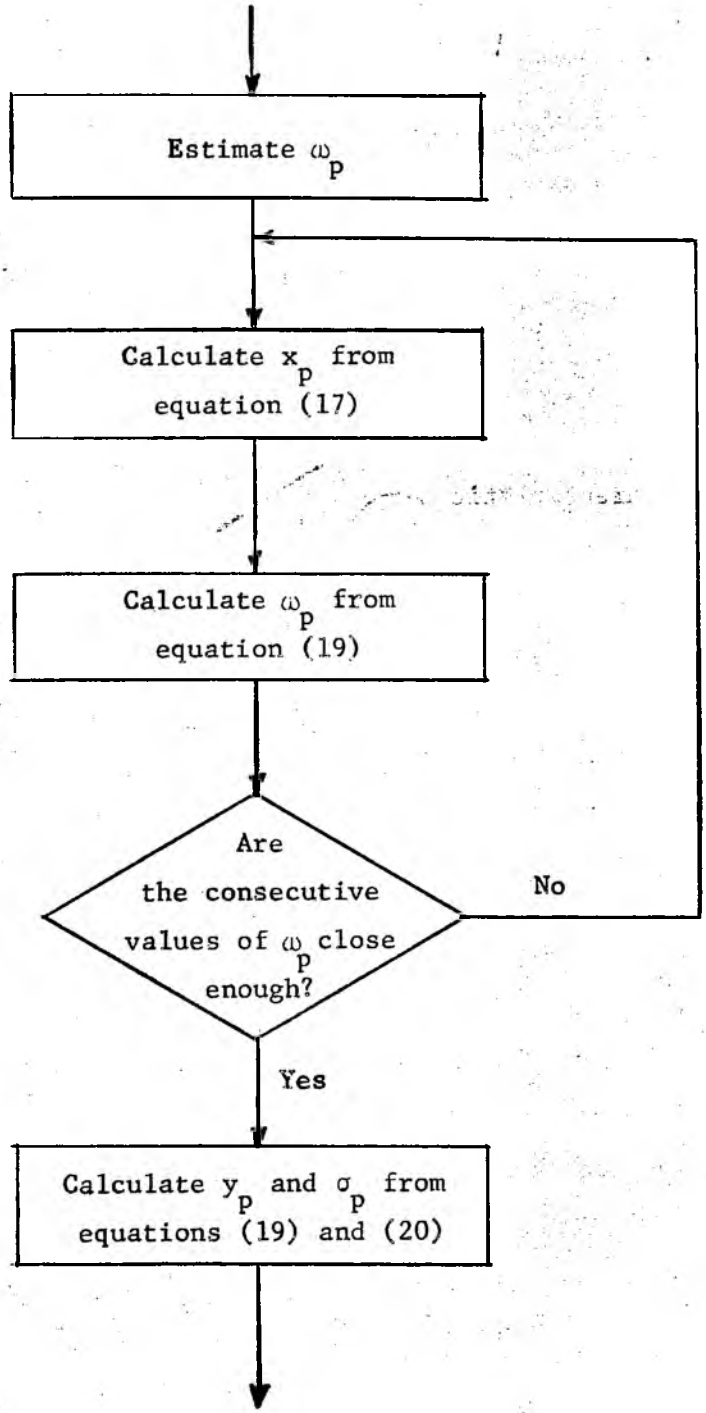

Figure 18

Flow chart for first basic stress calculation

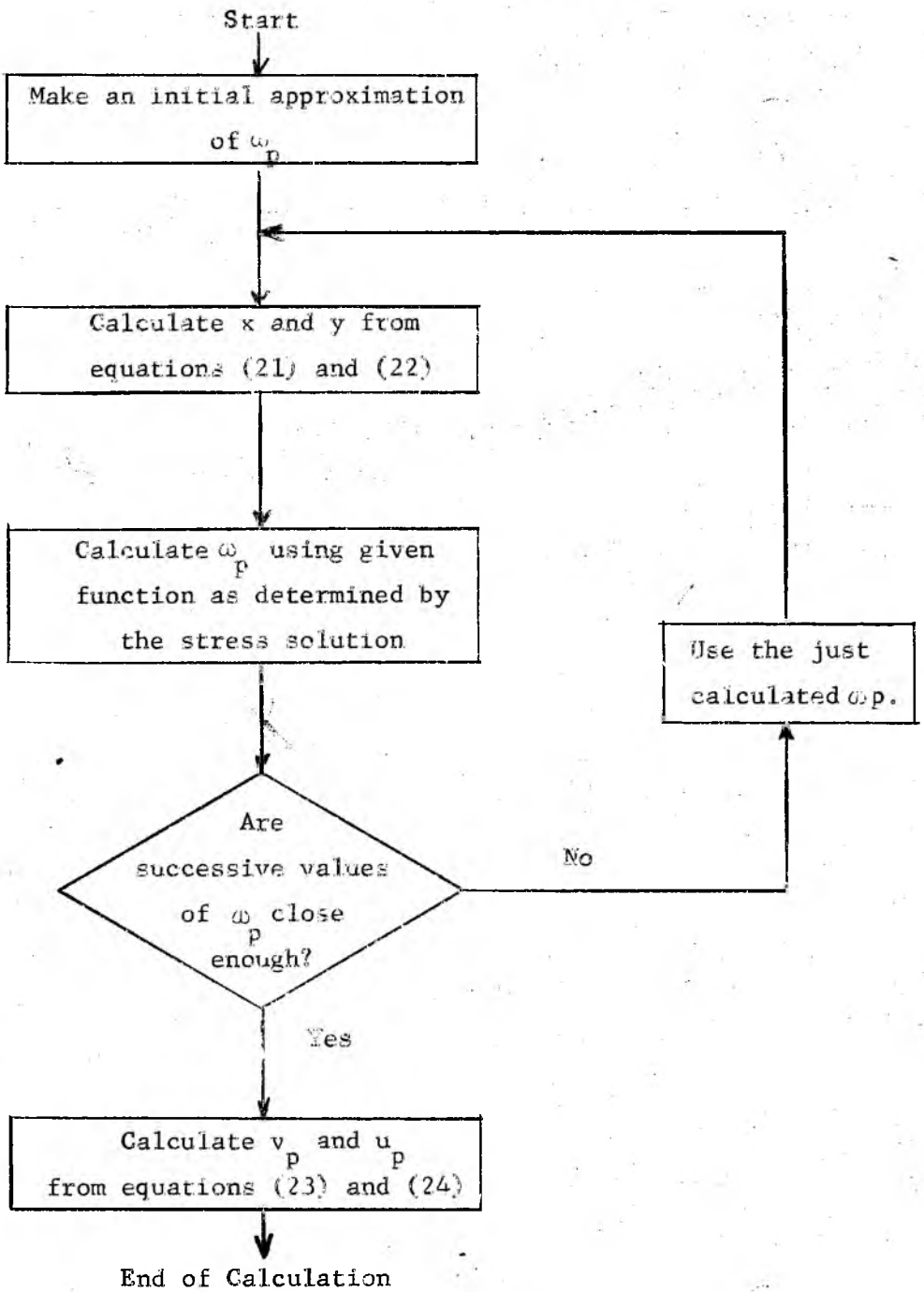

Figure 19

Flow chart for the first

basic velocity calculation

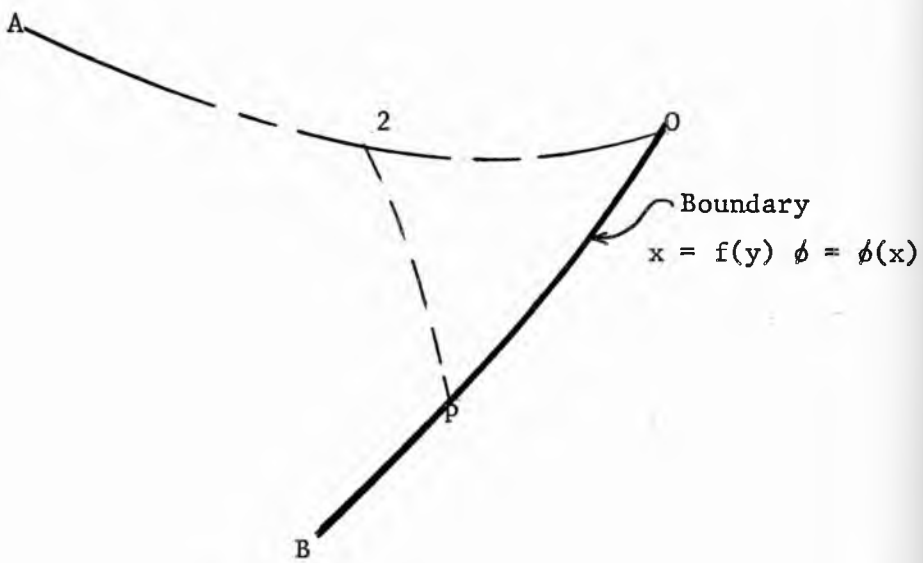

Figure 20.

The second basic calculation

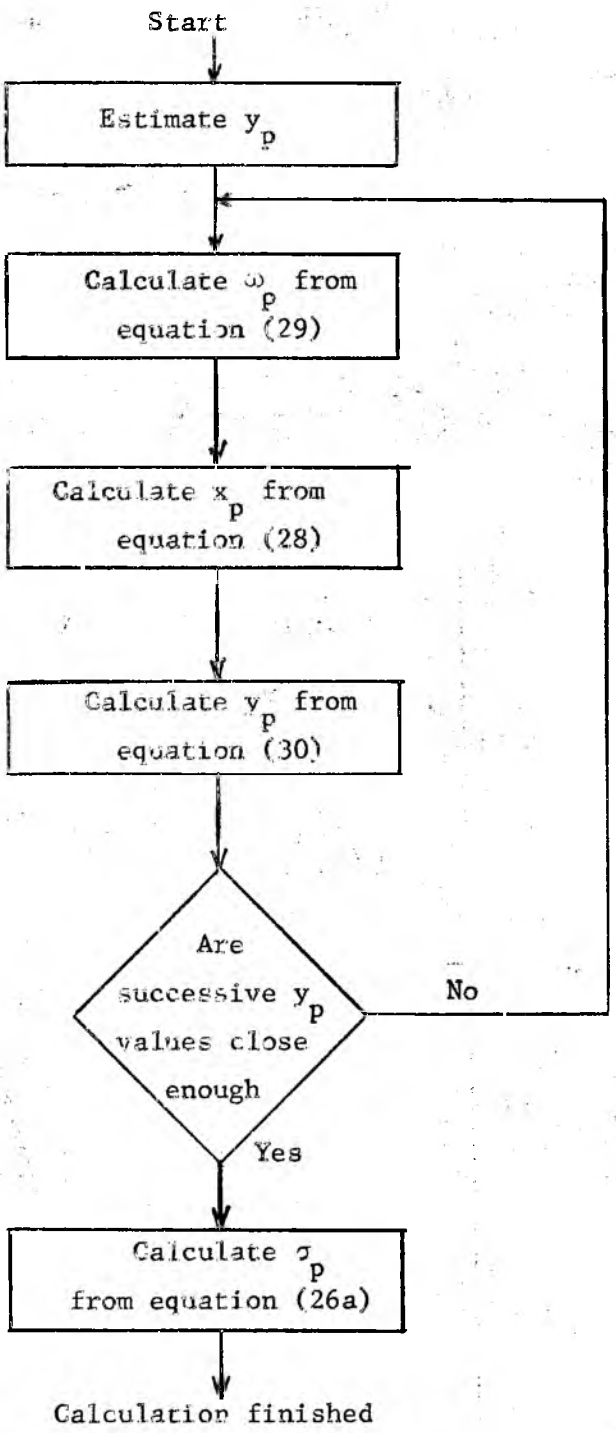

Figure 21

Flow chart for iterated second basic condition

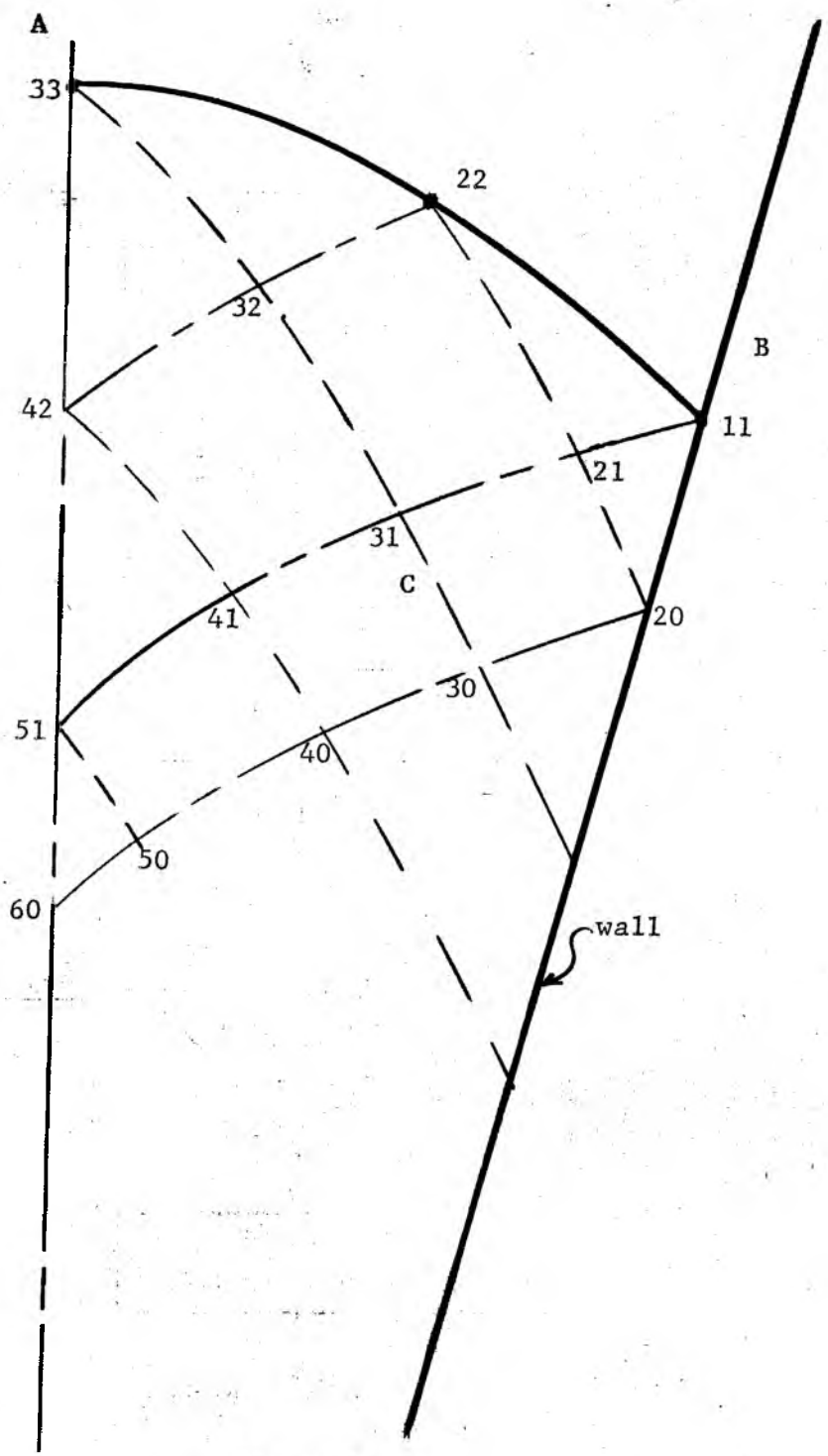

Figure 22.

Combining calculations into a complete solution

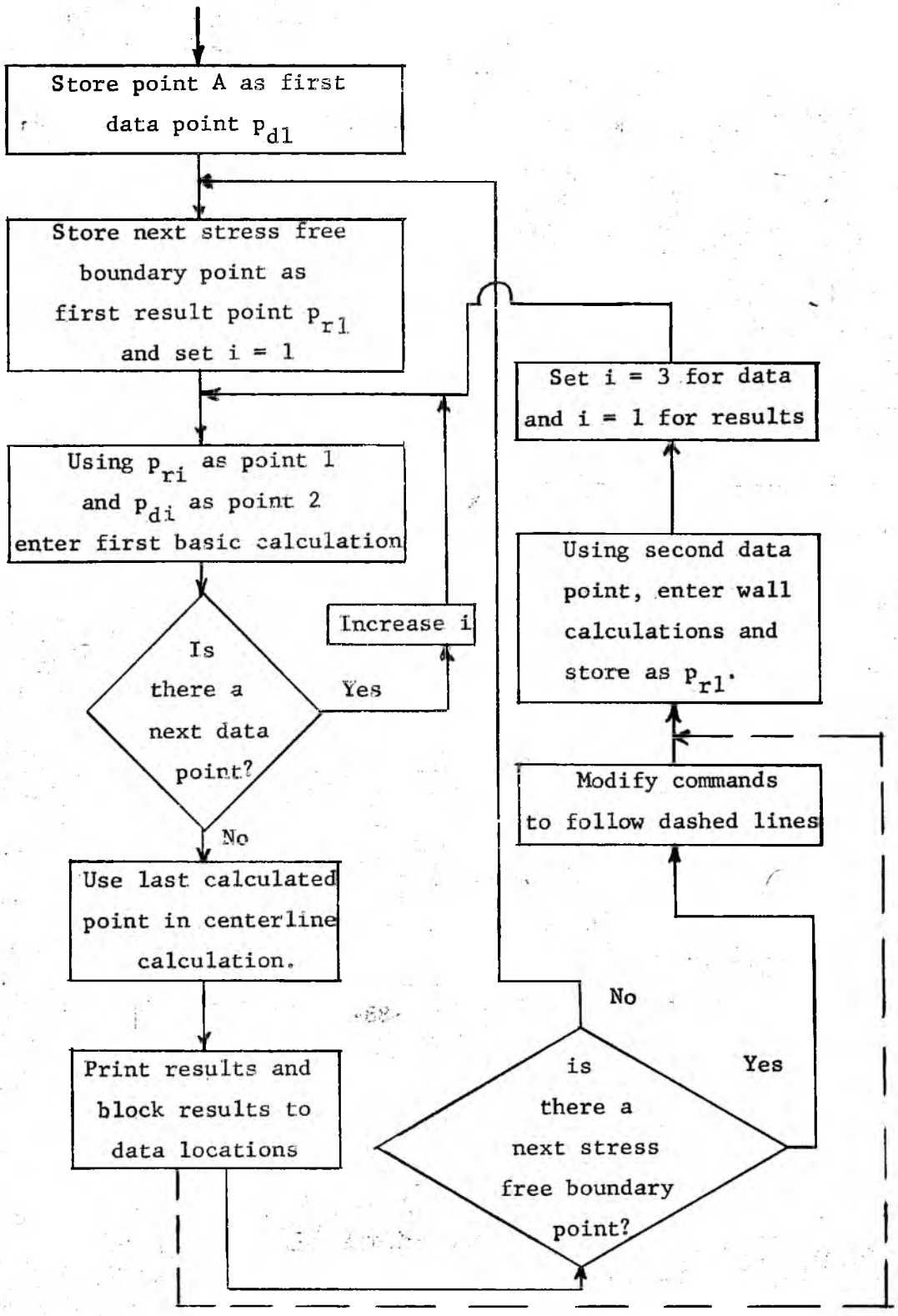

Figure 23

Flow chart for the correlation program

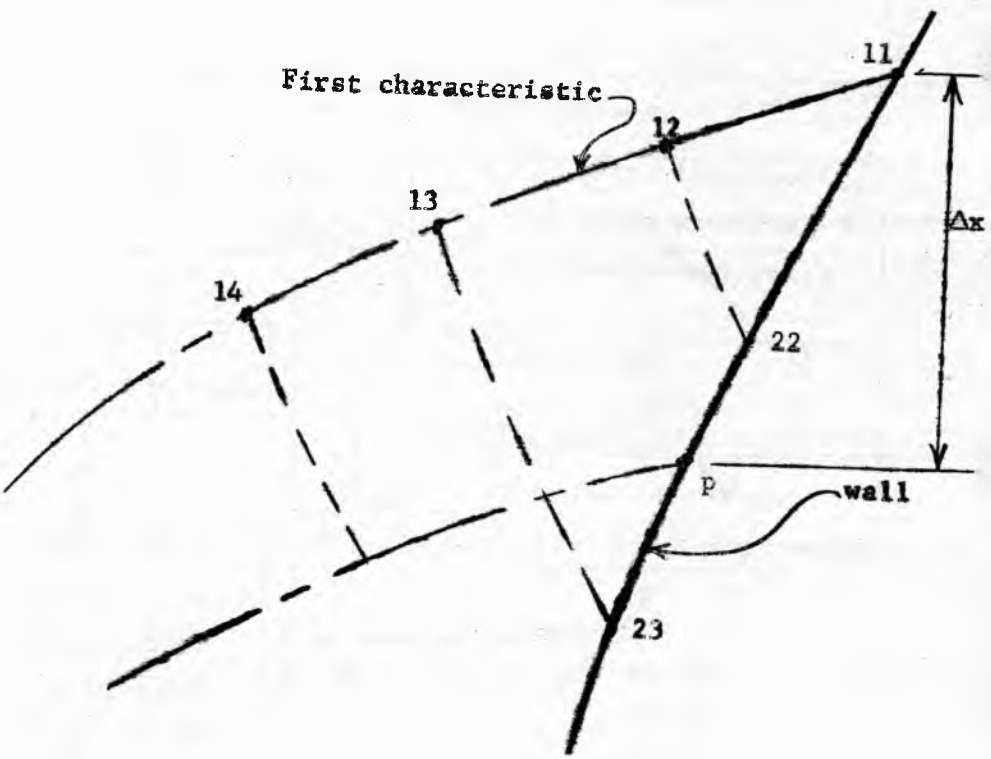

Figure 24

Typical wall calculation for equal spacing of points along the wall

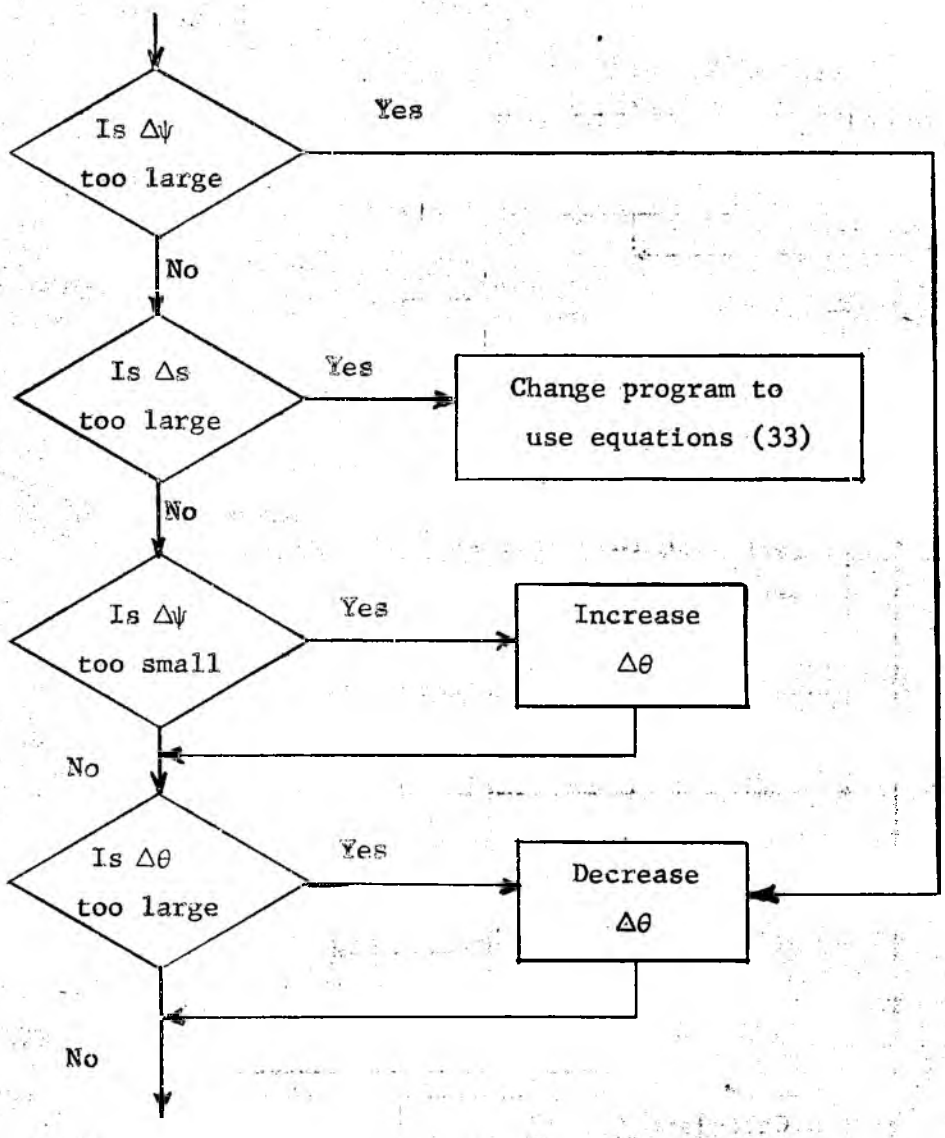

Figure 25

Flow chart for regulating the size of h in Runga-Kutta calculation

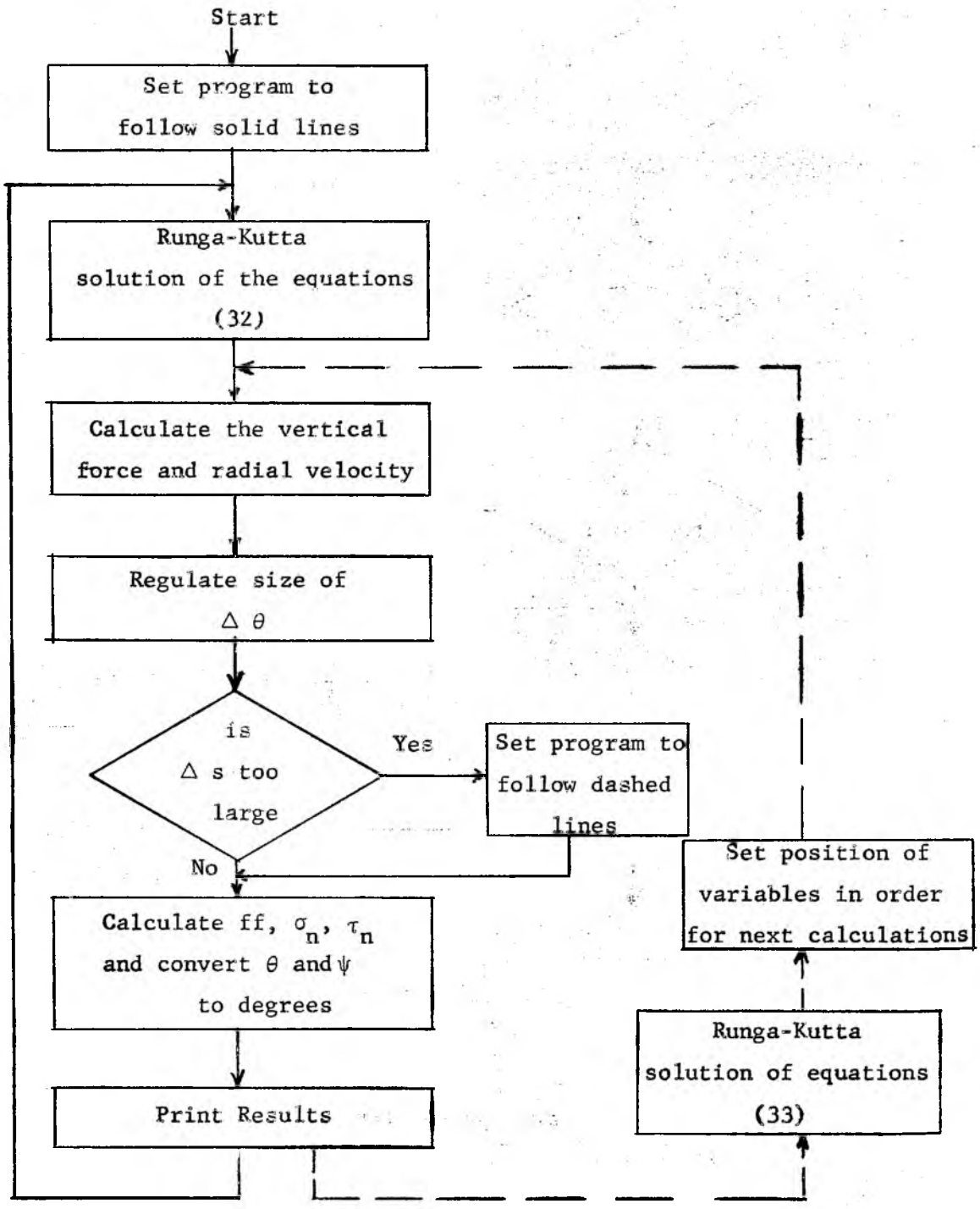

Figure 26

Flow chart for radial stress solution

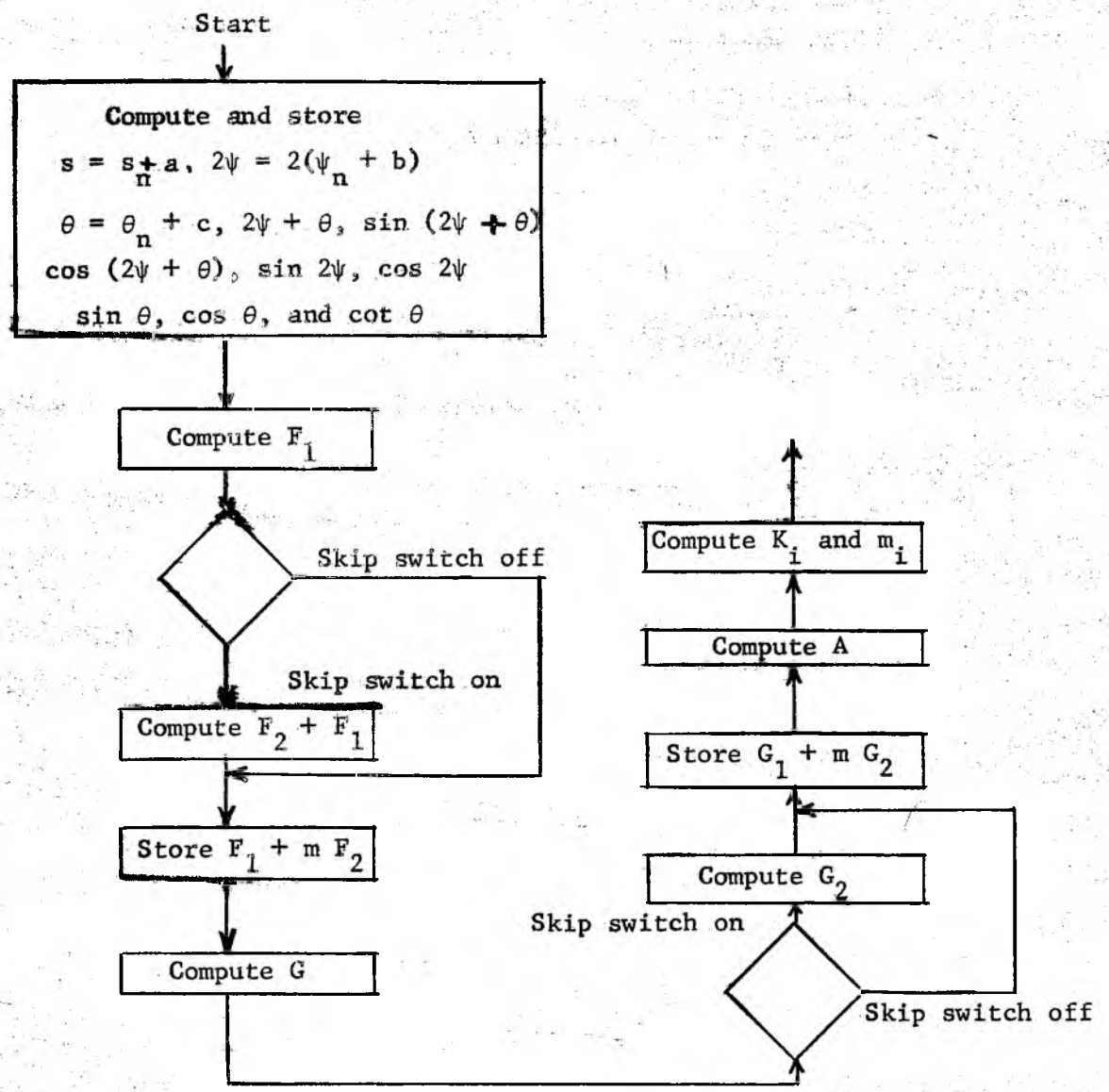

Figure 27

Flow chart to calculate K_i and m_i

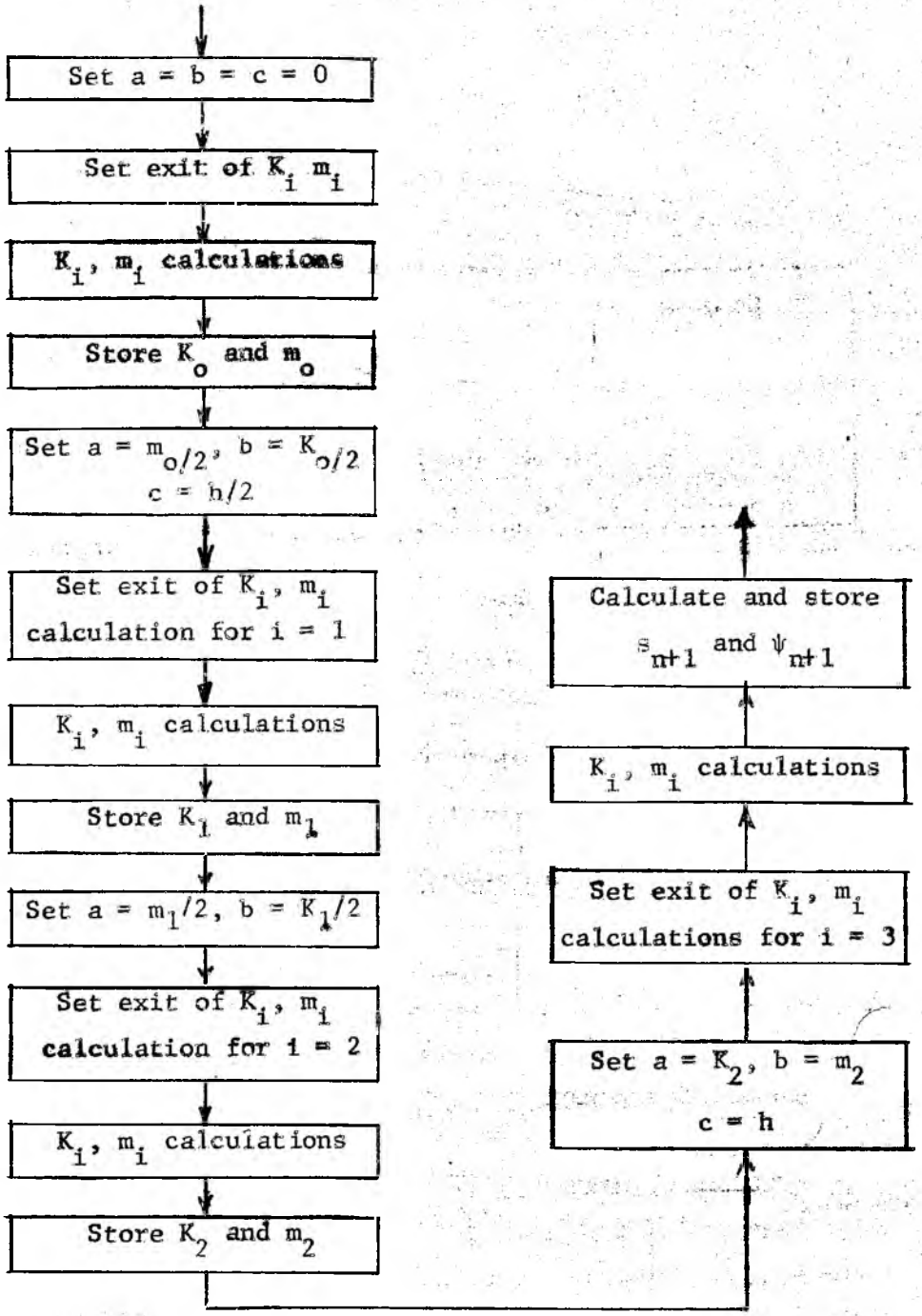

Figure 28

Flow chart for the Runga-Kutta solution

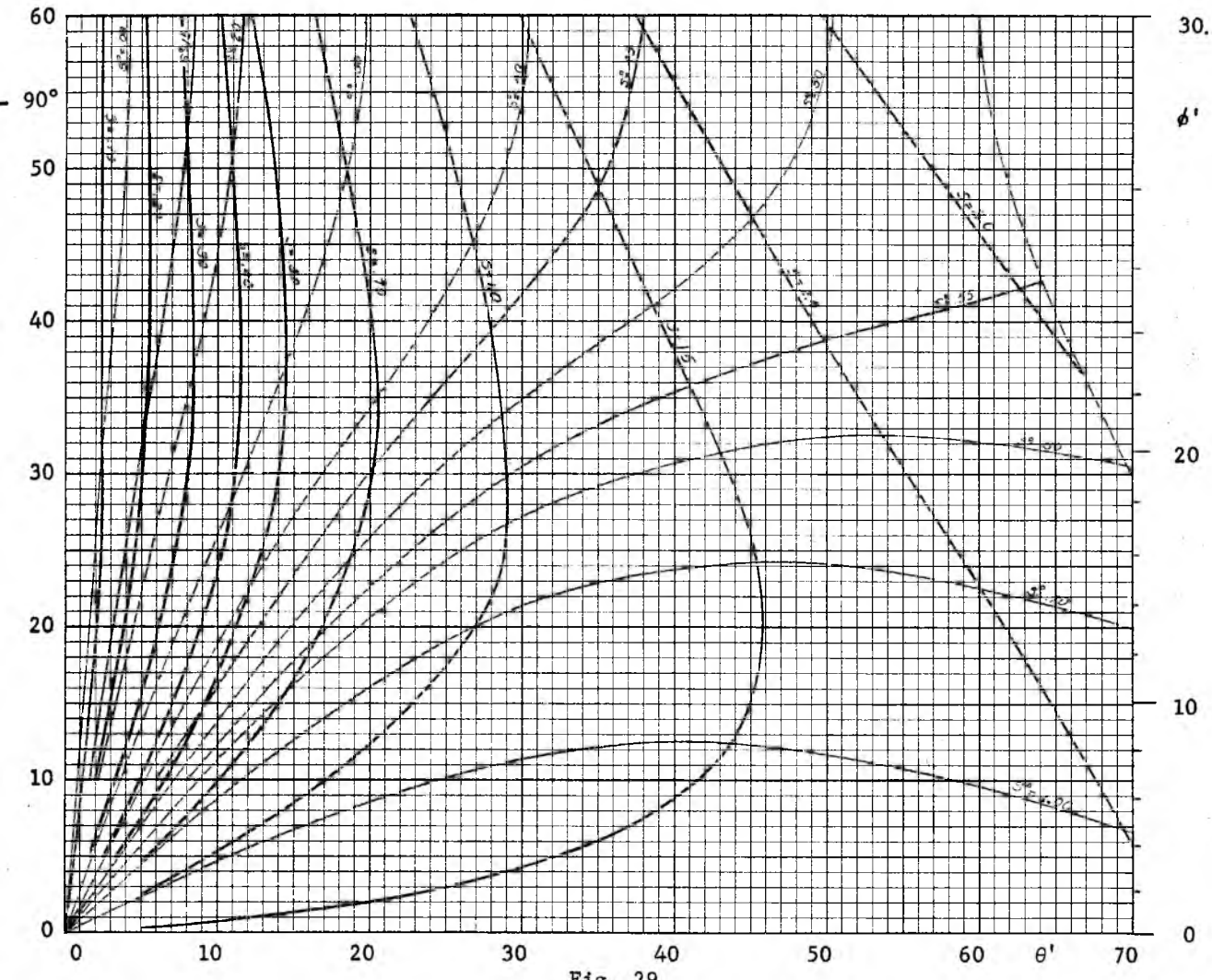

Fig. 29

Function s, $\delta = 30°$

Plane symmetry (symmetric plane flow)

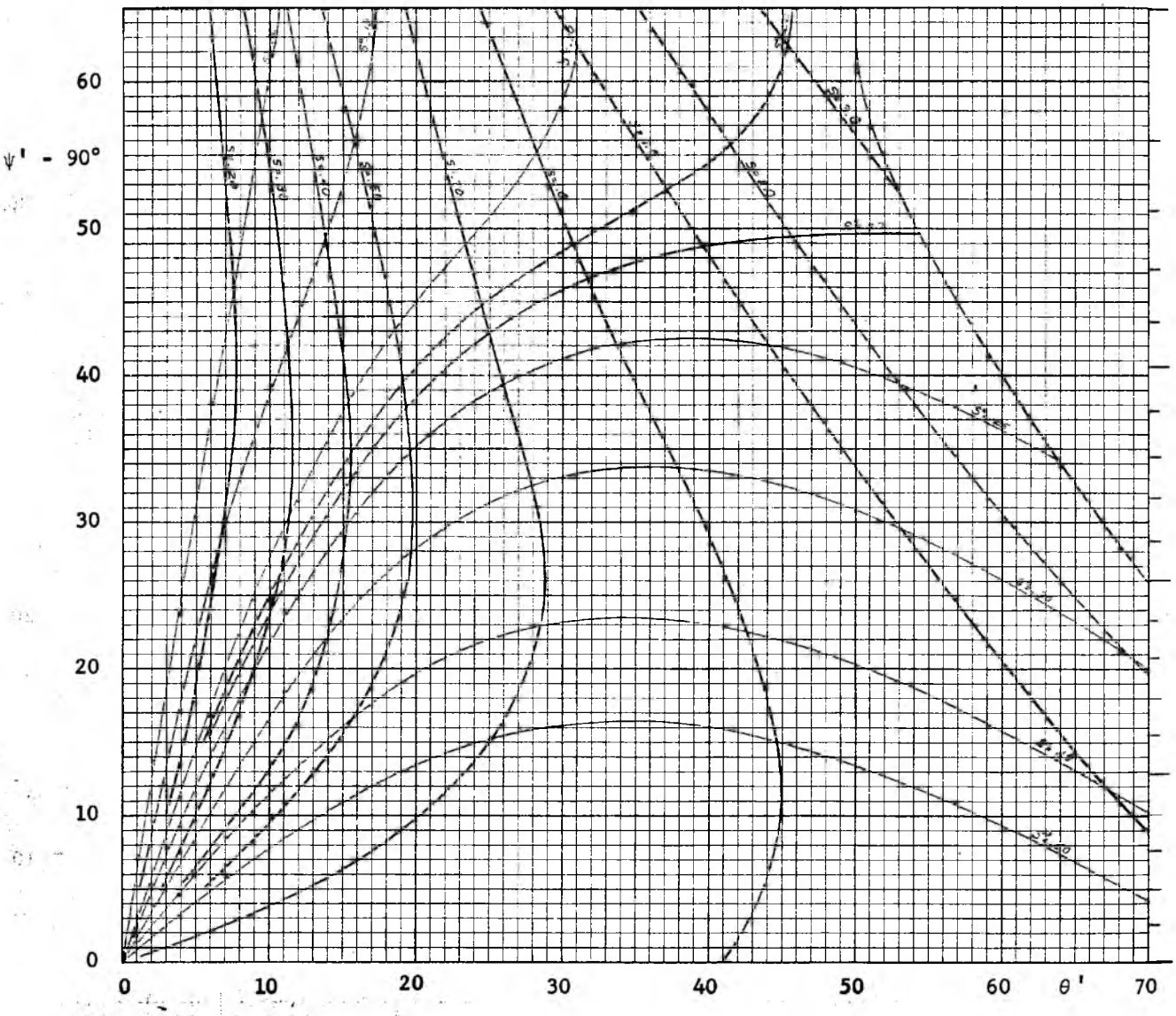

Fig. 30

Function s, $\delta = 40°$

Plane symmetry (symmetric plane flow)

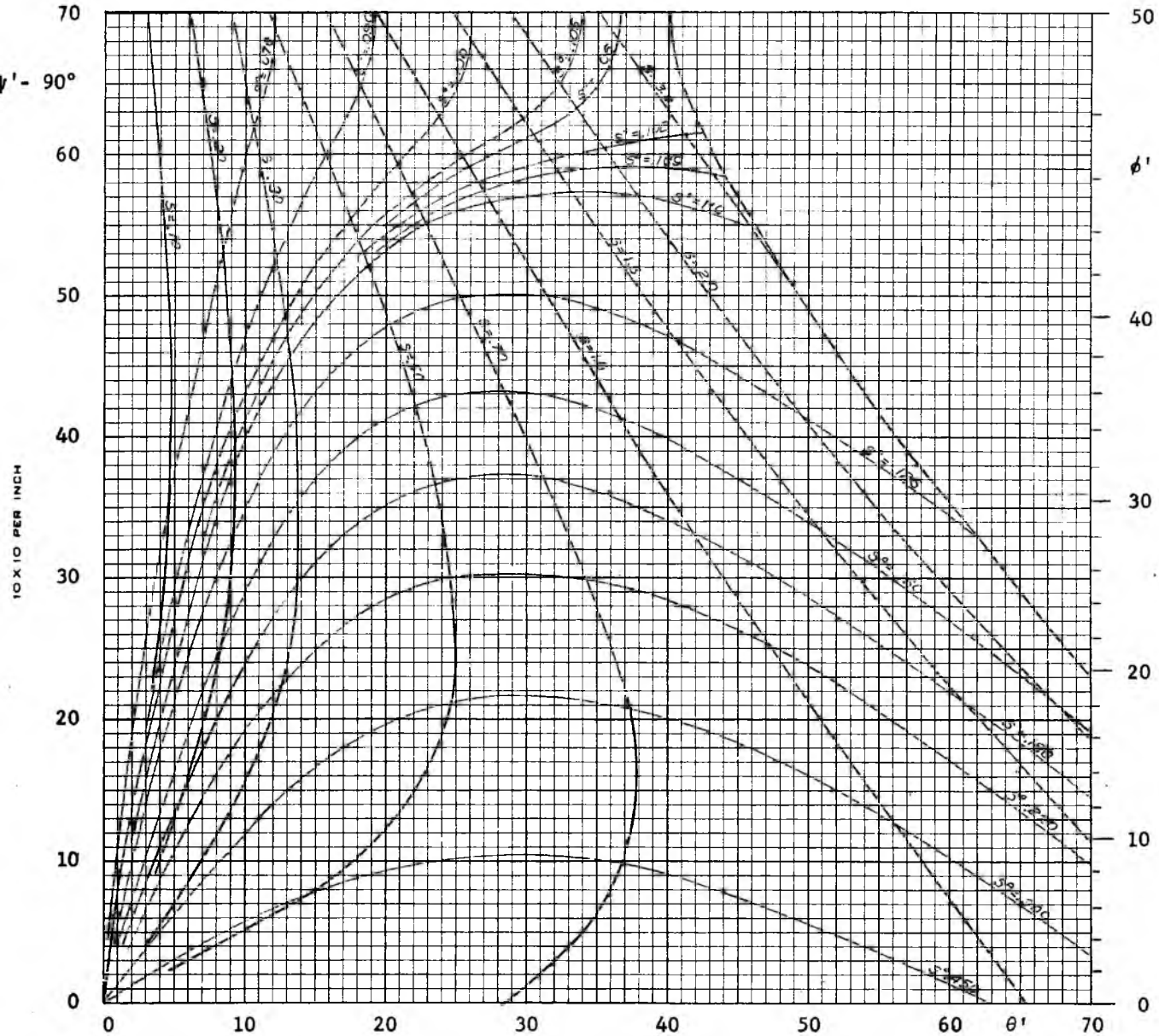

Fig. 31

Function s, $\delta = 50°$

Plane symmetry (symmetric plane flow)

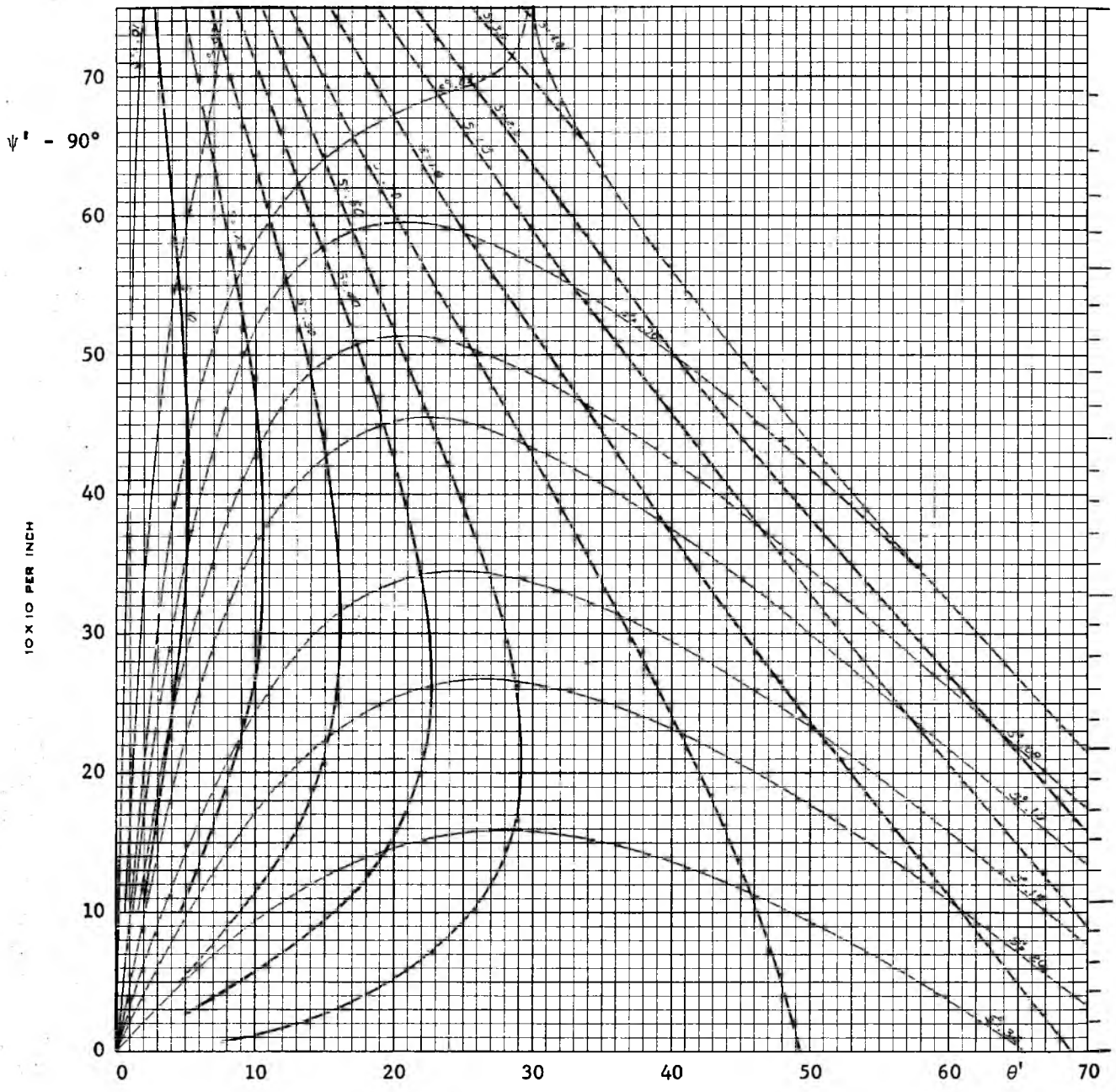

Fig. 32

Function s, $\delta = 60°$

Plane symmetry (symmetric plane flow)

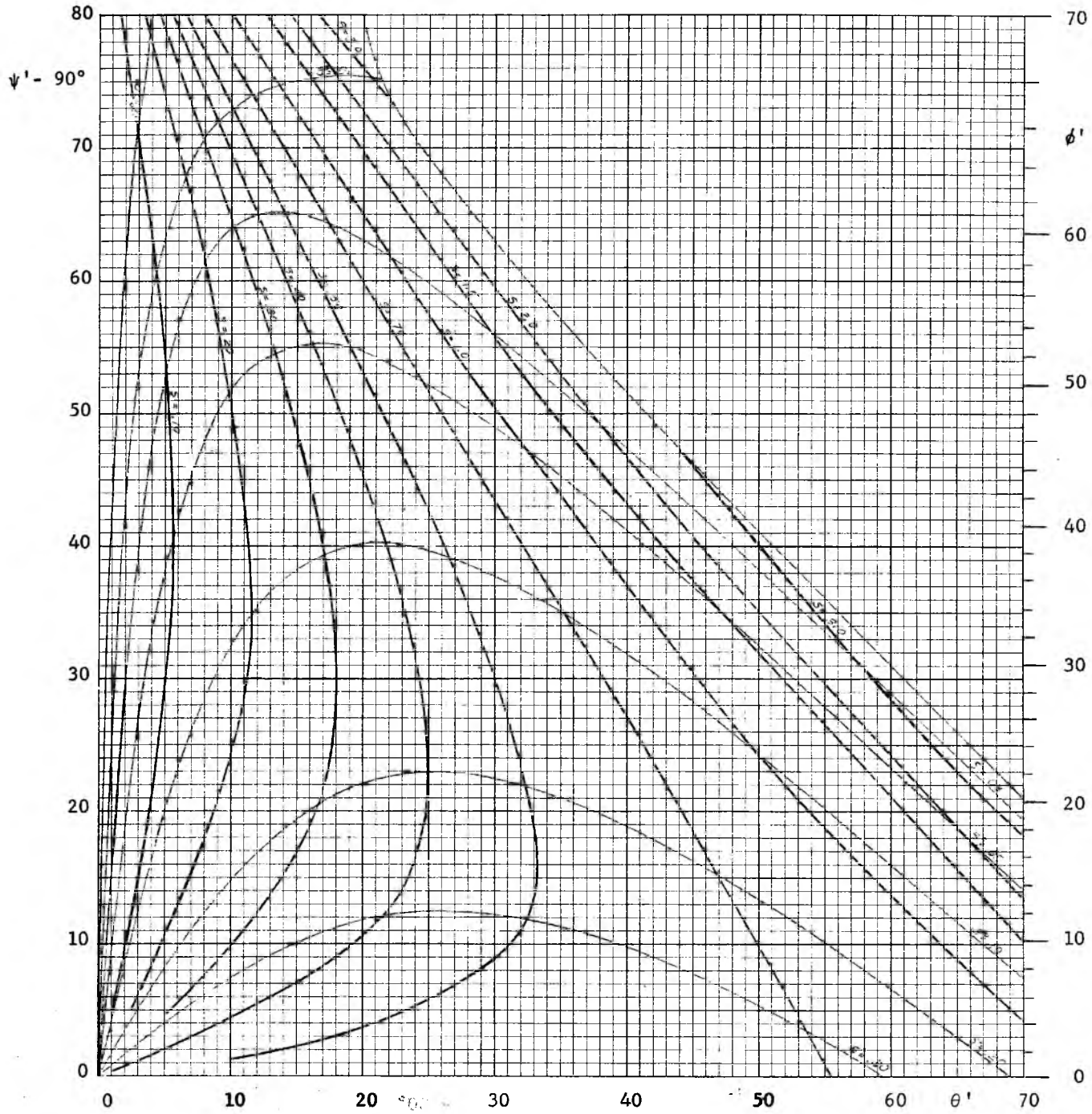

Fig. 33

Function s, $\delta = 70°$

Plane symmetry (symmetric plane flow)

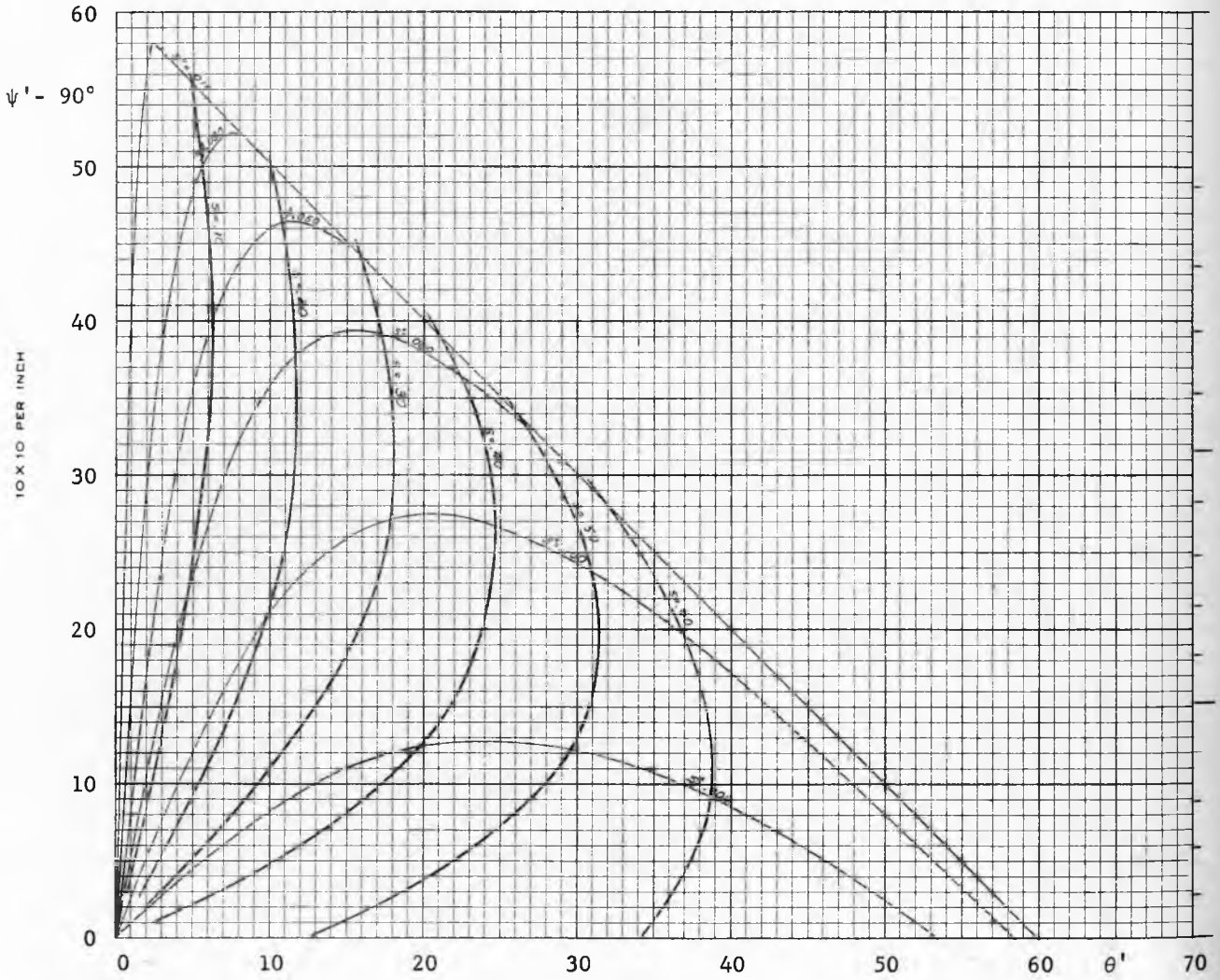

Fig. 34

Function s, $\delta = 30°$

Axial symmetry (conical flow)

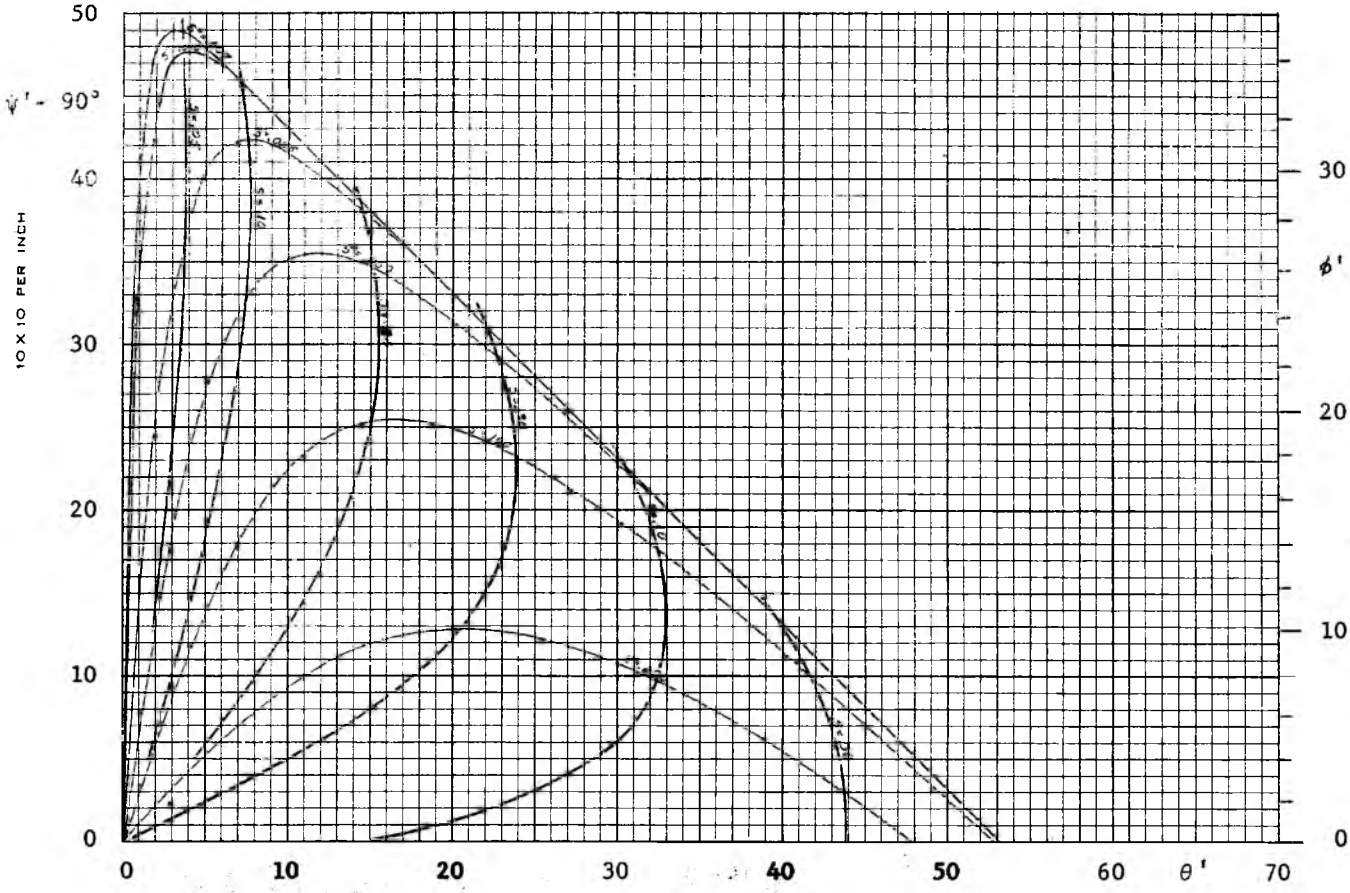

Fig. 35

Function s, $\delta = 40°$

Axial symmetry (conical flow)

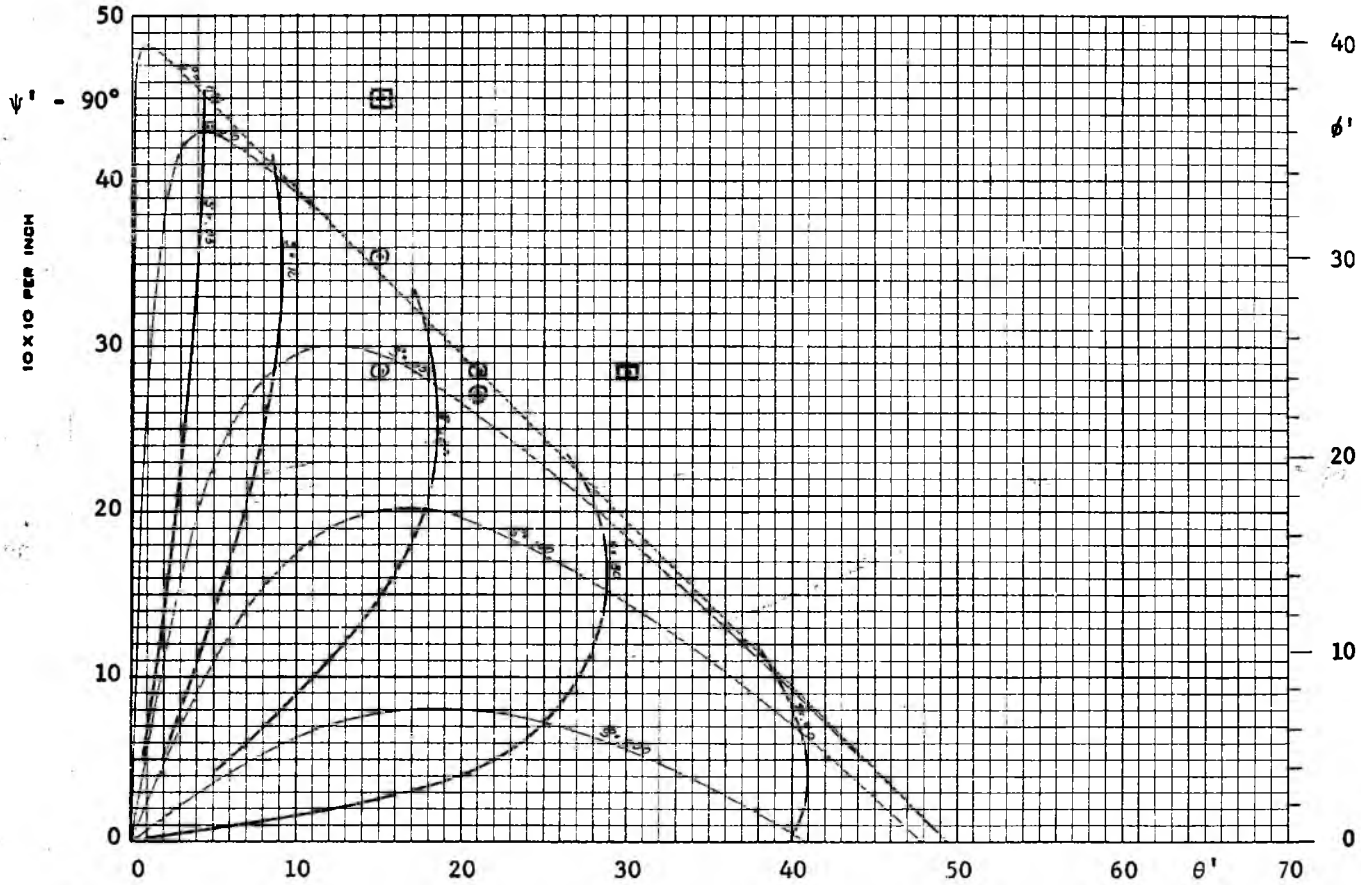

Fig. 36

Function s, $\delta = 50°$

Axial symmetry (conical flow)

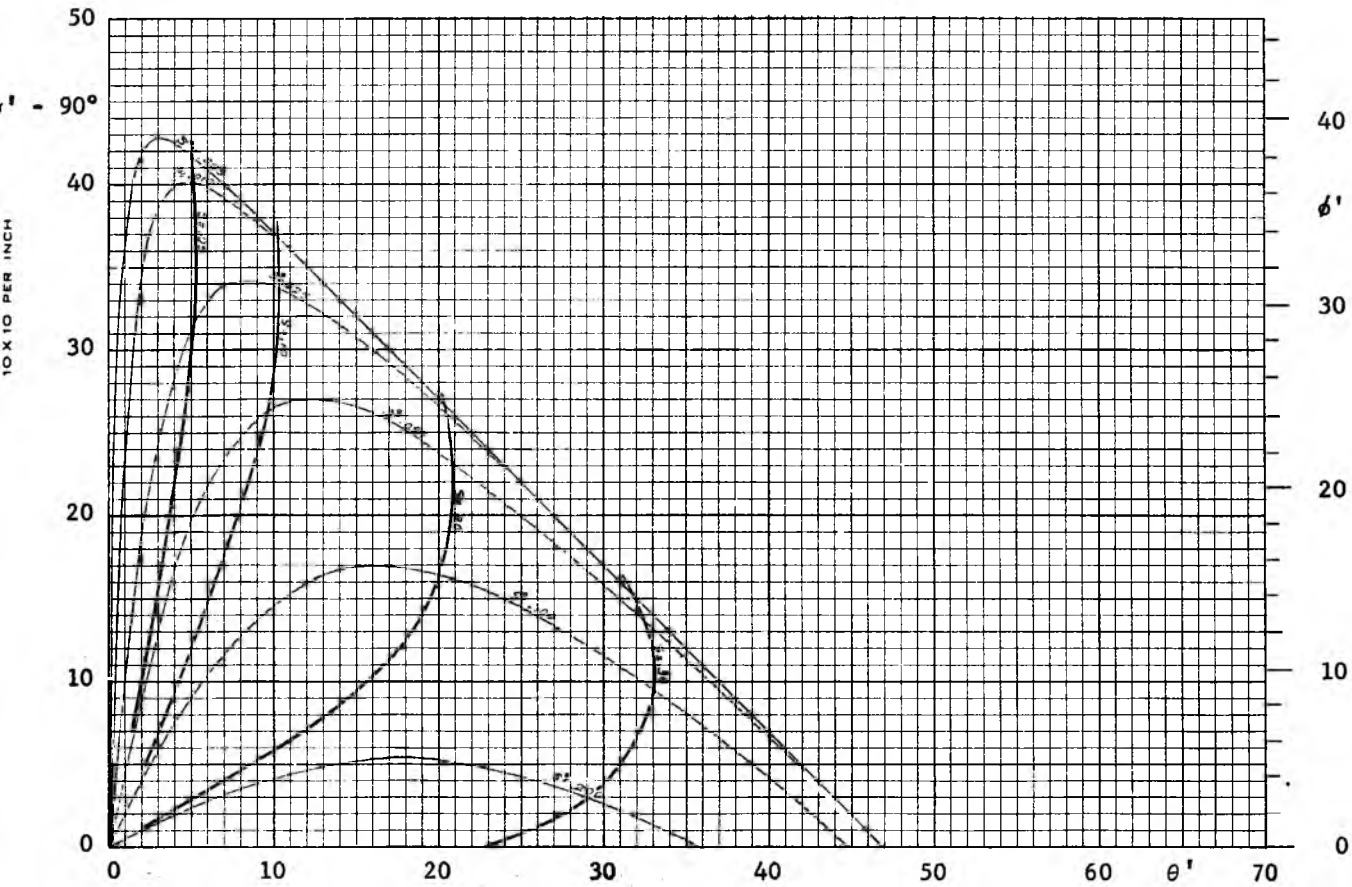

Fig 37

Function s, $\delta = 60°$

Axial symmetry (conical flow)

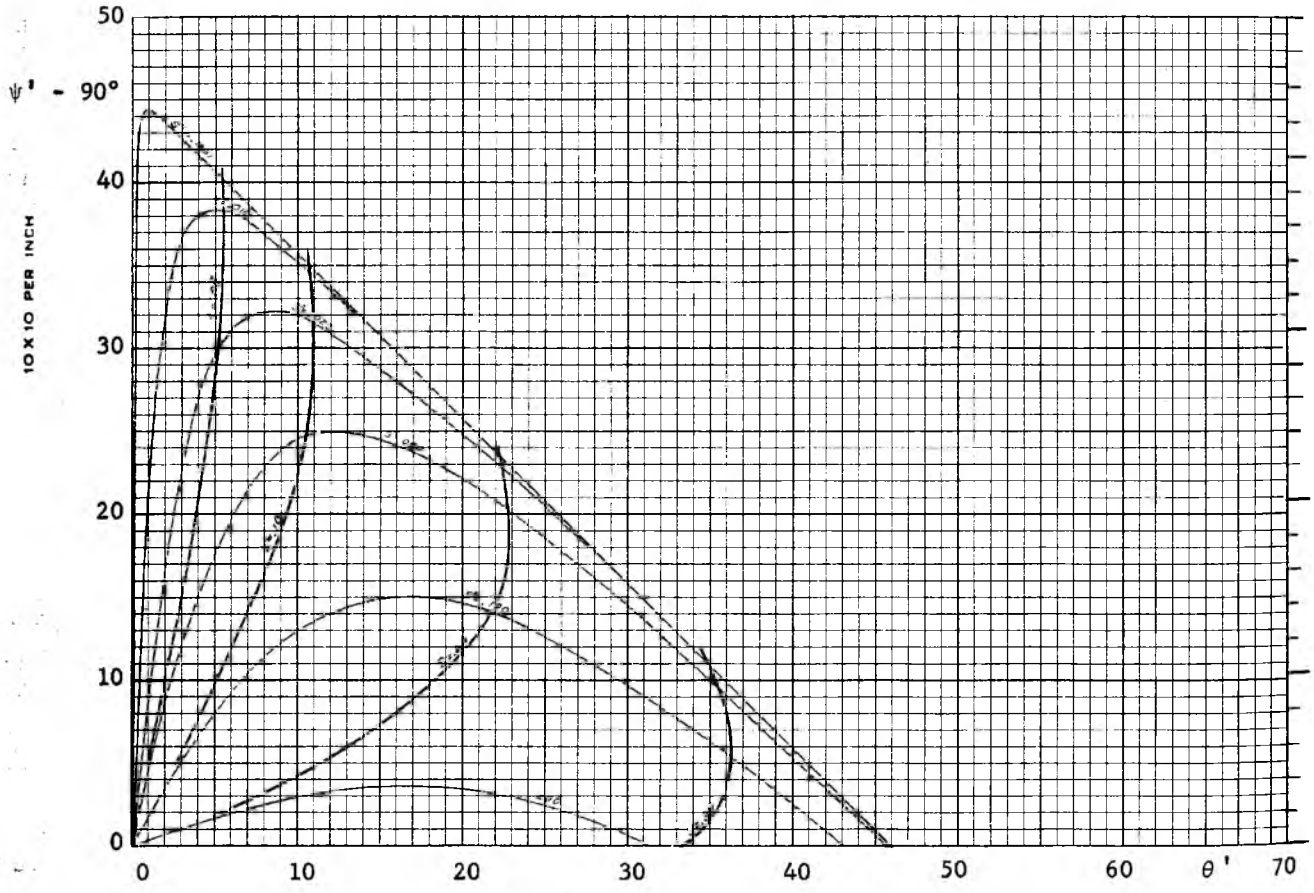

Fig. 38

Function s, $\delta = 70°$

Axial symmetry (conical flow)

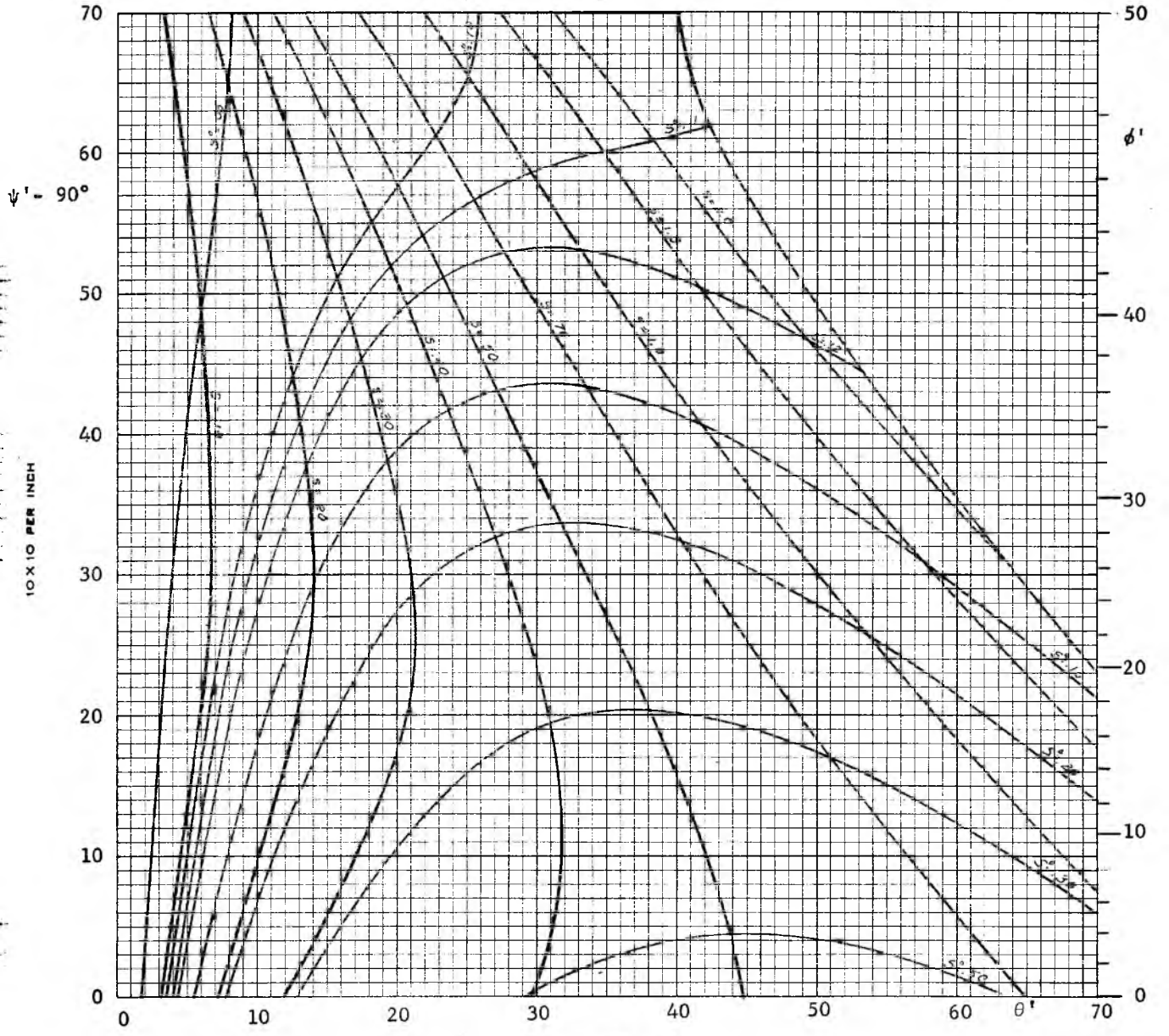

Fig. 39

Function s, $\delta = 50°$, $\phi^V = 20°$

Plane asymmetry (Plane flow - one vertical wall)

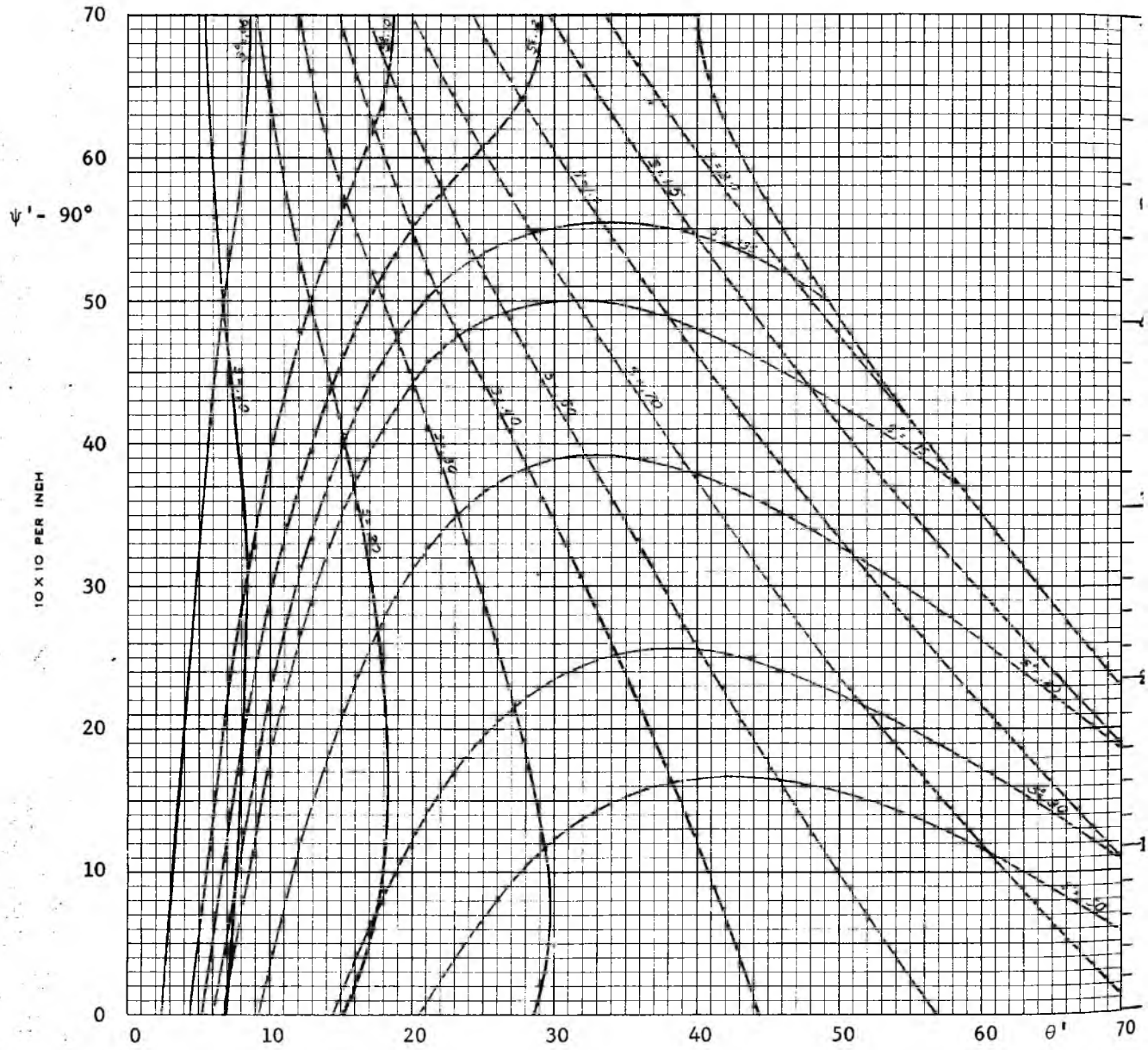

Fig. 40

Function s, $\delta = 50°$, $\phi^V = 30°$

Plane asymmetry (Plane flow - one vertical wall)

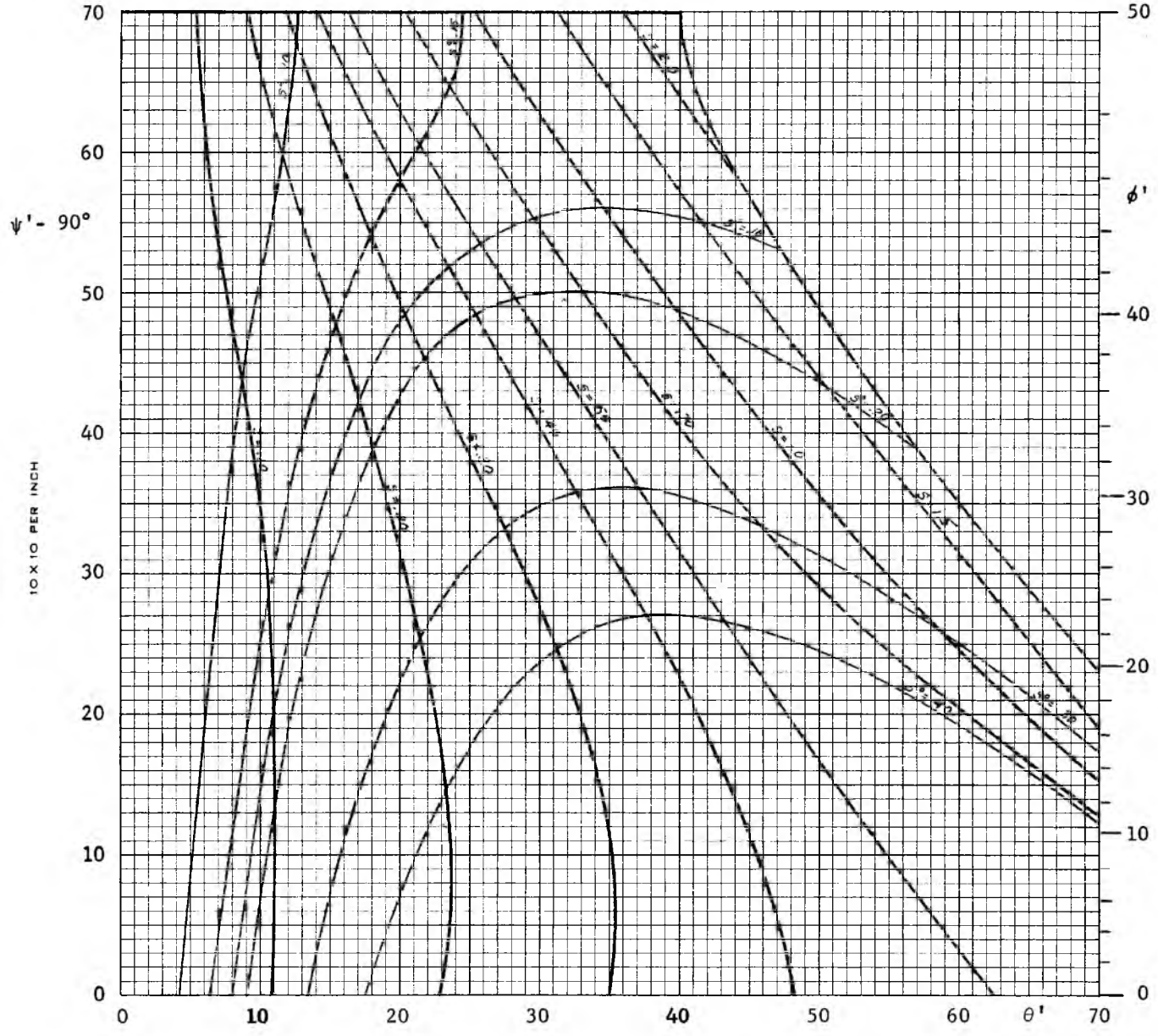

Fig. 41

Function s, $\delta = 50°$, $\phi^V = 40°$

Plane asymmetry (Plane flow - one vertical wall)

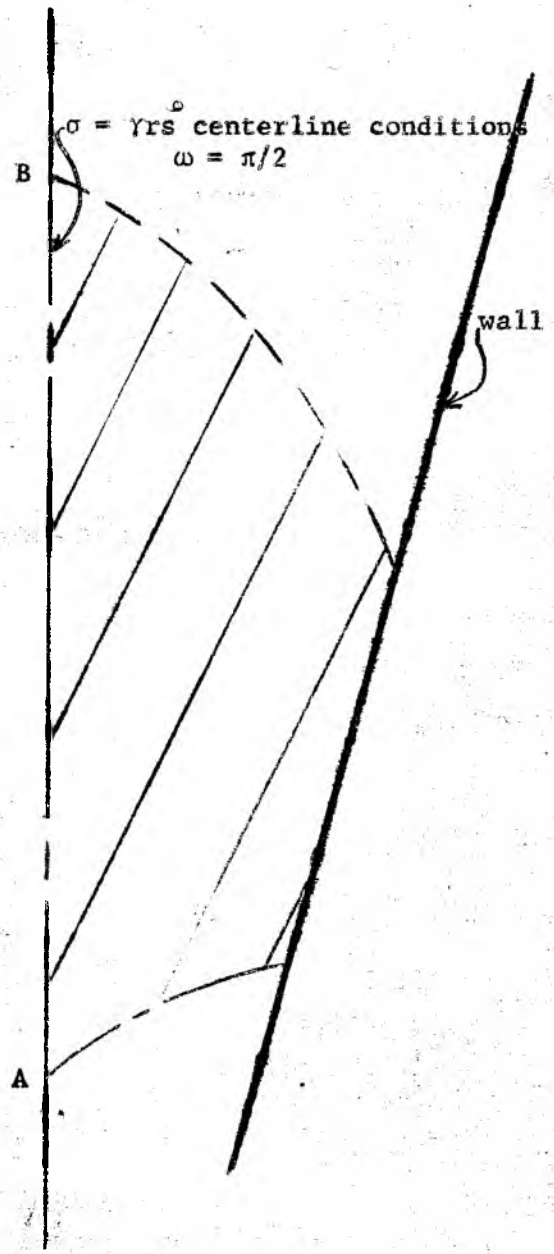

Figure 42

Region of Radial Stress Defined
$\sigma = \gamma r s^{\circ}$ along the centerline

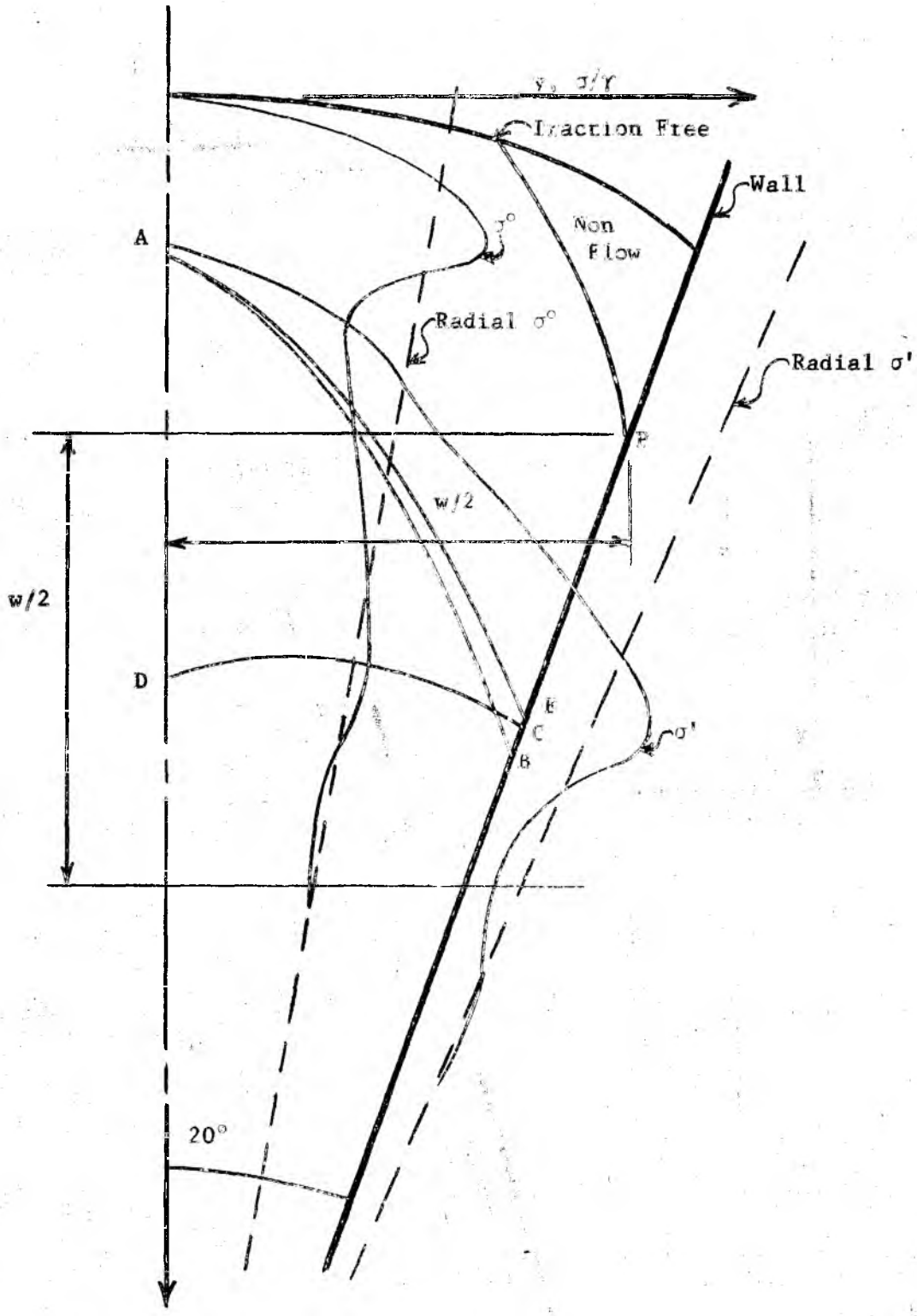

Figure 43

Stress in a converging channel

with a non-flow region

$\delta = 50°$, $\theta' = 20°$, $\phi' = 30°$

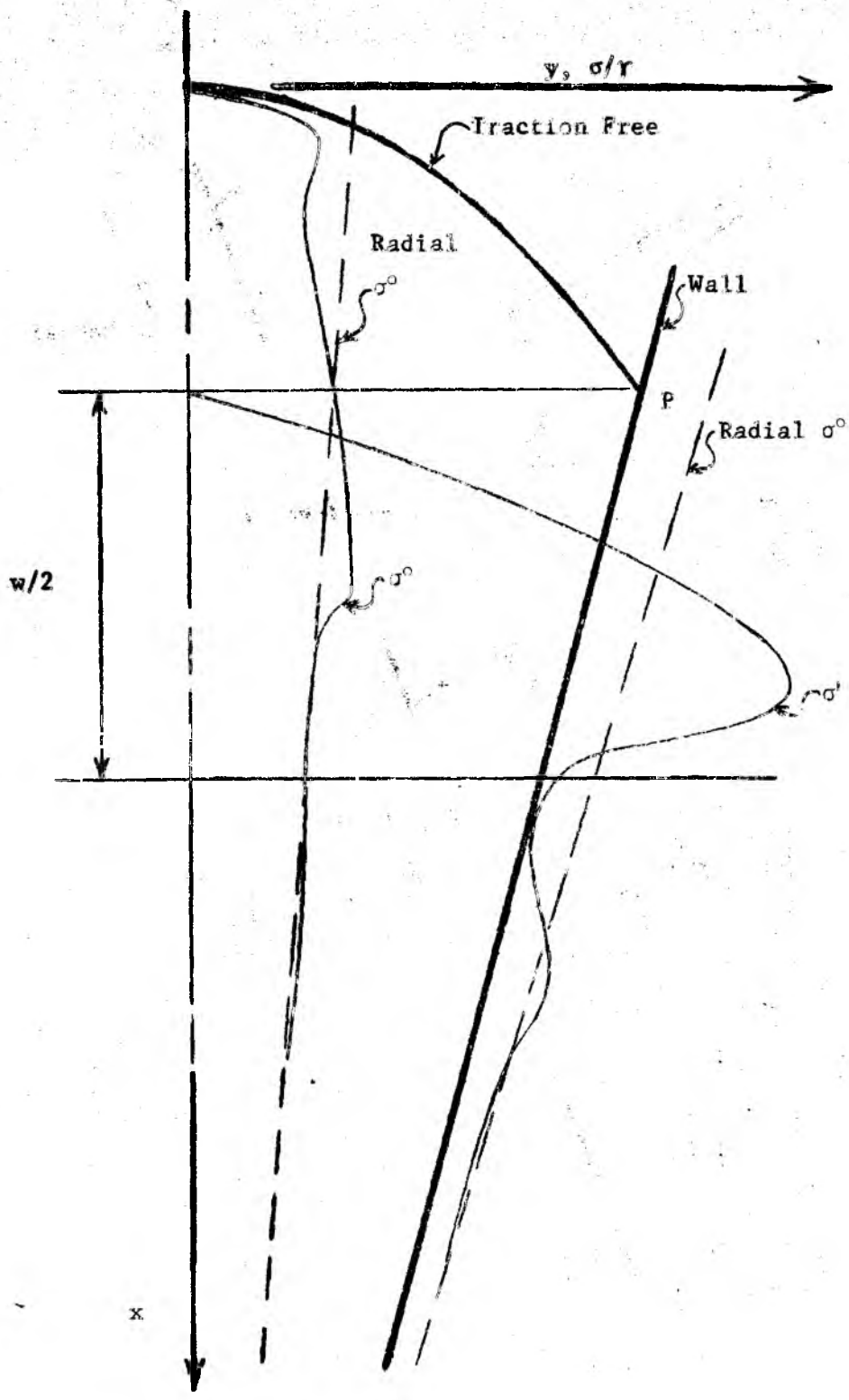

Figure 44

Stress in a converging channel

$\delta = 60°$, $\theta'' = 15°$, $\phi'' = 42°$

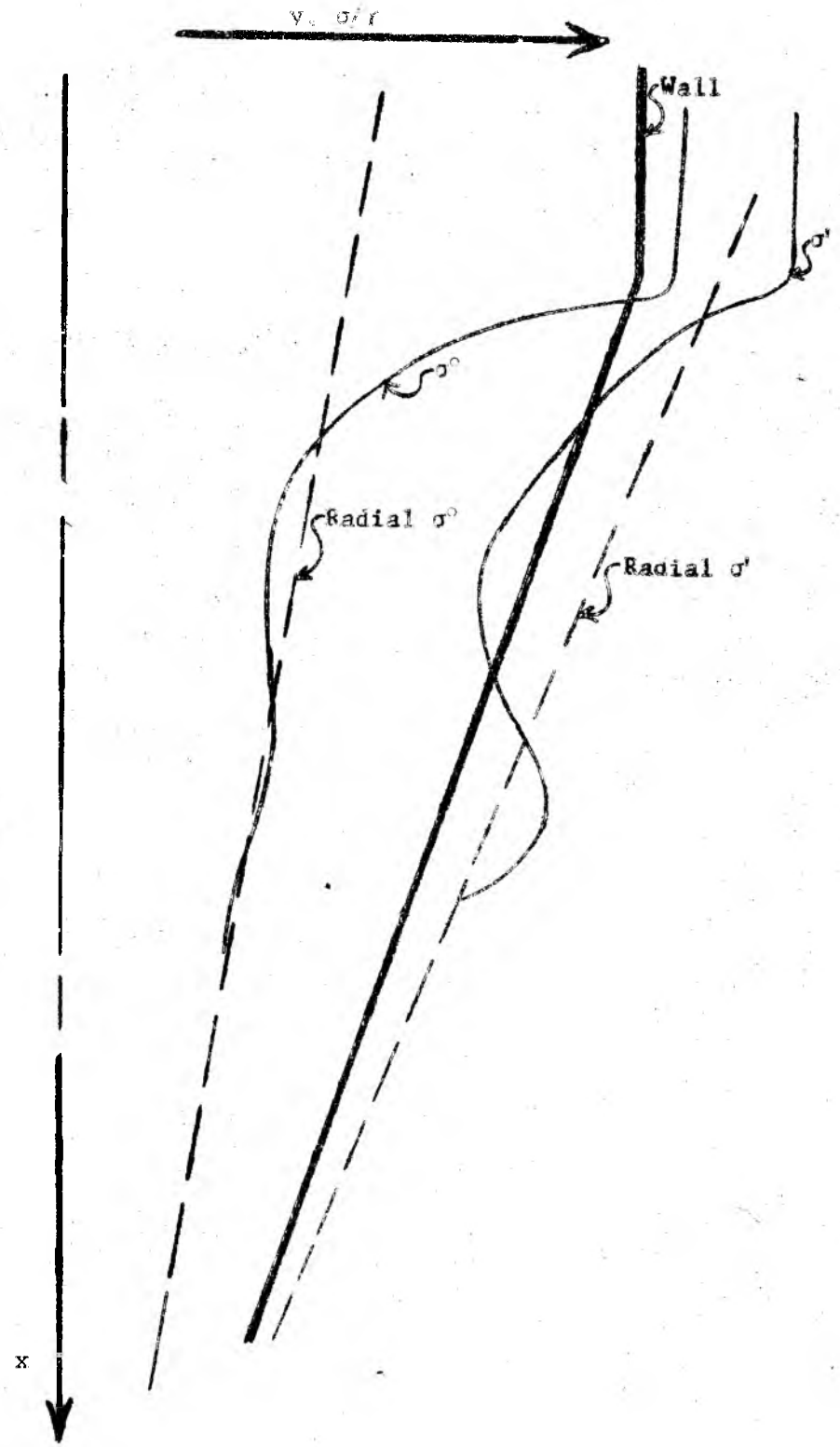

Figure 45

Stress in a transition from vertical wall to $\theta' = 20°$

$\delta = 50°$, $\phi' = 30°$

Figure 46

Equipment for plane strain testing

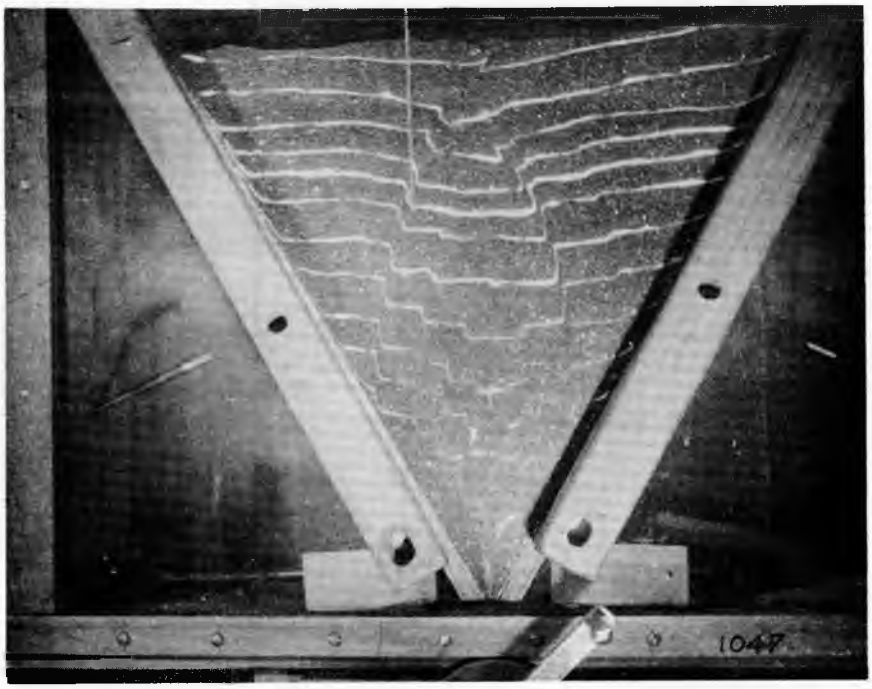

Figure 47

Plain strain model with a horizontal top boundary
$\delta = 50°$, $\theta' = 29°$, $\phi' = 24°$

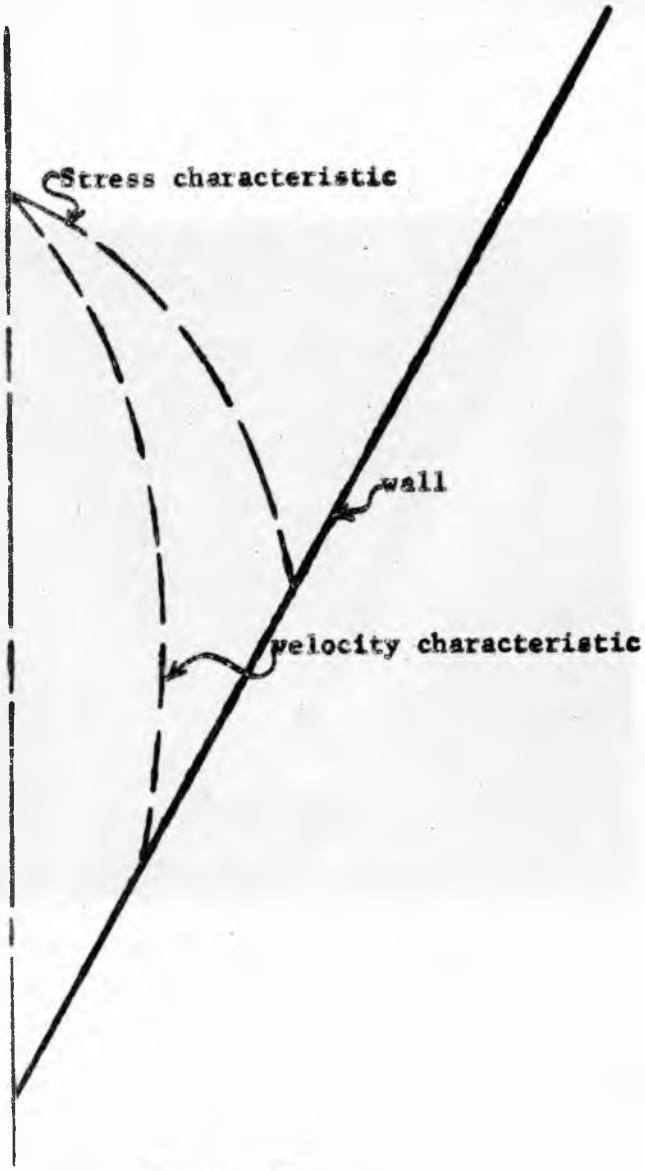

Figure 48.

Radial stress and velocity characteristics

$\delta = 50^\circ$, $\phi' = 24^\circ$ $\theta' = 29^\circ$

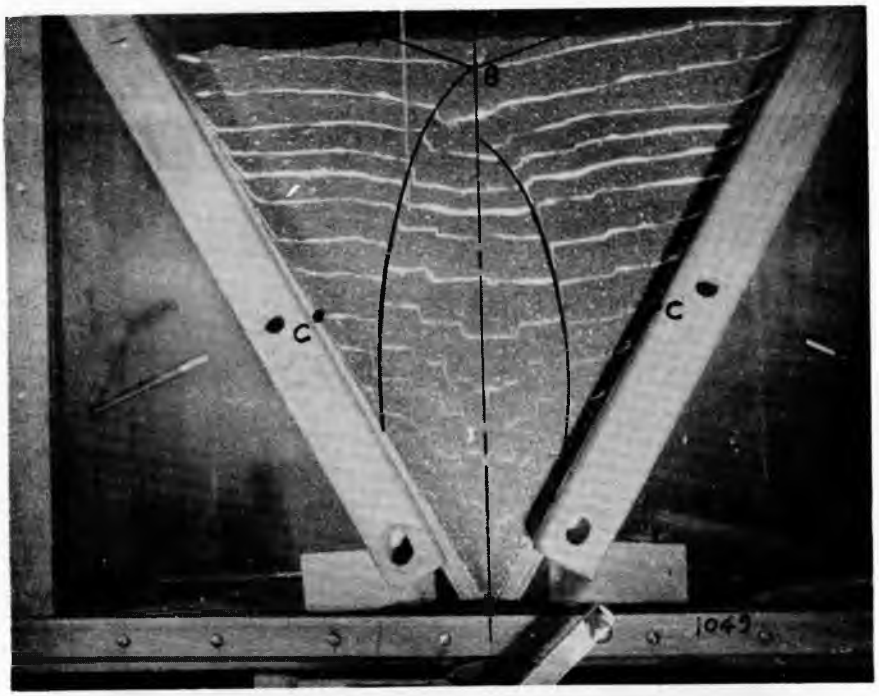

Figure 49

Plane strain model with radial velocity characteristics

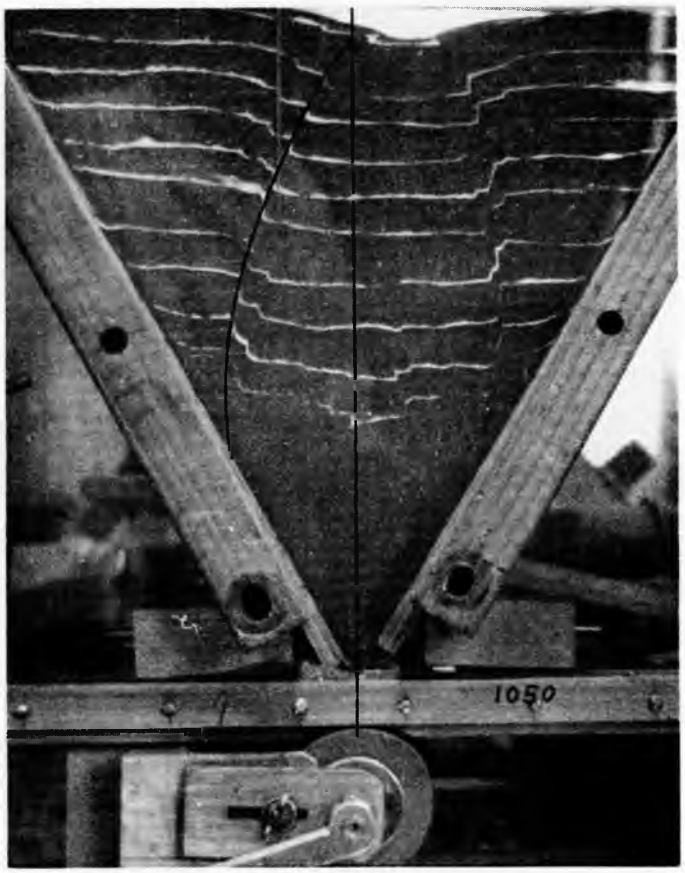

Figure 50

Plane strain model $\delta = 50°$, $\theta' = 29°$, $\phi' = 26.5°$

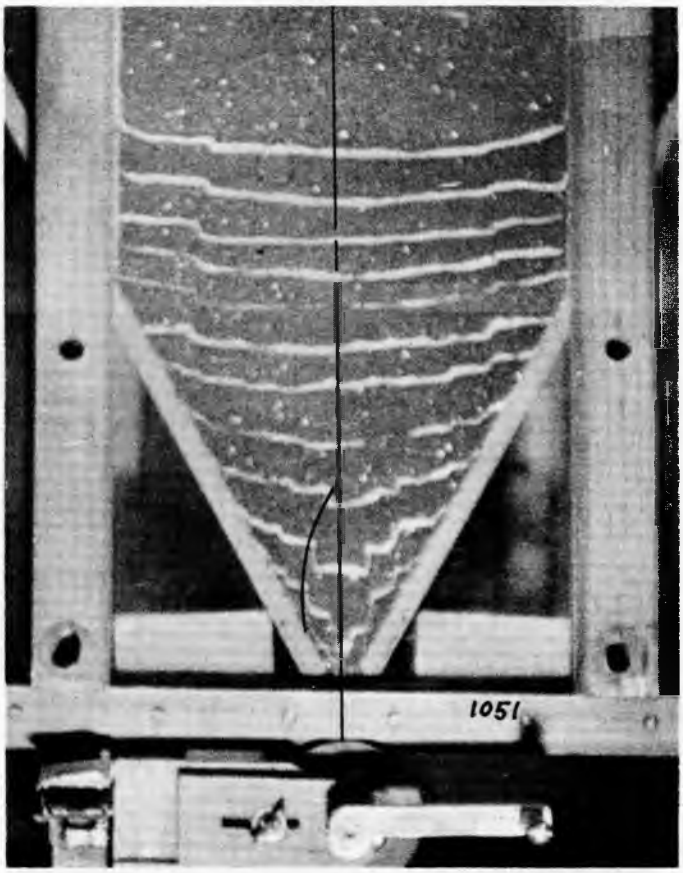

Figure 51

Plane strain model with a vertical section,
$\delta = 50°$, $\theta' = 29°$, $\phi' = 24°$

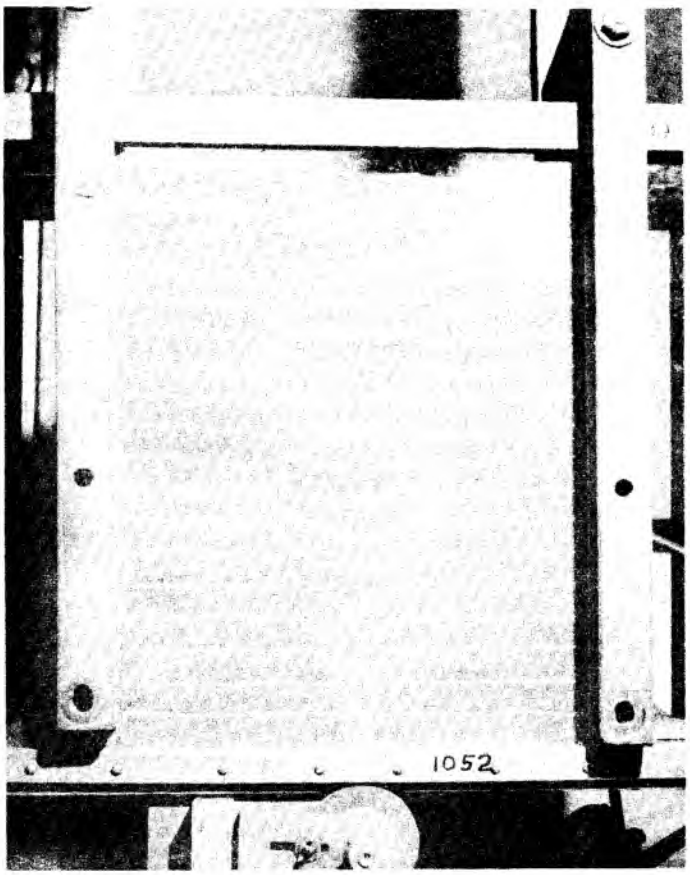

Figure 52

Plane strain flow pattern for flat bottom, $\delta = 50°$

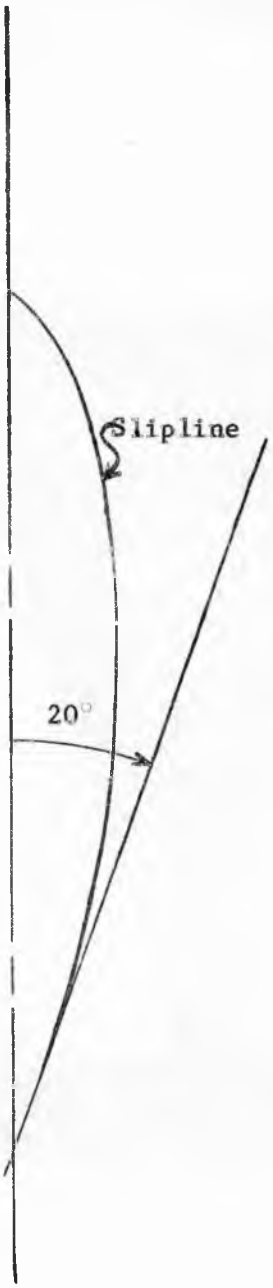

Figure 53.

Plane strain radial slipline
$\delta = 50^\circ$, $\theta' = 20^\circ$, $\phi = 33^\circ$

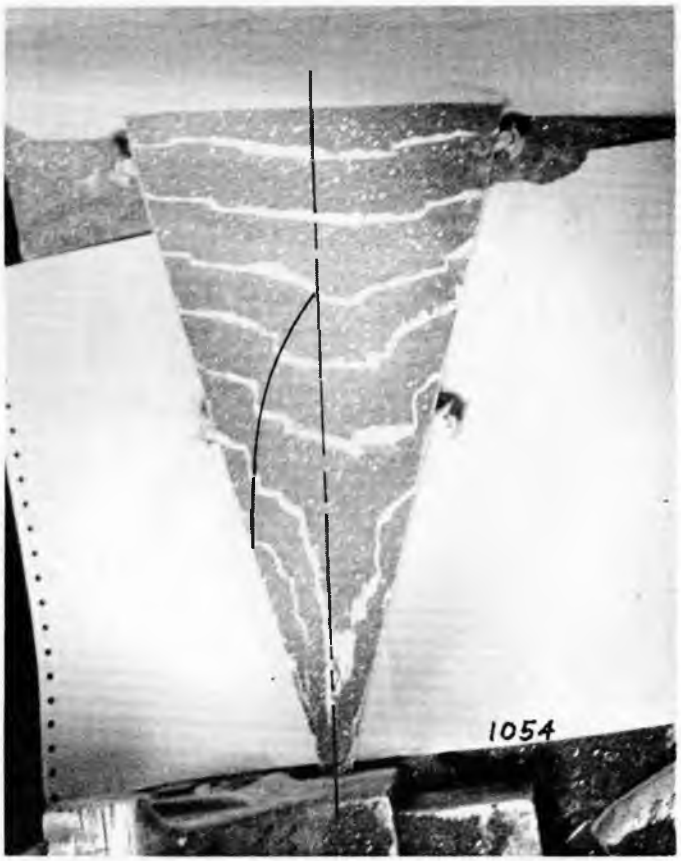

Figure 54

Axial symmetry model,
$\delta = 50°$, $\theta' = 15°$, $\phi' = 24°$

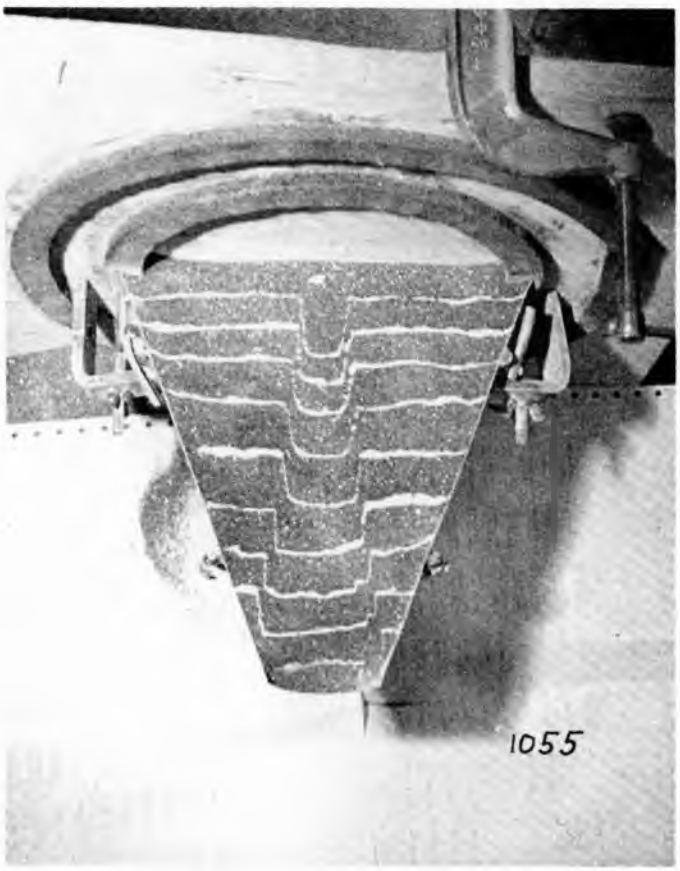

Figure 55

Axial symmetry model,
$\delta = 50°$, $\theta' = 21°$, $o' = 24°$

Figure 56

Axial symmetry model,
$\delta = 50°$, $\theta' = 30°$, $\phi' = 24°$

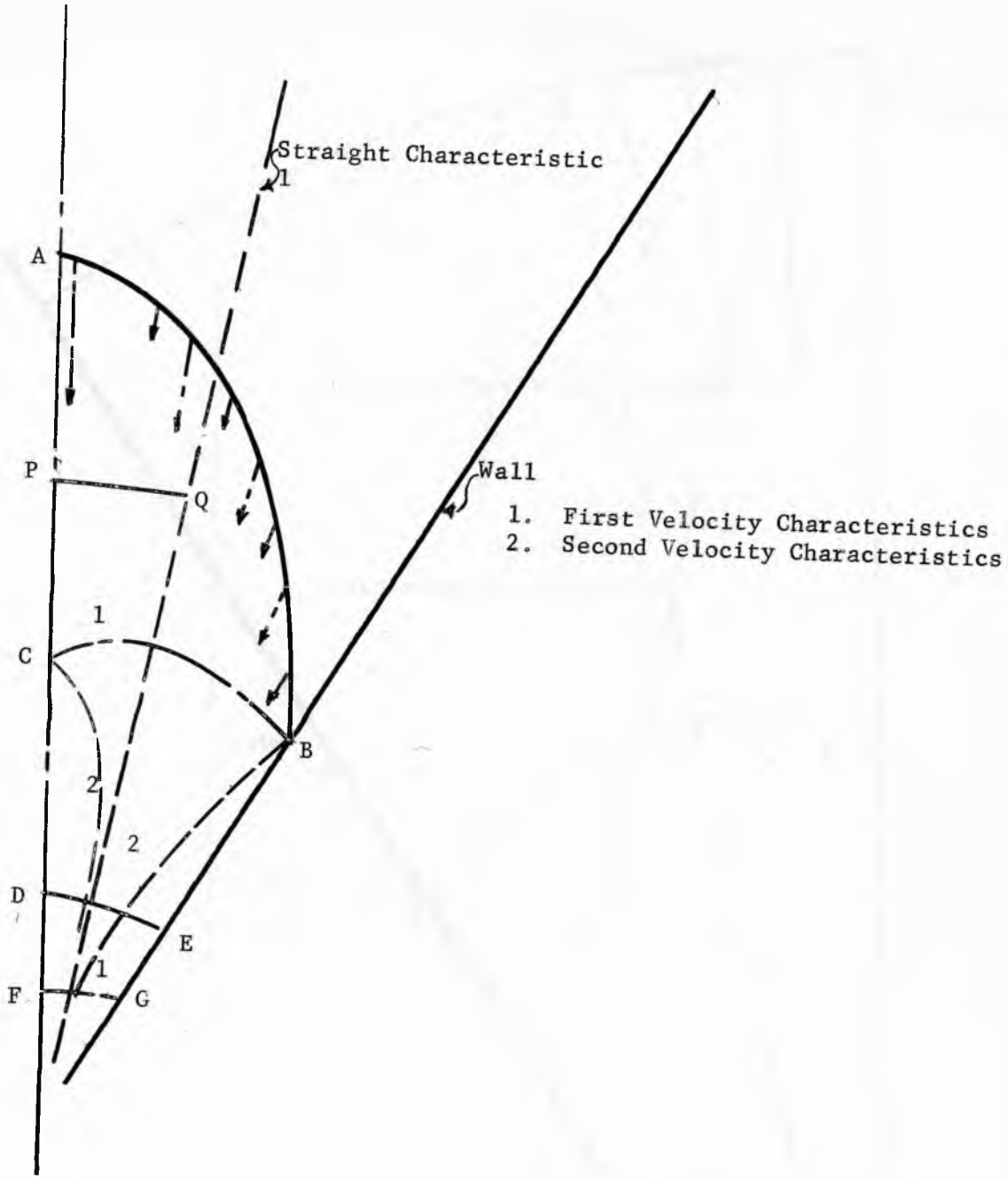

Figure 57
Velocity field characteristics for radial stress

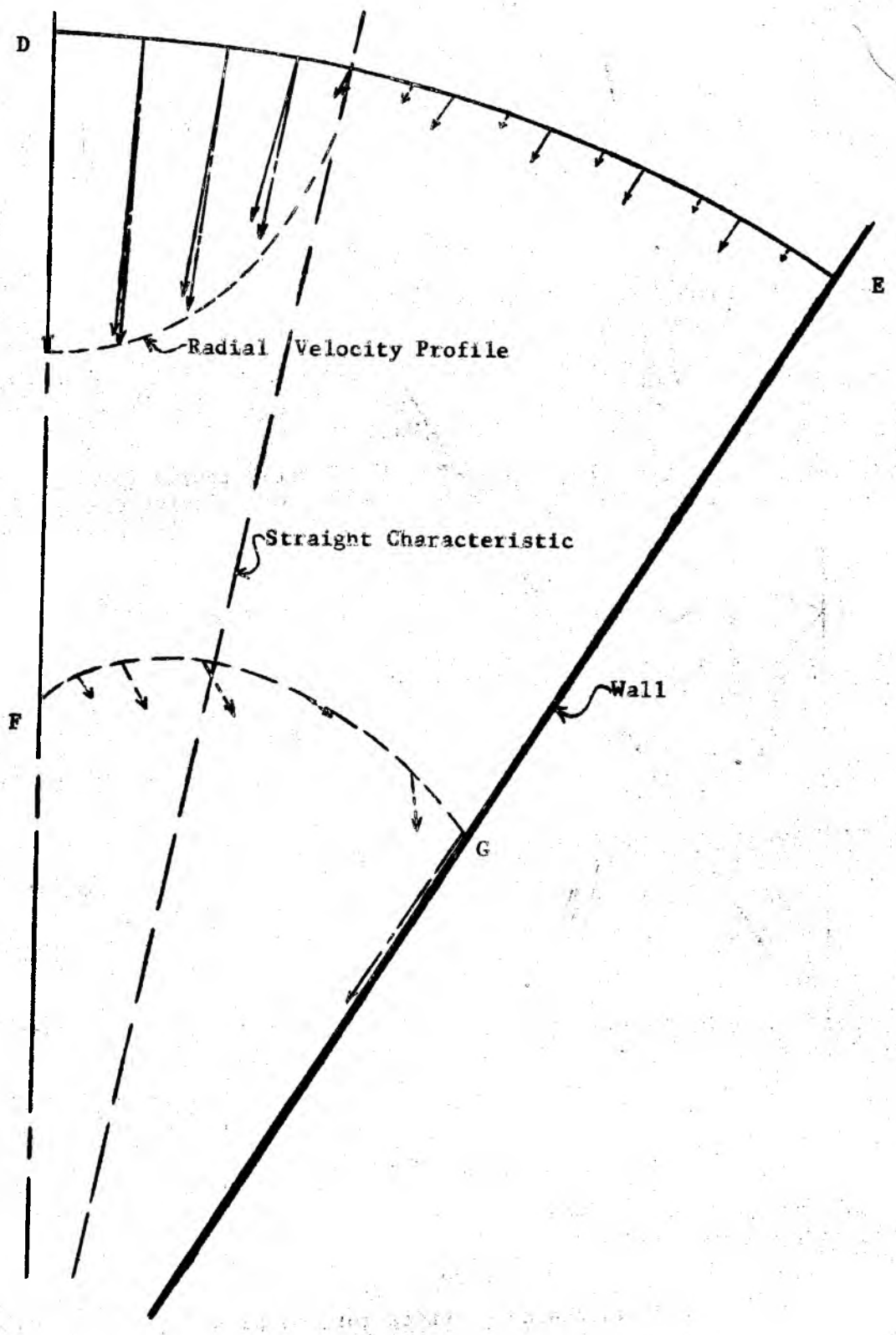

Figure 58

Examples of velocity with radial stress

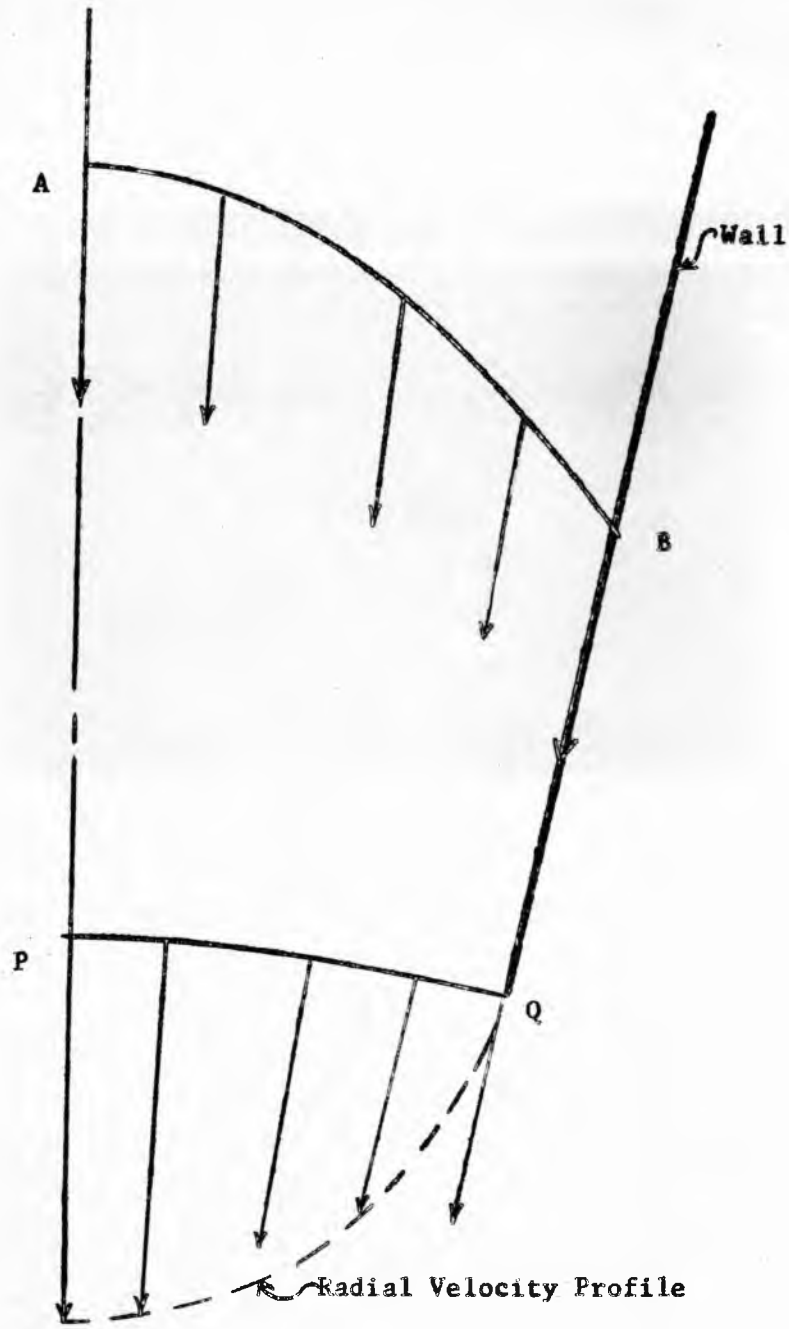

Figure 59

Radial stress velocity with the

straight characteristic as a wall

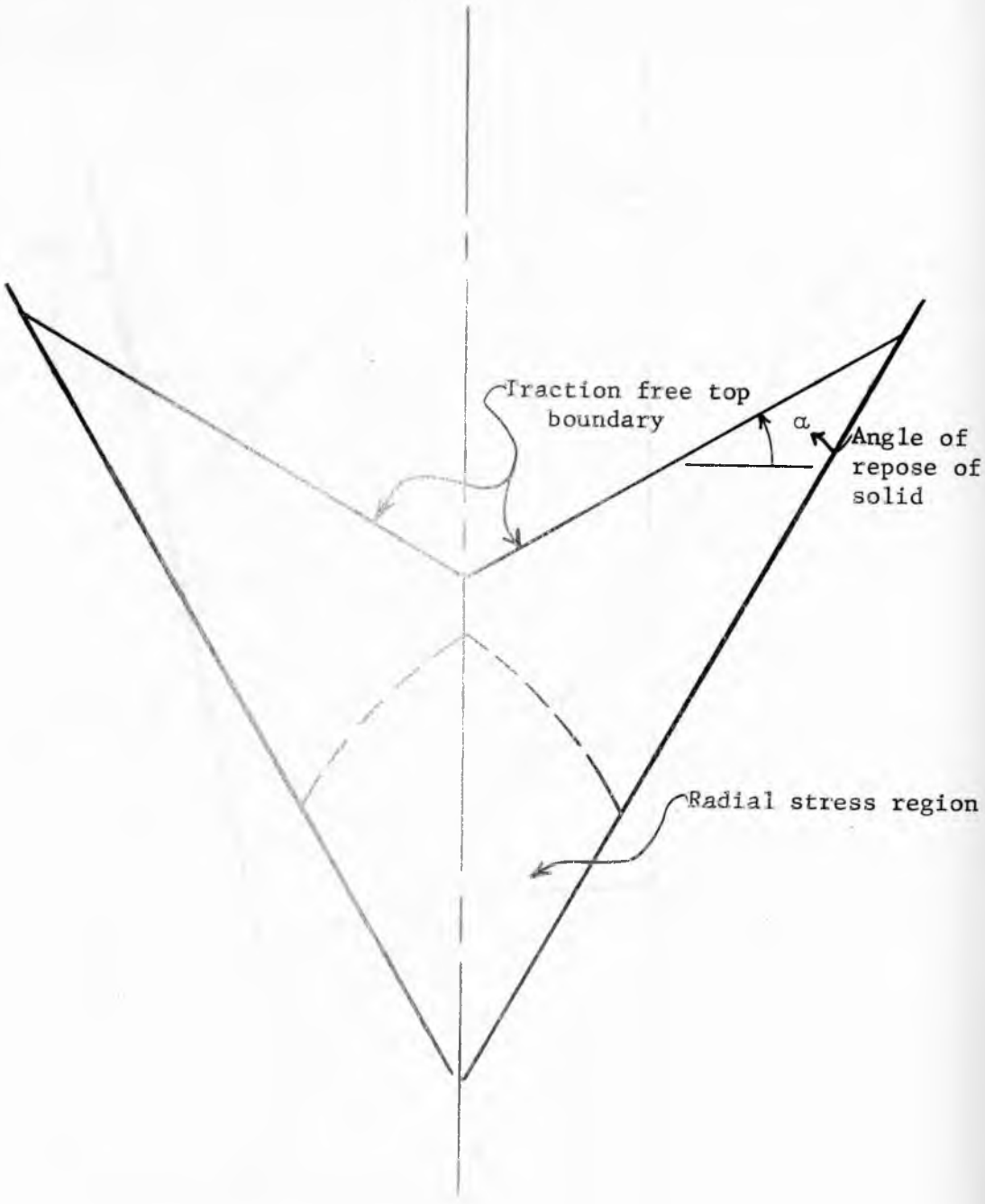

Figure 60.

Concave type top boundary

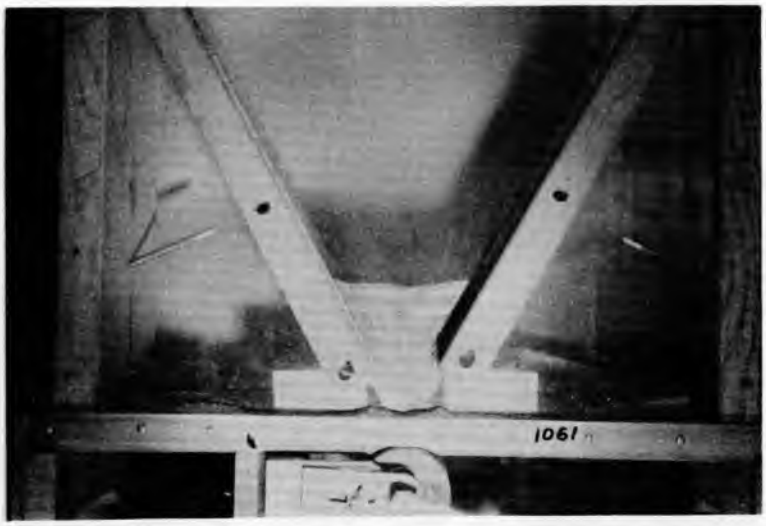

Figure 61

Plane strain model showing tendency of top boundary to remain horizontal, $\delta = 50°$, $\theta' = 29°$, $\phi' = 24°$

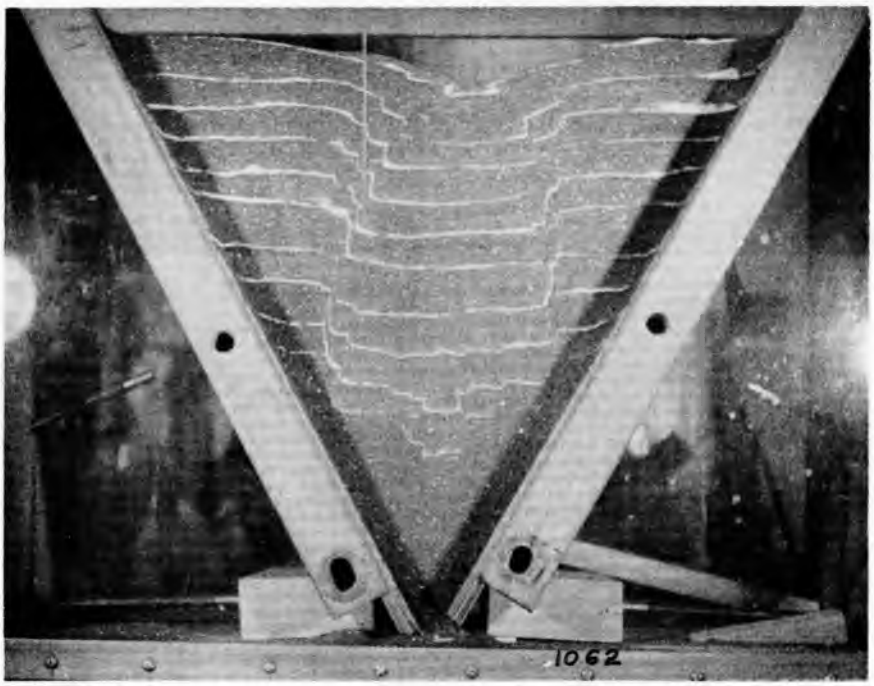

Figure 62

Plane strain model showing tendency of top boundary to
for concave shape, $\delta = 50°$, $\theta' = 29°$, $\phi' = 26.5°$

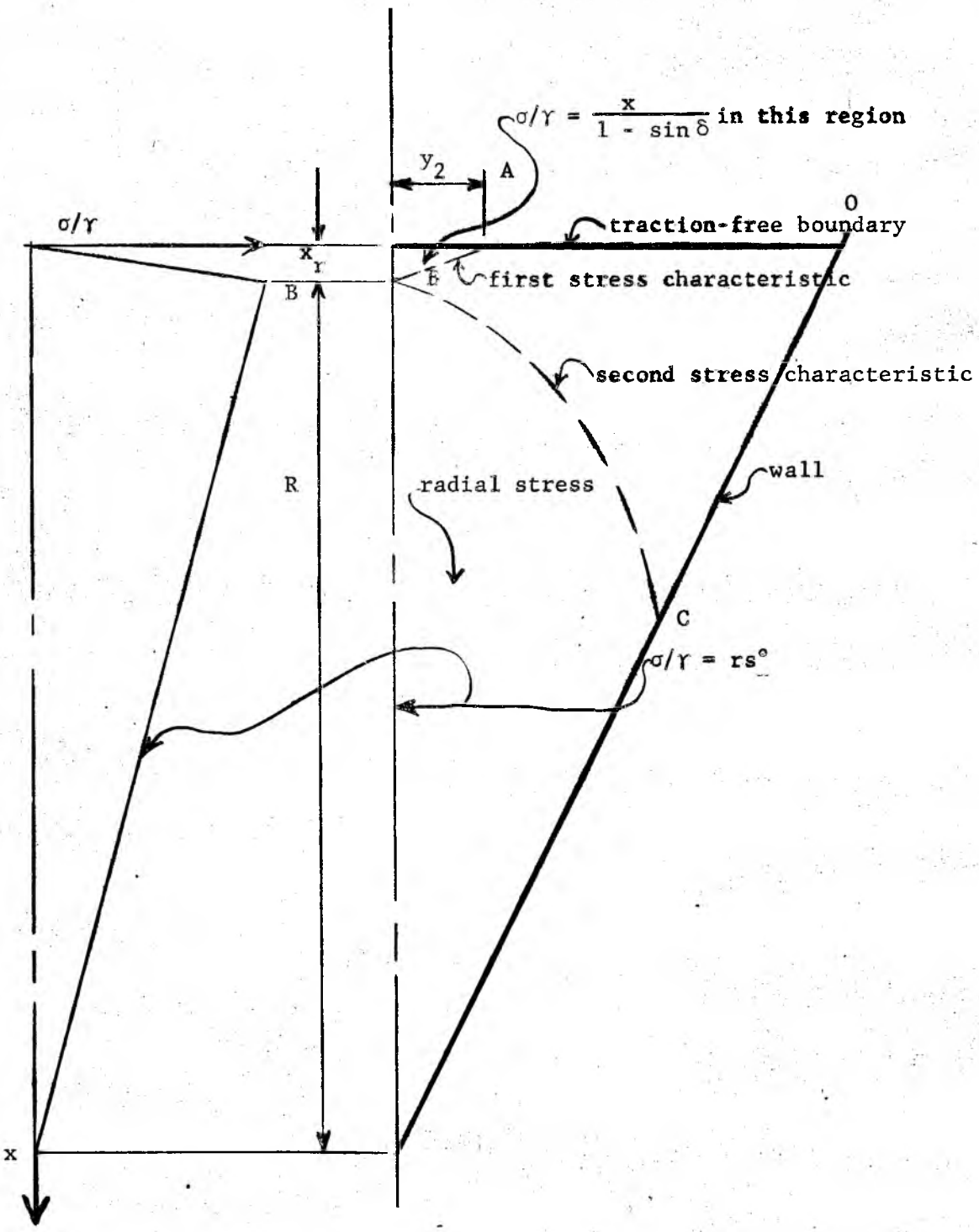

Figure 63.

Approximate stress field for converging channels with horizontal top boundaries

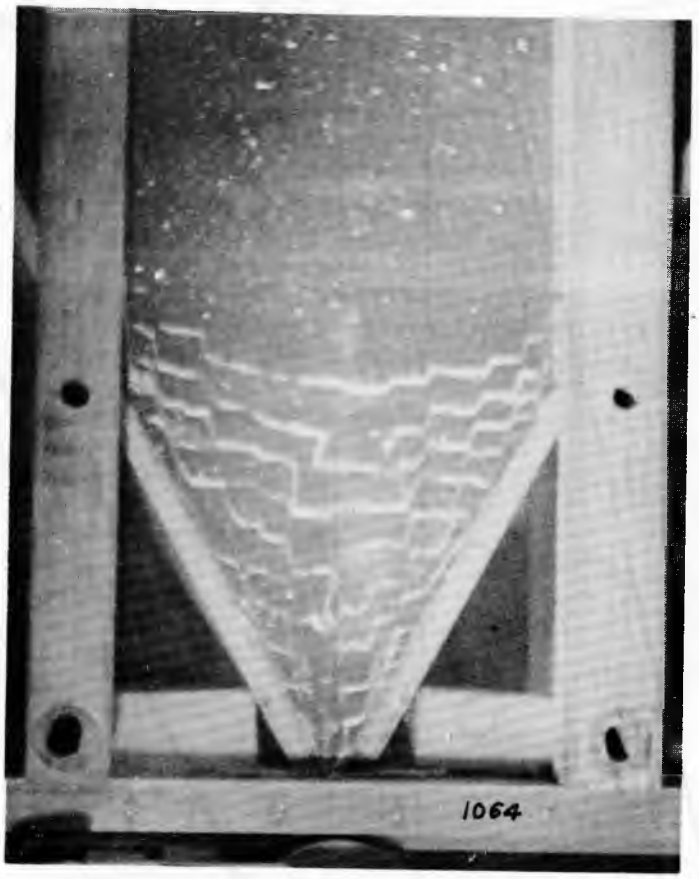

Figure 64

Plane strain flow pattern for a sharp transition from a vertical to a sloping wall, $\delta = 50°$, $\theta' = 29°$, $\phi' = 24°$

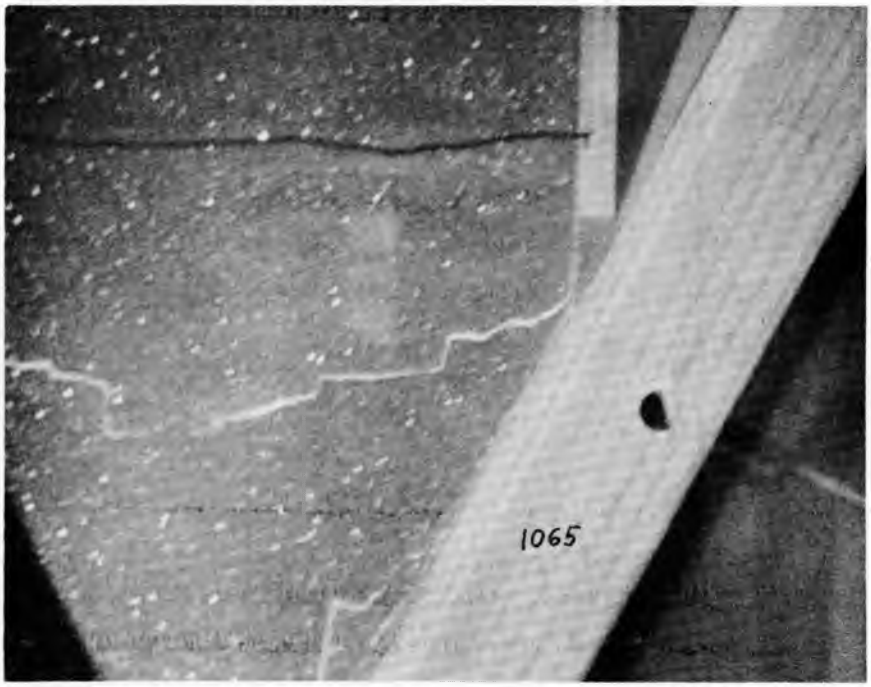

Figure 65

Details of the flow pattern near the transition

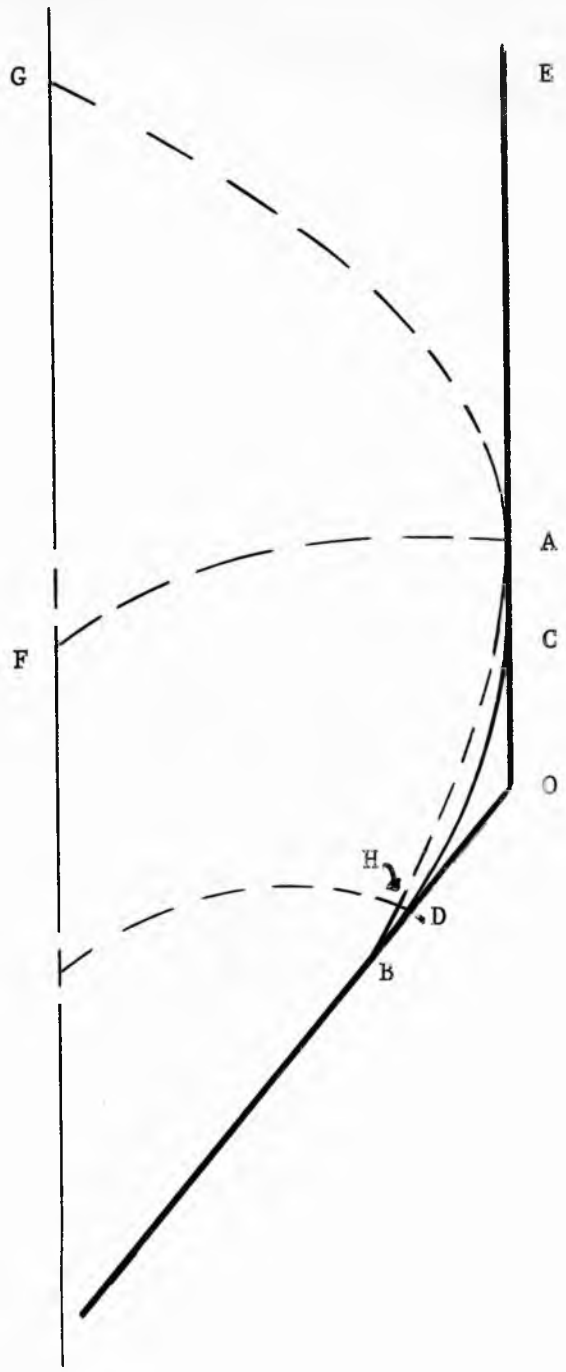

Figure 66

The velocity characteristics near the transition.

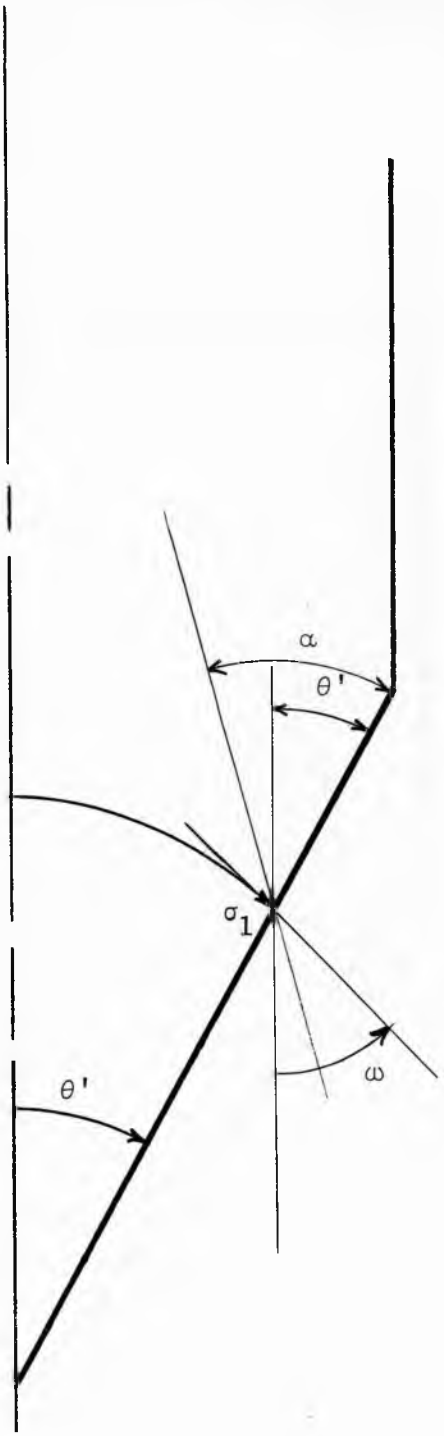

Figure 67

The relation between α and θ'

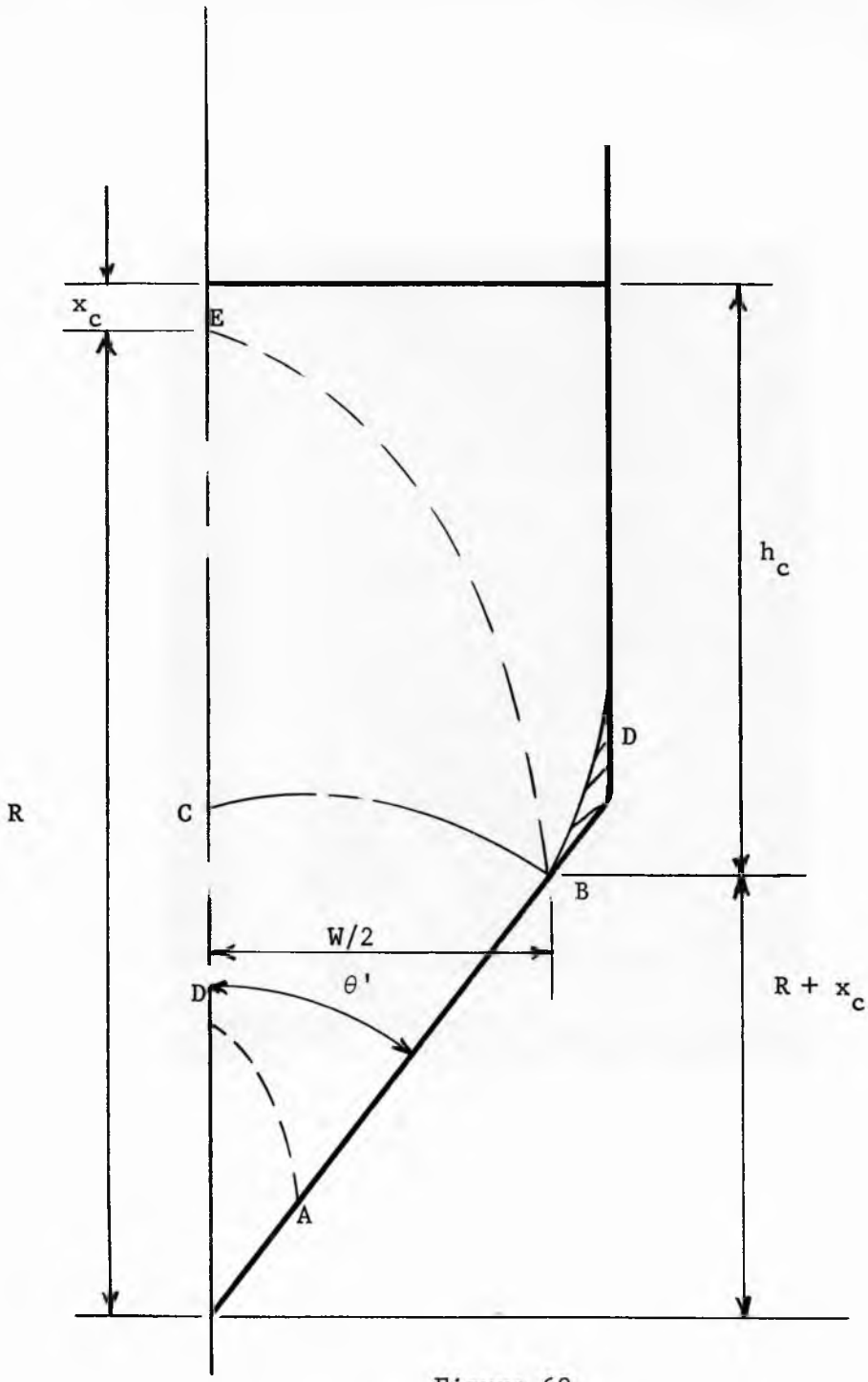

Figure 68.

Calculation of the critical height h_c

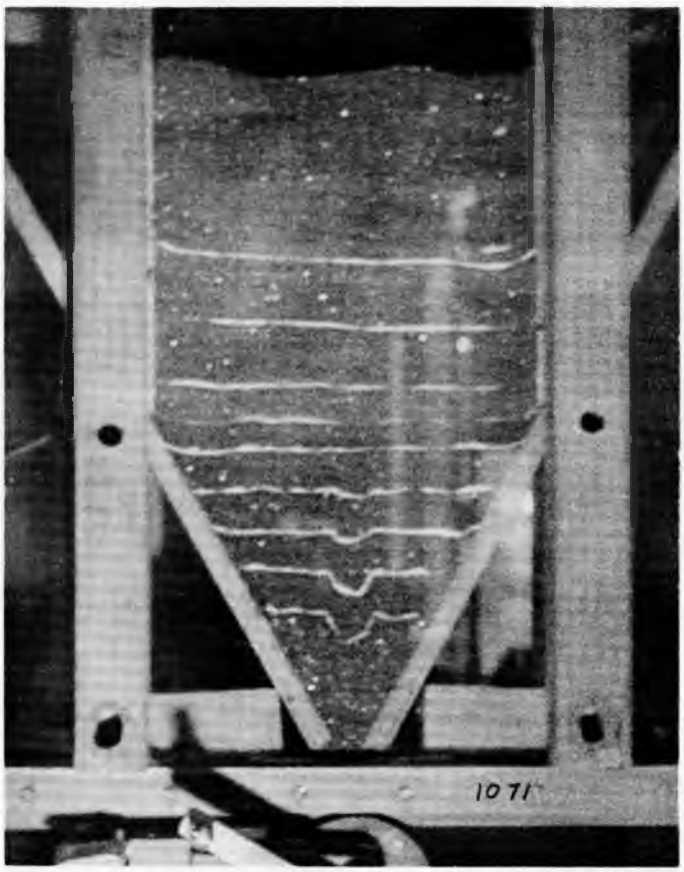

Figure 71

Plane strain sharp transition, $\delta = 50°$, $\theta' = 29°$, $\phi' = 24°$

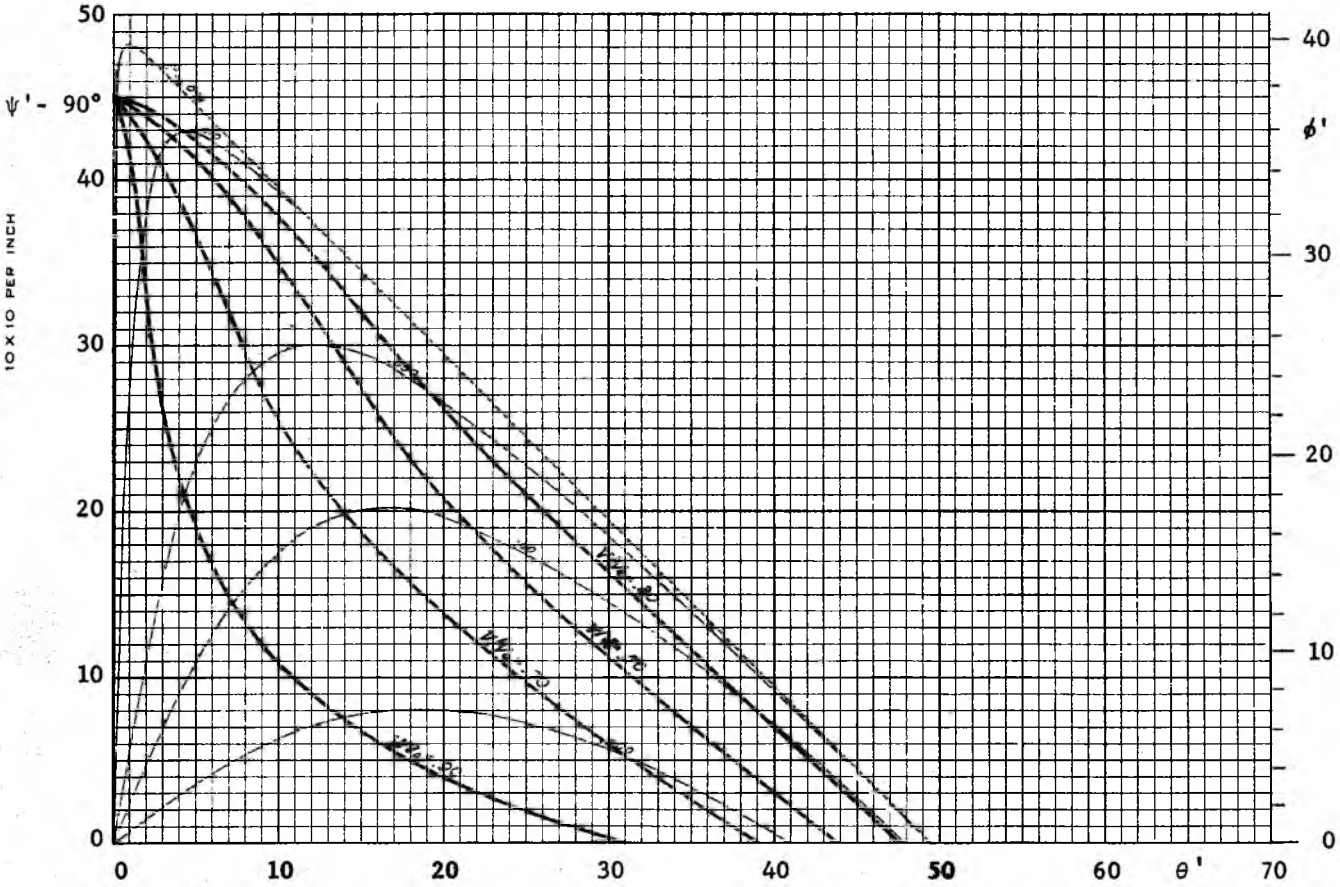

Fig. 70

Function V/V^{o}, $\delta = 50°$

Axial symmetry (conical flow)

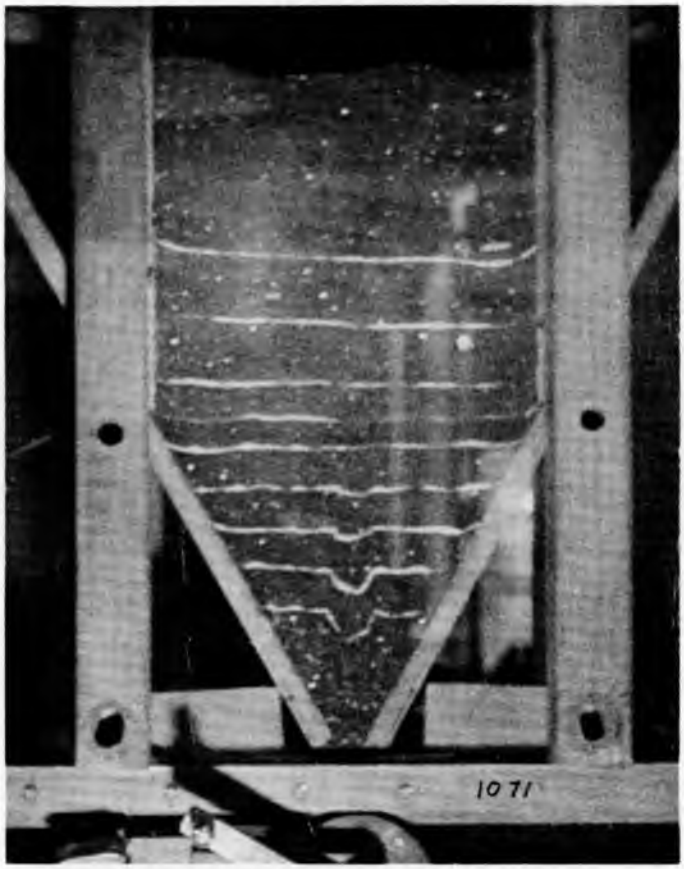

Figure 71

Plane strain sharp transition, $\delta = 50°$, $\theta' = 29°$, $\phi' = 24°$

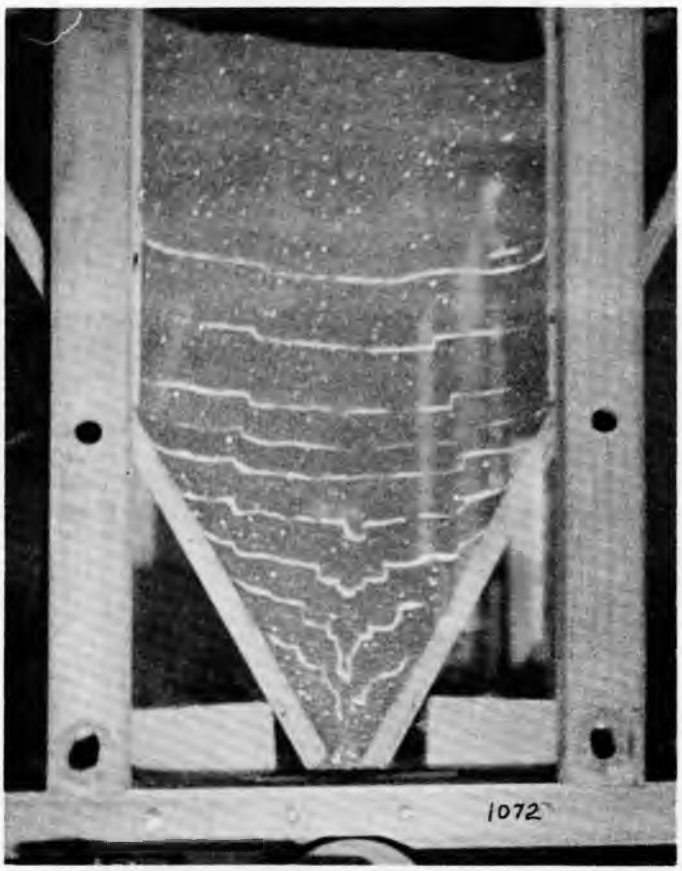

Figure 72

Plane strain sharp transition, $\delta = 50°$, $\theta' = 29°$, $\beta' = 24°$

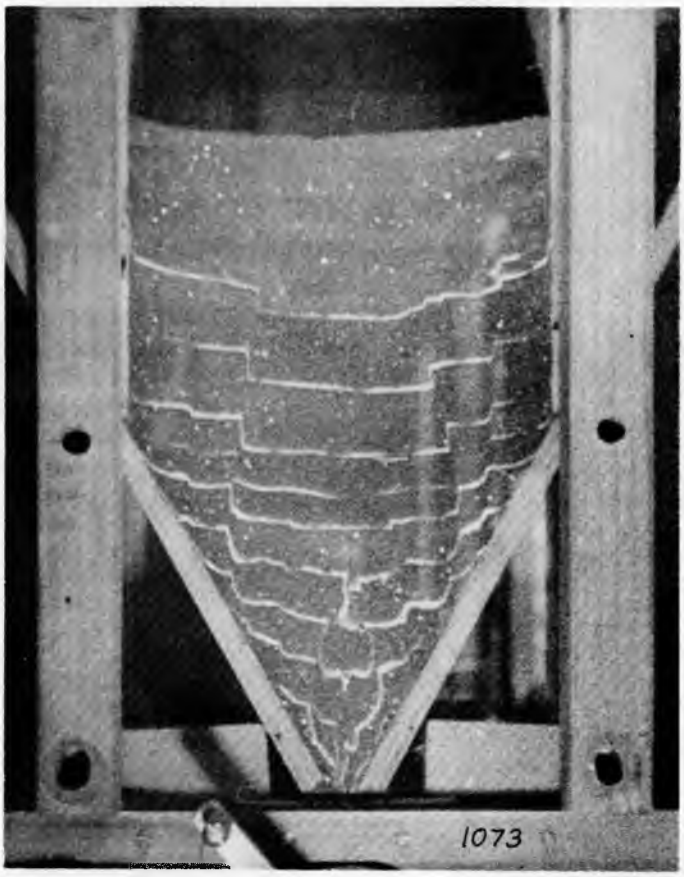

Figure 73

Plane strain sharp transition, $\delta = 50°$, $\theta' = 29°$, $\phi' = 24°$

BIBLIOGRAPHY

1. Jenike, Andrew W. Flow Properties of Bulk Solids, American Society for Testing Materials, Volume 60, 1960.

2. De Jong, G. De Josselin. Statics and Kinematics in the Failure Zone of a Granular Material. Waltman-Delft, Thesis for Ph.D. presented February 18, 1959.

3. Jenike, Andrew W., Shield, R. T. On the Plastic Flow of Coulomb Solids Beyond Original Failure, Journal of Applied Mechanics, 1959, 81B 599.

4. Drucker, D. C. A More Fundamental Approach to Plastic Stress-Strain Relations, Proc. 1st U. S. National Congress of Applied Mechanics, A.S.M.E. (1951) pp 487-491.

5. Jenike, Andrew W. Gravity Flow of Bulk Solids, Utah Engineering Experiment Station Bulletin No. 108, Vol. 52, No. 29, October, 1961.

6. Sokolovski, V. V., Statics of Soil Media, Butterworths Scientific Publications, 1960.

7. Forsythe, George E., Wasow, Wolfgang R. Finite - Difference Methods for Partial Differential Equations, John Wiley & Sons, Inc., 1960.

8. Petrovsky, I. G. Partial Differential Equations, Interscience Publishers, 1954, 1957.

9. Shield, R. T. On the Plastic Flow of Metals Under Conditions of Axial Symmetry, Proceedings of the Royal Society, A, Volume 233, pp 267-286, 1955.

10. Hildebrand, F. B. Introduction to Numerical Analysis, McGraw-Hill Book Company, Inc., 1956.